ÉCOLE DE TECHNOLOGIE SUPÉRIEURE
UNIVERSITÉ DU QUÉBEC

MANUSCRIPT-BASED THESIS
PRESENTED TO
ÉCOLE DE TECHNOLOGIE SUPÉRIEURE

IN PARTIAL FULFILLEMENT OF THE REQUIREMENTS FOR
THE DEGREE OF DOCTOR OF PHILOSOPHY
PH. D.

BY
Mehdi SABOORI

# MATERIAL MODELING FOR MULTISTAGE TUBE HYDROFORMING PROCESS SIMULATION

MONTREAL, JANUARY 08 2015

## BOARD OF EXAMINERS

THIS THESIS HAS BEEN EVALUATED

BY THE FOLLOWING BOARD OF EXAMINERS

Prof. Natalia Nuño, ETS, présidente
Département de génie de la production automatisée, École de technologie supérieure

Prof. Henri Champliaud, ETS, directeur de thèse
Département de génie mécanique, École de technologie supérieure

Dr. Javad Gholipour Baradari, CNRC, codirecteur de thèse
National Research Council, Institute for Aerospace Research, Aerospace Manufacturing Technologies Center

Prof. Augustin Gakwaya, Université Laval, co-directeur de thèse
Département de génie mécanique, univertisté Laval

Prof. Ngan Van Lê, ETS, membre du jury
Département de génie mécanique, École de technologie supérieure

Prof. Philippe Bocher, ETS, membre du jury
Département de génie mécanique, École de technologie supérieure

Prof. Zengtao Chen, University of Alberta, Membre externe independent
Department of Mechanical Engineering, university of Alberta

THIS THESIS WAS PRENSENTED AND DEFENDED

IN THE PRESENCE OF A BOARD OF EXAMINERS AND PUBLIC

NOVEMBER 28 2014

AT ÉCOLE DE TECHNOLOGIE SUPÉRIEURE

**This dissertation is dedicated to my loving parents and my beloved spouse**

For their love, endless supports and encouragement

# ACKNOWLEDGMENT

I would like to express my sincere gratitude to my supervisor Prof. Henri Champliaud for guiding me and helping me reach my potential. Prof. Champliaud has both the personal and professional attributes that I strive for, and I will always consider it a tremendous honor to have studied under his guidance.

I would like to extend my special thanks to my co-supervisor Dr. Javad Gholipour Baradari from National Research Council of Canada (NRC)-Aerospace, who supported me at every important moment of my PhD experience at NRC. Without his thrust, guidance, patience and supports, my research would not have been successful. Undoubtedly, he was one of the most influential person during my Ph.D.

Also, I would like to thank my co-supervisor Prof. Agustin Gakwaya from Laval University in a special way, I express my heartfelt gratefulness for his guide and support that I believed I learned from the best.

I also sincerely thank to Dr. Jean Savoie from Pratt & Whitney Canada for his enthusiastic support and pertinent suggestions all along the Project. This dissertation would not have been possible without the financial support of Pratt & Whitney Canada, NRC-Aerospace, Natural Sciences and Engineering Research Council of Canada (NSERC) and Consortium de recherche et d'innovation en aérospatiale au Québec (CRIAQ). A partially financial support by Fonds Québécois de la Recherche sur la Nature et les Technologies (FQRNT) is gratefully acknowledged.

I would also like to give thanks and a special acknowledgement to Dr. Priti Wanajara for providing valuable comments supporting me at writing stages of all my publication.

A very special acknowledgement goes to my wife Somayeh, who loved and supported me during the final, critical months of my dissertation, and made me feel like anything was possible. I love you, Somayeh. I would also like to acknowledge my parents, as well as my

wife's parents, for their unwavering supports, kind words, well-wishing and patience for abiding by my absence.

I am particularly grateful to my friends and colleagues who put up with me during the hard and the joyful times.

Finally, Thank you my God for many beautiful thinks cannot be seen our touched, they are left within the heart. What you have done for me is one of them. And thank you from the bottom of my heart.

# MATERIAL MODELING FOR MULTISTAGE TUBE HYDROFORMING PROCESS SIMULATION

Mehdi SABOORI

## ABSTRACT

The Aerospace industries of the 21st century demand the use of cutting edge materials and manufacturing technology. New manufacturing methods such as hydroforming are relatively new and are being used to produce commercial vehicles. This process allows for part consolidation and reducing the number of parts in an assembly compared to conventional methods such as stamping, press forming and welding of multiple components. Hydroforming in particular, provides an endless opportunity to achieve multiple cross-sectional shapes in a single tube. A single tube can be pre-bent and subsequently hydroformed to create an entire component assembly instead of welding many smaller sheet metal sections together. The knowledge of tube hydroforming for aerospace materials is not well developed yet, thus new methods are required to predict and study the formability, and the critical forming limits for aerospace materials.

In order to have a better understanding of the formability and the mechanical properties of aerospace materials, a novel online measurement approach based on free expansion test is developed using a 3D automated deformation measurement system (Aramis®) to extract the coordinates of the bulge profile during the test. These coordinates are used to calculate the circumferential and longitudinal curvatures, which are utilized to determine the effective stresses and effective strains at different stages of the tube hydroforming process.

In the second step, two different methods, a weighted average method and a new hardening function are utilized to define accurately the true stress-strain curve for post-necking regime of different aerospace alloys, such as inconel 718 (IN 718), stainless steel 321 (SS 321) and titanium (Ti6Al4V). The flow curves are employed in the simulation of the dome height test, which is utilized for generating the forming limit diagrams (FLDs).

Then, the effect of stress triaxiality, the stress concentration factor and the effective plastic strain on the nucleation, growth and coalescence of voids are investigated through a new user material for burst prediction during tube hydroforming. A numerical procedure for both plasticity and fracture is developed and implemented into 3D explicit commercial finite element software (LS-DYNA) through a new user material subroutine. The FLDs and predicted bursting pressure results are compared to the experimental data to validate the models.

Finally, the new user material model is used to predict the bursting point of some real tube hydroforming parts such as round to square and round to V parts. Then, the predicted bursting pressure results are compared to the experimental data to validate the models in real and multistep tube hydroforming processes.

**Keywords:** Hydroforming, Forming Limit Diagram, Stress triaxiality, Inconel, Stainless steel

# MATERIAL MODELING FOR MULTISTAGE TUBE HYDROFORMING PROCESS SIMULATION

Mehdi SABOORI

## RÉSUMÉ

L'industrie aéronautique du 21e siècle est en forte demande de technologie de fabrication et de matériaux de pointe. Des méthodes avancées de fabrication telles que l'hydroformage sont relativement nouvelle et actuellement utilisée pour produire des véhicules commerciaux. Ce procédé permet à travers la consolidation de pièces de réduire le nombre de pièces dans un assemblage comparativement aux méthodes conventionnelles de mise en forme du métal en feuille comme l'emboutissage, la mise en forme par presse et soudage de multiple composantes. Un simple tube peut être pré-déformé par pliage ou écrasé puis hydroformé pour créer un assemblage de composants en lieu et place d'une pièce constituée de plusieurs petites sections de métal soudées ensemble. Les connaissances sur l'hydroformage de tubes en alliages aéronautiques ne sont pas encore très développées. Ainsi, Il est nécessaire de mettre en place de nouvelles méthodes pour prédire et étudier la formabilité et les limites critiques de mise en forme des matériaux aéronautiques.

Afin de mieux comprendre la formabilité et les propriétés mécaniques des matériaux aéronautiques, une approche novatrice de mesure en ligne basée sur des essais d'expansion libre a été développée. Elle utilise un système automatique 3D de mesure de déformation (Aramis®) pour extraire les coordonnées du profil de gonflement du tube pendant l'essai. Ces coordonnées sont utilisées pour calculer les courbures circonférentiel et longitudinale, qui elles servent à déterminer les contraintes et déformations effectives à différentes étapes du procédé d'hydroformage de tube.

Dans un deuxième temps, deux différentes méthodes : une méthode de moyenne pondérée et une nouvelle fonction de durcissement ont été utilisés pour définir avec précision la courbe contrainte vraie-déformation vraie pour la section après striction de différents alliages aéronautiques, tels que l'inconel 718 (IN 718), l'acier inoxydable 321 (SS 321) et le titane (Ti6Al14V). Les courbes d'écoulement ont été employées dans la simulation du test de hauteur de dôme qui sert à générer les diagrammes de limites de mise en forme (FLDs).

Ensuite, les effets de la triaxialité de contraintes, du facteur de concentration de contraintes et de la déformation plastique effective sur la nucléation, la croissance et la coalescence des cavités sont étudiés à travers un nouveau matériel pour la prédiction de la rupture pendant un essai d'hydroformage de tube. Une procédure numérique pour, à la fois, la plasticité et la rupture a été développée et implémentée dans le logiciel d'éléments finis commercial 3D explicite (LS-DYNA) à travers une nouvelle matérielle sous-routine. Les FLDs ainsi que les prédictions de pression à la rupture sont comparés aux données expérimentales pour valider les modèles.

Enfin, le nouveau modèle matériau a été utilisé pour prédire le point de rupture de quelques pièces réelles hydroformées de type « ronde à carré » et « rond à V ». Puis, les résultats de prédiction de la pression de rupture ont été comparés avec les résultats expérimentaux pour valider les modèles en procédés de mise en forme par hydroformage réel et multi-étapes.

**Mots-clés** : Hydroformage, diagramme de mise en forme limite, triaxialité des contraintes, inconel, acier inoxyable

## TABLE OF CONTENTS

Page

# LIST OF TABLES

# LIST OF FIGURES

# LIST OF ABREVIATIONS

| | |
|---|---|
| THF | Tube Hydroforming |
| FE | Finite Element |
| SS 321 | Stainless Steel 321 |
| SS 304L | Stainless Steel 321 |
| AA 6061 | Aluminum Alloy 6061 |
| IN 718 | Inconel 718 |
| n-value | Strain Hardening Exponent |
| r-value | Material Anisotropy |
| FLD | Failure Limit Diagram |
| FLC | Failure Limit Curve |
| FLDf | Forming Limit at Fracture |
| FLDn | Forming Limit at Necking |
| NRC | National Research Council of Canada |
| W | Length of the Expansion Zone |
| r | Die Radius |
| $t_0$ | Initial Thickness of the Tube |
| p | Internal Pressure |
| h | Bulge Height |
| t | Thickness at the Maximum Bulge Height |
| $r_\theta$ | Bulge Circumferential Radius |
| $r_z$ | Bulge Longitudinal Radius |
| $p_i$ | Internal Pressure at Time i |
| $t_i$ | Wall Thickness at Stage i |
| $\sigma_\theta$ | Circumferential Stress |
| $\sigma_z$ | Longitudinal Stress |
| $r_{\theta p}$ | Maximum Circumferential Radius |
| $r_z$ | Bulge Curvature or Longitudinal Radius |
| $t_p$ | Wall Thickness at the Maximum Bulge Height |

| | |
|---|---|
| $\overline{\sigma}$ | Effective Stress |
| $\varepsilon_\theta$ | Strains in the Circumferential Direction |
| $\varepsilon_t$ | Strains in the Thickness Direction |
| $\varepsilon_z$ | Strains in the Longitudinal Direction |
| $\varepsilon_0$ | Initial Plastic Strain |
| $\bar{\varepsilon}_p$ | Effective Plastic Strain |
| k | Strength Coefficient |
| n | Strain Hardening |
| $n_s$ | Strain Hardening for Swift |
| $n_h$ | Strain Hardening for Hollomon |
| F | Tensile Load |
| A | Cross Sectional Area of the Sample at the Gauge Length |
| $\overline{\sigma}_{neck}$ | Effective Stress at the Neck |
| $\bar{\varepsilon}_{neck}$ | Effective Strain at the Neck |
| $\alpha$ | Weight Constant |
| $\delta$ | Square Errors |
| $\sigma_s$ | Steady-State Flow Stress |
| $\sigma_m$ | Hydrostatic Stress |
| $\frac{\sigma_m}{\overline{\sigma}}$ | Triaxiality Stress Ratio |
| D | Physical Property |
| $\sigma^*$ | Maximum Principal Stress |
| $\frac{\sigma^*}{\overline{\sigma}}$ | Stress Concentration Factor |
| $\bar{\varepsilon}_i$ | Magnitude of Equivalent Strain |
| $C_1$ to $C_6$ | Material Constants |
| $D_1$ | Damage Accumulation Caused by Nucleation of the Voids |
| $D_2$ | Damage Accumulation Caused by Growth of the Voids |
| $D_3$ | Damage Cccumulation Caused by Coalescence of the Voids, |
| Sij | Stress Deviator |

| | |
|---|---|
| $\Delta\varepsilon$ | Strain Increment |
| $B^{ep}$ | Elasto-Plastic Constitutive Matrix |
| $\sigma_{ij}{}^{*}$ | Trial Stress Tensor |
| $G, \ d\varepsilon_m$ | Plastic Shear Modulus |
| $\lambda$ | Lamé Modulus, |
| $d\varepsilon_m$ | Incremental Hydrostatic Strain |
| $Y(\bar{\varepsilon}^p)$ | True Stress–True Strain Curve |
| $\delta_{ij}$ | Kronecker Delta |
| H | Effective Plastic Strain Incremental |

# INTRODUCTION

Cost saving and product improvement have always been important goals in advanced metal forming processes. To achieve to these goals, metal forming processes need to be optimized. Tube hydroforming (THF) is one of the most popular advanced metal forming processes that is widely used to produce various tubular components. The principle of tube hydroforming is displayed in Figure 0.1. The tube is first clamped between the two halves of the die as shown in (Figure 0.1.a). The tube ends are then sealed using two plungers, (Figure 0.1.b). Pressurized fluid is then introduced into the tube through the end plungers and, in this way, the tube is then forced to adopt the inner contour of the die by the application of internal pressure and axial forces (via plungers) simultaneously (Figure 0.1.c). With increasing internal pressure, expansion of the tube occurs and at its limit the tube bursts. For limited applications, the tube can be formed by the increasing internal pressure only. This means that the axial plungers do not feed more material into the expansion zone.

Establishment of this process goes back to 1939 when Grey et al (Gray, Devereaux and Parker, 1940) investigated manufacturing of seamless copper fittings with T and X branches using a combination of internal pressure and axial load. During the last decays THF process contributed to automobile industries and more recently this process was implemented in aerospace industry due to its capability of manufacturing complex shapes with a simpler procedure than traditional stamping and welding processes. Hydroforming also has some further advantages such as weight reduction through more efficient section design, improved structural strength, and lower tooling cost due to fewer die components (Hwang and Lin, 2002; Lang et al., 2004). Increasing acceptance and use of THF technology within the aerospace industry demands a comprehensive understanding of critical issues such as material characteristics, friction condition and hydroformability of the material. To fulfill these requirements the feasibility study of the THF in aerospace industry should be well understood and its parameters optimized. The reliable application of finite element (FE) modeling could be contributed to a well-designed feasibility study. More recently the possibility of coupling FE modeling to mathematical failure algorithms is offering an opportunity to design/study more precisely instead of only feasible ones. Throughout intensive research works during the last decays, the knowledge on the mechanisms of forming stages, material behavior and failure modes is understood to a good extent, followed by introduction of integrated strategies for precise FE modeling of THF process. Despite of all achievements, there are still many challenges on understanding, precise study of THF process for aerospace materials, by means of FE modeling and consequently time reduction in feasibility and design study.

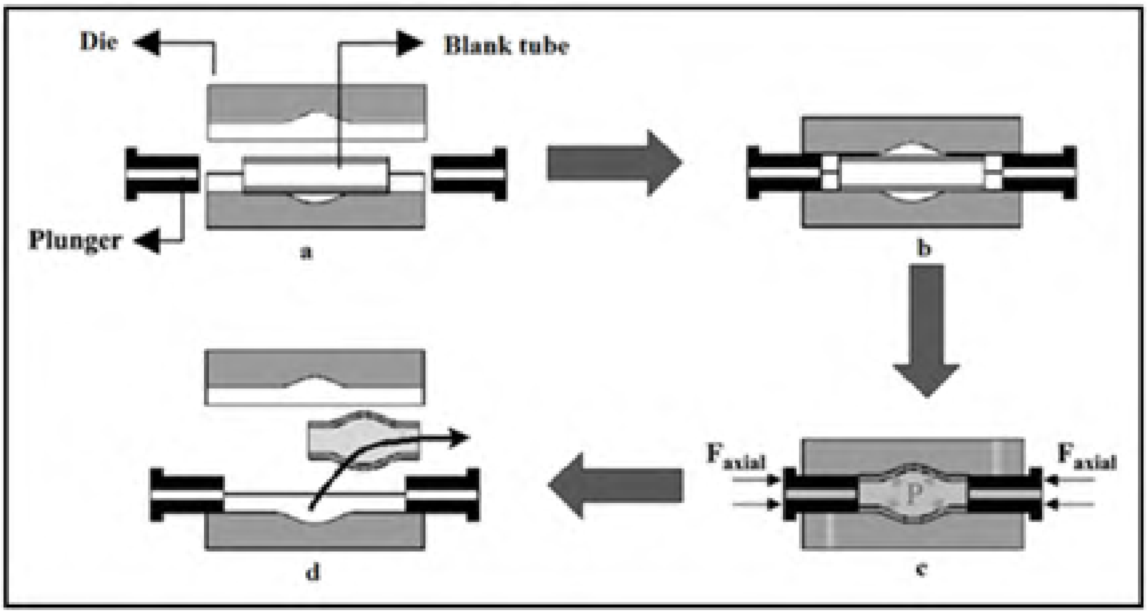

Figure 0.1: Typical tube hydroforming process (Guan, Pourboghrat and Yu, 2006).

## Defining the problem

The application of the THF process in the aerospace sector is comparatively recent with many challenges due to the high strength and/or limited formability of aerospace materials. This is plagued with long lead times, which result from much iteration of tryouts either on trial-and-error based FE modeling or on expensive prototype tooling. To avoid these undesirable expenses, study precisely the hydroformability of aerospace material is a key factor. However, The hydroformability of tubular parts is affected by a large number of parameters such as mechanical properties (before and after onset on instability), tube geometry, complex die-tube interface lubrication, and process parameters, i.e. loading paths (Ahmed and Hashmi, 1997; Koc and Altan, 2002; Vollertsen and Plancak, 2002). However it is a complicated task as formability is remarkably influenced by direct and interaction effects between process parameters.

The main concerns when dealing with hydroformability is mechanical properties and proper selection process to determine the true stress-true strain behavior of tube to implement in any finite element software. Generally, the mechanical response is defined by the stress-strain behavior that can be determined from tensile testing of the specimens extracted either from the sheet used for roll forming of the tubes or directly from the tubes. More recently, free expansion testing has been used to characterize the mechanical response of the material for hydroforming applications (Hwang and Lin, 2002; Hwang, Lin and Altan, 2007; Saboori et al., 2013b; Song, Kim and Kang, 2007; Song et al., 2010). The free expansion test can emulate process conditions similar to those found during THF, and, as such, can be used to obtain reliable and accurate information on the mechanical response/properties of the tubular material (Saboori et al., 2014a).

Among mechanical properties, in the case of large plastic deformations, determination of true stress-true strain curves is usually performed in the pre-necking phase of the tensile testing. The post necking phase is usually ignored as deformation occurs at a localized region, i.e. the uniform stress state vanishes after the neck. The material behavior up to the onset of necking has been determined by different constitutive models, but a good knowledge of the material behavior after necking has not been fully addressed yet. Knowing the material behavior after neck is essential for performing an accurate FE modeling of metal forming processes (Cooreman et al., 2007). A few studies (Bohme et al., 1992; Bridgman, 1952; Ling, 1996; Mirone, 2004; Zhang et al., 1999) on analytical and FE modeling of material behavior after onset of instability have been reported. Hence, most of the previous investigations have employed experimental or FE modeling approaches for round specimens, while in the THF, the mechanical properties of sheet is necessarily for FE modeling (Saboori et al., 2012a).

The correct prediction of possible damage and failures in the reliable numerical simulation of THF is of most significant. Although FE model to predict the deformation behavior of THF before failure are increasingly available, reliable prediction of failure remains still open. In order to effectively design and manufacture a hydroformed aerospace part, it is critical that a reliable failure criterion be used in this process. To evaluate the forming severity of THF process studies have been performed on two main important failures; (i) necking and (ii) ductile fracture. However, in practical cases, the necking criterion may not predict the forming limit in a wide range of hydroforming process. Especially, in some materials, such as austenitic stainless and high strength steel alloys where strain hardening constants are greater than 0.4 ductile fracture is more common mode than necking since these alloys fail with negligible thickness reduction ((Bressan and Williams, 1983) (Korhonen and Manninen, 2008); Lou et al. 2012) . Moreover, onset of the necking take place in tension while ductile fracture is observed not only in tension but also in shear and compression (Lou et al., 2012); (Lou and Huh, 2012). Various ductile fracture criteria have been studied to gain the onset of fracture, (Lei, Kang and Kang, 2001). as well as (Lei, Kim and Kang, 2002) developed ductile fracture criterions (DFCs) to predict the forming limit of simple stamping part. A DFC at various stress triaxialities was presented by (Michael et al., 2008) to study the effect of stress triaxiality on the onset and evolution of damage inductile metals. (Farzin et al., 2006) as well as (Yu et al., 2007) investigated the effects of various damage criterions on the blanking parameters. Bao and Wierzbicki (Bai and Wierzbicki, 2010; Bao and Wierzbicki, 2004), Ko (Ko et al., 2007), Lou (Lou et al., 2012), and Lou and Huh (Lou and Huh, 2012) developed different phenomenological damage models based on nucleation, growth and coalescence of microscopic voids.

Many researchers (Han and Kim, 2003); (Ozturk and Lee, 2004); (Liu et al., 2009); (Chen, Zhou and Chen, 2010); (Lou et al., 2012); (Lou and Huh, 2013) verified the applicability of the phenomenological damage models to predict the formability of sheet metals. Although many studies of ductile fracture have already been undertaken, these are not applicable to estimate bursting failure in THF and all attempts involved with bursting failure in hydroforming process are based on experiment and few basic criteria ductile damage models, (Lei, Kim and Kang, 2002); (Kim et al., 2004b);(Song et al., 2005); Saboori et al., 2011).

## Research objectives

The goal of this research project is to propose new strategies for understating and modeling material behavior of THF process for aerospace materials. The ultimate goal of this work is to implement the new formability and failure study in a real hydroformed part/ multistage hydroforming process.

The specific research objectives can be summarized as follows:

1. To investigate and validate the formability/mechanical response of aerospace alloys before the onset of necking by using new combined experimental-analytical free expansion process.
2. To study and validate the flow behavior of aerospace alloy after the onset of the instability.
3. To suggest and validate a new damage model to study of failure and forming limit diagram at fracture for FE modeling of THF process of aerospace alloys.

## Structure of thesis

This thesis comprises 5 chapters. It starts with an introduction, followed by chapter one on literature review, three other chapters on various research tasks, and a chapter on summary of the work presented, which links the outcomes of each chapter to proposed research objectives.

The thesis is organized as follows:

**Chapter 1** a literature review concerning tube hydroforming process, formability and bursting failure are presented. An overview of failure methods is presented, followed by a conclusion of the literature review.

**Chapter 2** presents the first goal of this research. A set of analytical and experimental works to understand the hydroformability of austenitic stainless steel types 321 (SS 321), 304L (SS 304L), Inconel alloy 718 (IN 718) and aluminum alloy 6061 (Al 6061) in the annealed “0’’ temper condition (AA 6061-0) is presented. Detailed stress-strain behavior of the material during free expansion is carried out for selected aerospace alloys.

**Chapter 3** presents the second goal of this research. A set of analytical, experimental and FE analysis works is carried out to understand the true stress-strain curve for post-necking regime of different aerospace alloys, such as SS 321, IN 718 and Titanium (Ti6Al4V). A new hardening model is also adopted and validated to predict the material behavior after onset of necking.

**Chapter 4** presents a new decoupled damage model for THF process of ductile materials based on the effect of the stress thriaxiality and the concentration factor. A new user material is also developed and implemented in 3D commercial finite element software, Ls-Dyna.

**Chapter 5** presents damage prediction in two real THF processes based on the new decoupled damage model that is developed in chapter 4.

**Chapter 6** presents a summary of research work presented in chapters 2-5. It links the outcomes of this work and the previous studies, and helps clarifying certain aspects and shortcomings that were identified in the problematic and research objectives.
Finally, some concluding remarks and recommendations will be presented.

# CHAPTER 1

# LITERATURE REVIEW

Tube hydroforming (THF) is among the most advanced metal forming process. The application of THF in the aerospace industries is relatively new and substantially needs more study and knowledge compared to that of automobile alloys. Therefore, there is a growing need for generating databases for aerospace alloys. This chapter presents an overview of major various aspects of THF. When proper conditions such as mechanical properties, material behavior and failure behavior are used, the feasibility and the design steps of this forming process for any aerospace application will be acquired. First, the design parameters and process condition that affect the forming process is presented. After that, the failure modes that usually occur during the process and the technique to predict and avoid these failure modes are discussed.

## Introduction

THF is a forming process in which by applying controlled pressure and axial feed. The shape of the tube material is changed to the desired shape applications of THF can be found in the automotive, the aircraft industries (Ahmetoglu et al., 2000). Figure 1.1 shows some typical hydroformed parts.

The main components and key issues of a complete THF system (Figure 1.2) can be listed as follows:

A. Quality and properties of incoming tube materials.

B. Preforming design.

C. Die and tool design guidelines.

D. Interface issues between die and workpiece: wear and friction.

E. Mechanics of the different deformation zones.

F. Equipment, press and environment related issues.

G. Specifications and requirement of the hydroformed part.

Figure 1.1: Typical hydroformed parts (Hartl, 2005).

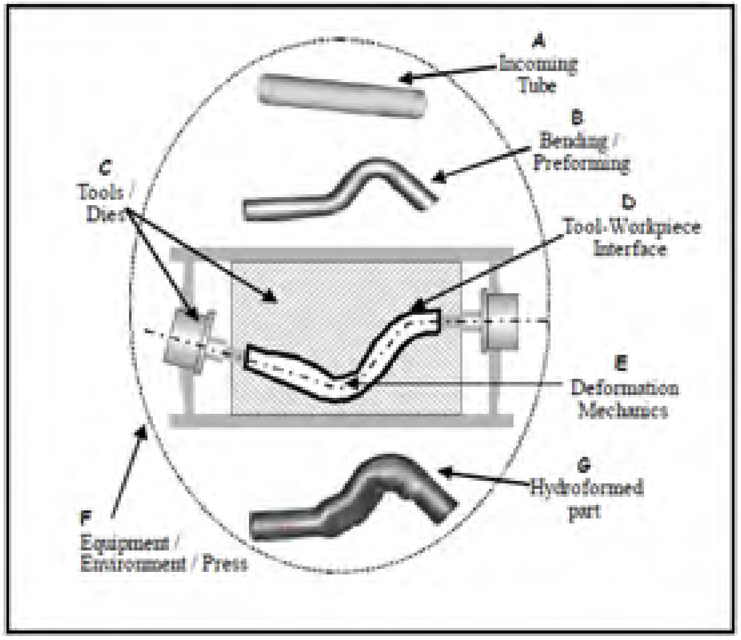

Figure 1.2: The tube hydroforming system
(Strano et al., 2004).

Use of hydrostatic pressure in metal forming processes, in particular, for bulging of tubular parts was first reported in the late 1960s (FUCHS, 1966; Ogura, 1970). In 1970s, research on different aspects of bulge forming continued both experimentally and theoretically, new shapes, materials, different tooling configurations and new machine concepts were introduced by various authors, whereas the fundamentals remained the same. Starting from 1980s, researchers in Japan concentrated on determining the material properties and their effects on tube bulging operations (Hashmi and Crampton, 1985). The process started to spread industrially in the late eighties, and a lot of work was conducted, based on the previous theoretical studies, along with real and new industrial applications of this technology (Dohmann and Hartl, 1997). Some of the advantages of the THF in comparison with conventional stamping technology are: part consolidation, weight reduction, higher part quality, fewer secondary operations, reduced dimensional variations, reduced scrap, less springback, and improved structural strength and stiffness. But this process has also some drawbacks, such as slow cycle time, expensive equipment and lack of extensive knowledge base for process and tool design (Ahmetoglu et al., 2000; Jirathearanat, Hartl and Altan, 2004). In order to increase the implementation of this technology in the stamping industry, some issues need to be addressed: the preparation of the tubes (material selection and quality of the incoming tube), pre-form design and production method, application of computer simulations, selection of effective lubricants and enhancement of the tribological performance, and improvement of the formability of the tube.

## Classification of tube hydroformed part

Nowadays, Hydroformed tubular parts vary over a wide range of shapes and materials. This variety goes from a simple bulged tube to complex shape such as an engine cradle with multiple part features. It is necessary to classify the THF parts into different categories with respect to characteristics that they have in order to manage the design process more efficiently. Mainly, as shown in Figure 1.3 THF parts have the following common features on them (Koc and Altan, 1998).

**Bend:** a tube is bent in order to obtain a designed spline geometry that accommodates alignment of the tube in the THF die cavity.

**Crushing:** a crushed shape is given into a tube in the pre-forming stage not only to facilitate the tube alignment into the die but also to accumulate the tube material locally for the subsequence expansion process. Crushed geometries are found frequently in automotive structural parts.

**Bulge:** bulges are typically tube expansions, mostly axisymmetric about the tube axis.

**Protrusion:** protrusions are local expansions, stemmed out from the tube axis. They are normally manufactured as connectors, i.e. T-shapes and Y-shapes, used particularly in exhaust manifolds.

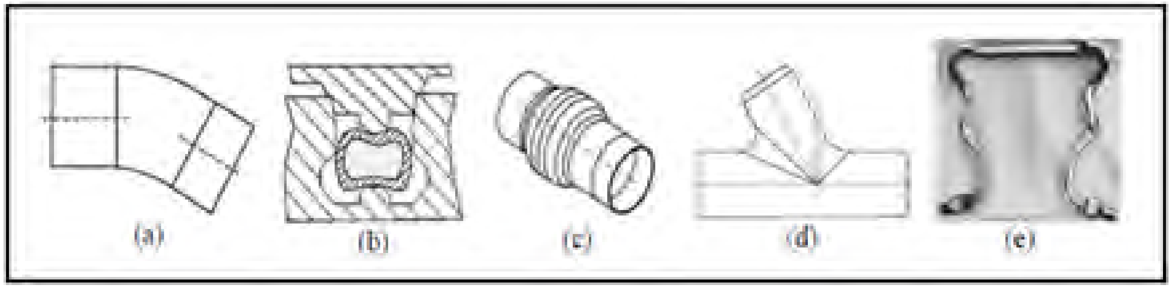

Figure 1.3: Tube hydroformed part features (a) bent feature, (b) crushed feature, (c) bulge feature, (d) protrusion feature (referred as Y-shape), and (e) automotive hydroformed structural part (SPS, Germany).

## Tube hydroforming process parameters

### 1.1.1 Tube material

The process variables introduced by the tube material are:

1) Mechanical properties: chemical composition, yield strength, ultimate tensile strength, percent elongation and flow characteristics.

2) Dimensions: tube diameter and wall thickness of the tube.

3) Quality of the raw tube and method of preparation of the tube, which can be welded or seamless.

All these variables are critical for the success of the THF process and must be determined based on the final part requirements (Ahmetoglu and Altan, 2000; Ahmetoglu et al., 2000; Carleer et al., 2000). There are several tests used in industry to determine the material properties. The most widely used test are:

#### 1.1.1.1 The tensile test Tube material

One of the simplest methods to measure the formability of tube is to carry out tensile tests on specimens taken from the tube or sheet. The stress–strain curve and the mechanical properties (yield stress, tensile stress, strain hardening exponent, anisotropy can be determined. It is common to take sample specimens at certain positions around the tube such as 90°, 180° and 270° from the weld seam. Figure 1.4 shows tensile specimens generally machined according to the ASTM standard.

In conclusion, the flow stress of the tube specimen is most likely to be different from that of the sheet specimen from which the tube was manufactured (Saboori et al., 2014a; Saboori et al., 2012b)

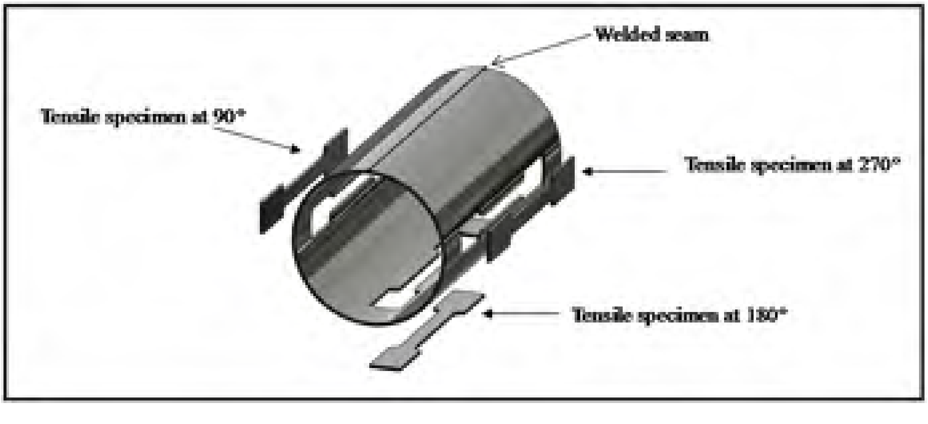

Figure 1.4: Schematic to show how tensile specimens are taken from a tube (Saboori et al., 2014a).

#### 1.1.1.2 The tube bulge test

In order to obtain reliable data on material properties of the tube, a test procedure should be used, that is as close as possible to the hydroforming process. Although the results of the tensile test can provide information about the stress-strain relationship and anisotropy parameters, they can hardly be used to evaluate formability of tubes for hydroforming, since the tensile test induces a uniaxial state of stress, while the THF process is mainly biaxial. In other words, a test generating a biaxial tensile stress state in the sample (such as a bulging test) would be closer to the real process conditions and this would insure a much more effective evaluation of formability (Hwang, Lin and Altan, 2007; Koç, Aue-u-lan and Altan, 2001; Saboori et al., 2014a).

Table 1.1 shows a comparison of two commonly tests used. The biaxial bulge test is increasingly being applied by the European automotive industry for obtaining sheet material flow stress data for process simulation. The principle of the bulge test is very simple: a metal tubular specimen is loaded with internal pressure (usually hydraulic) and expands, undergoing plastic deformation until bursting occurs. By measuring the internal pressure and the tube deformation at the crown of the tube, much information on its mechanical properties can be attained.

Koç, (Koç, Aue-u-lan and Altan, 2001) and Sokolowski (Sokolowski et al., 2000) determined stress-strain relations behavior based on isotropic assumption. Hwang (Hwang and Lin, 2002), Manabe (Manabe and Amino, 2002) studed the influence of different parameters on formability. The parameters that were studies included strain hardening coefficient (n), anisotropy parameter (r), initial thickness and length of the tube. In their study they found that n and r have impact on the shape of the bulged tube and on the strain distribution. Higher values for r and n result in more evenly distributed strain and will favour larger deformations.

Table 1.1: Advantages of biaxial test over uniaxial test (Yadav, 2008).

| | Tensile test | Hydraulic bulge test |
|---|---|---|
| 1. State of stress | Does not very close to stress conditions in production. | Closer to biaxial stresses seen in production. |
| 2. Flow stress data | Flow stress data collection is limited by local necking of tensile specimen. For FE modeling, flow stress data is extrapolated to large strains. | Flow stress data is obtained for up to twice the strain range in tensile test. Thus, no extrapolation is needed in FE modeling. |
| 3. Formability | 'n' values or strain-hardening exponent of the material (for materials that follow power law fit $\overline{\sigma} = k\overline{\epsilon}^n$) is used as a measure of material formability. | Dome height/ bulge height at burst is a good measure of formability. This test is a quick-and-easy check on incoming sheet/tube quality. |

### 1.1.2 Loading path

The formability of THF is not influenced only by the mechanical properties of the tube material, but also by the loading path and the tube size (Kang, Kim and Kang, 2005). An improper loading path condition will lead to failure. The most common modes of failure in THF are: bursting due to formation of a localized necking which leads to fracture, and wrinkling due to local buckling.

The axial feeding has to be coordinated with the internal pressure. If the internal pressure is applied with a high rate or rapidly and the axial feeding slowly, the process will fail, because there is not enough material to flow into the die cavities. However, if the internal pressure is applied slowly and the axial feeding rapidly, there will be wrinkling or bulking on the tube (Jansson, Nilsson and Simonsson, 2008; Yuan et al., 2007). The optimum loading path (internal pressure and the axial feed) is very difficult to achieve via experiments. Therefore, finite element analysis is used to verify and optimize the initial design step before the real hard tooling is built.

The loading path for round to Square and round to v shape s was investigated through finite element simulations (Mojarad Farimani, 2013). The purpose of these simulations was to study the effect of the axial feed on thickness variation and internal pressure. The authors demonstrated that the forming process is very sensitive to the axial feeding. The results indicated a decrease in the thinning of the tube wall when the axial feeding distance was increased.

### 1.1.3 Tribological aspects in tube hydroforming

The frictional conditions have a significant influence on the THF process. Due to high contact pressures and large contact surfaces, high friction forces between the tube and the die will result. These forces will affect not only the process parameters but also the quality of the component, such as the wall-thickness distribution. Therefore, decreasing the friction and its negative influence in THF is very important (Ngaile et al., 2006; Plancak, Vollertsen and Woitschig, 2005; Vollertsen and Plancak, 2002). Their conclusion was that during the forming process, the surface micro geometry will change continuously and therefore the friction conditions will also be changed. Lubricant, material properties (yield strength), surface texture and the die surface finish, die hardness and die surface treatment, and coating are the main parameters that affect the friction condition in THF. The lubricant trapped between the asperities on the tube and die surfaces may provide better lubrication at the interface due to the potential for hydrostatic lubrication. Figure 1.5 presents the THF for T-shape. From the friction point of view it is possible to identify three different zones: guided, transition and expansion zones. Due to the difference in the material flow and the state of stress, these three zones exhibit different tribological conditions (Koç, 2003; Ngaile, Jaeger and Altan, 2004). Therefore the lubricants can perform differently, these zones have to be evaluated separately to determine the friction characteristics.

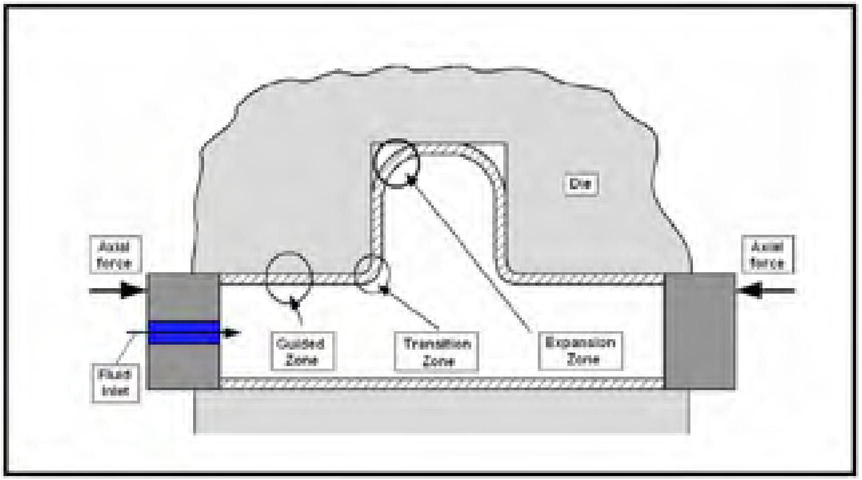

Figure 1.5: Friction zones in tube hydroforming
(Ngaile et al., 2006).

### 1.1.4 Formability in sheet and tube metal forming

The sheet or tube metal formability is a measure of its ability to deform plastically during forming processes in order to produce a part with definite requirements on mechanics, dimension and appearance, being mainly limited by the occurrence of flow localization or instability. Formability strong dependence on both the constitutive properties of the sheet metal and the factors involved in a practical forming operation turned the correct choice of these parameters to be one of the main aims in modern industry. A good understanding of the deformation processes of the plastic flow localization and of the factors limiting the forming of the tube or sheet metal in of key importance in monitoring the formability issue (Xu, 2006).

In THF, the instability modes are wrinkling, buckling and necking or bursting load (Chu and Xu, 2004; 2008; Kim et al., 2004a; 2005; Koc and Altan, 2002; Nefussi and Combescure, 2002), these instability shown schematically in Figure 1.6. Wrinkling and buckling occurs when the axial feeding (compressive stress) exceeds the strength of the material and the internal pressure is not high enough to produce expansion. Buckling is observed mostly in long tubes with thick walls, and wrinkling in short tubes with thin walls with high end feeding condition. Bursting is a consequence of necking, which is due to large tensile stresses, when the plastic deformation reached a point at which the deformation will continue under a falling pressure.

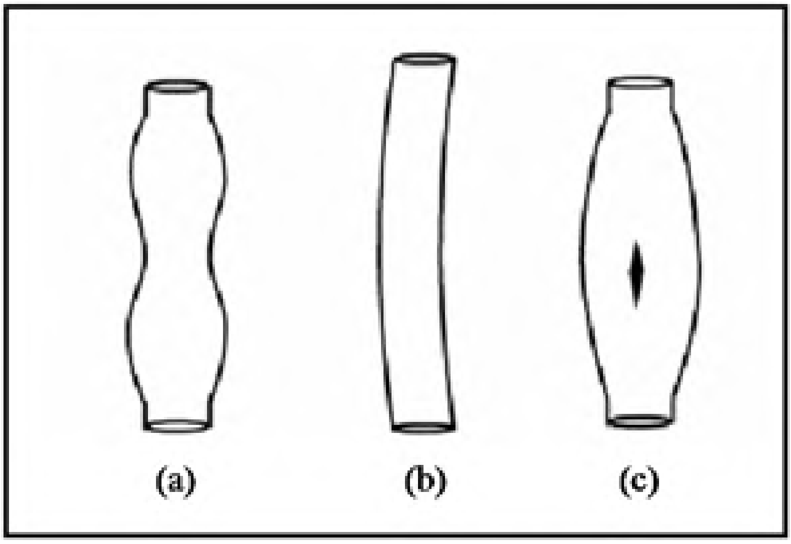

Figure 1.6: Failure modes in tube hydroforming:
(a) wrinkling, (b) buckling, and (c) bursting
(Koc and Altan, 2002).

### Formability in hydroforming

It has been a well known fact that material and some external parameters are important factors that affect formability in hydroforming. Most of the studies in the literature will be presented next.

### 1.1.5 Strain hardening

Strain hardening or work hardening is the ability of materials to strengthen or harden with increasing strain level (Wagoner and Chenot, 1997). It is one of the most important properties influencing the formability of THF (Dohmann and Hartl, 1997; Manabe and Amino, 2002). When a material is cold worked, its strength and hardness increase because of strain hardening. However, a consequence of that is also reducing of the remaining ductility. During metal forming (plastic deformation), a region undergoing thinning can resist further deformation because of strain hardening and can spread deformation to its neighboring regions, thus further deformation case uniform thinning. The parameter reflecting this behavior is strain hardening index, $n = d(ln\sigma)/d(ln\epsilon)$ the uniform elongation (strain on the material until a neck forms) is mostly controlled by n. Thus a high n delays the onset of necking and improves formability. According to Considèred criterion, the end of uniform elongation occurs when the true work-hardening rate, equals the true strain (Chow and Yang, 2002; Saboori et al., 2012b). In order to obtain hydroformed parts with uniform wall thickness, the greater the strain-hardening of a tube, the better it performs in processes where there is considerable stretching as the straining will be more uniformly distributed and the tube will resist bursting (Manabe and Amino, 2002).

### 1.1.6 Anisotropy

Anisotropy in sheet and tube metal forming is the variation in its plastic behavior with orientation. It can be expressed by the normal anisotropy coefficient, $R = \frac{\epsilon_w}{\epsilon_t}$. Thus it is the ratio of plastic strain in the width direction to that in the thickness direction in the specimen (Zribi, Khalfallah and BelHadjSalah, 2013). The difference in properties for a tube aligned with the rolling, transverse ($45^o$) directions is referred to as planer anisotropy. If R is greater than unity, it indicates that the material has a high thinning resistance due to greater strength in the through-thickness direction. It also mean high strength in biaxial tension, while a low R-value indicates easy thinning and hence a low biaxial strength. In sheet metal forming, a high value of R allows deeper parts to be drawn and higher value reduces wrinkling (Manabe and Amino, 2002; Zribi, Khalfallah and BelHadjSalah, 2013).

### 1.1.7 Damage accumulation

The damage of materials is the progressive physical process by which they break. the mechanics of damage is the study of the following mechanisms when materials are subjected to loading (Lemaitre and Lippmann, 1996):

a) The accumulation of micro stresses in the neighborhood of defects or interfaces and the breaking of bonds, which both damage the material at the microscale level.

b) The growth and the coalescence of micro cracks or micro voids which together initiate one crack.

c) The growth of that crack at the macro scale level.

The first two stages may be studied by means of damage variables of the mechanics of continuous media. The third stage is usually studied using fracture mechanics.

Damage criteria can be divided into two:

a) Empirical and Semiempirical models and the damage criteria using theoretical void coalescence and growth (decoupled model).

This model taking into account a variable extern which predicts the damage when a critical value is reached (The damage calculated does not interact on the mechanical characteristics of the material).

b) Coupled model.

This model reports the decline of mechanical properties due to the development of the damage.

#### 1.1.7.1 Damage Criteria using Empirical and Semiempirical Models

Most ductile fractures are usually based on combinations of stress with strain or strain rate, rather than on either of these quantities separately.

All the integrated stress–strain criteria based on empirical and semiempirical approach are versions of Freudenthal’s critical plastic work per unit of volume,

$$\int_0^{\bar{\varepsilon}_f} \bar{\sigma}\overline{d\varepsilon} = C_i \tag{1.1}$$

where $\bar{\sigma}$ is the effective stress, $\overline{d\varepsilon}$ is effective strain increment and $\bar{\varepsilon}_f$ is the effective strain at fracture. $C_i$ , where i :1,2,... are critical damage values.

Cockcroft and Latham have suggested an alternative fracture criterion based on maximum principal stress (Cockcroft and Latham, 1968).

$$\int_0^{\bar{\varepsilon}_f} \sigma_1\overline{d\varepsilon} = C_1 \tag{1.2}$$

where $\sigma_1$ is the largest principal stress.

The normalized version of this criterion can be written as (Oh, Chen and Kobayashi, 1979a):

$$\int_0^{\bar{\varepsilon}_f} \frac{\sigma_1}{\bar{\sigma}}\,\overline{d\varepsilon} = C_3 \tag{1.3}$$

Explicit dependence on the level of both the largest (tensile) principal stress, $\sigma_1$, and the hydrostatic stress $\sigma_m$, was proposed by Brozzo by means of an empirical modification of the above-mentioned criterion (Brozzo, Deluca and Rendina, 1972):

$$\int_0^{\bar{\varepsilon}_f} \frac{2\sigma_1}{3(\sigma_1 - \sigma_m)}\,\overline{d\varepsilon} = C_4 \tag{1.4}$$

#### 1.1.7.2 Damage criteria using theoretical void coalescence and growth-decoupled damage

Metals are organized in crystals/ grains, a regular array of atoms except on many lines of dislocations where atoms are missing. If a shear stress is applied to the metallic materials, the dislocations may move by the displacement of bonds, thus a plastic strain created by slipping.

Debonding is the first stage in the beginning of the damage process. If the dislocation is stopped by a micro defect concentration, it creates a constrained zone in which another dislocation may be stopped. This process occurs with debonding, where several arrests of dislocations nucleate a micro crack (Lemaitre and Lippmann, 1996).

Elasticity is one of the material properties that is directly influenced by the damage, since the number of atomic bonds responsible for elasticity decreases with damage. Plasticity is directly related to slips. In metals, slips occur by movement of dislocations. Damage influences plastic strains because the decrease in the elementary area of resistance, resulting from the decrease in the number of bonds, increases the effective stress.

Kachanov (Kachanov, 1986) explained the 'one-dimensional surface damage variable' by considering a damaged body and a representative volume element (RVE) at a point *M* oriented by a plane defined by its normal $\vec{n}$ and its abscissa *x* along the direction $\vec{n}$ (see Figure 1.7)

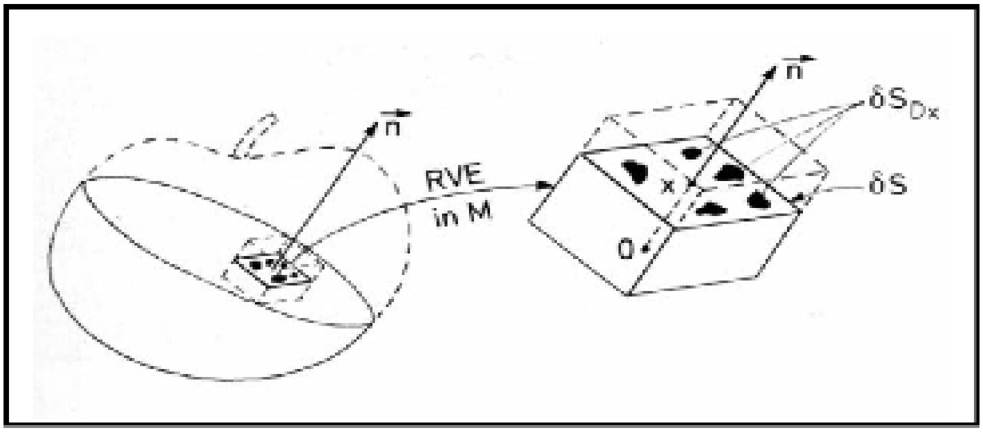

Figure 1.7: Damaged RVE in a damaged body (Lemaitre, 1996).

The value of the damage *D (M,* $\vec{n}$*,x)* attached to the point M in the direction $\vec{n}$ and the abscissa *x* is:

$$D\ (M, \vec{n}, x) = \frac{\delta S_{Dx}}{\delta S} \tag{1.5}$$

where, $\delta S_{Dx}$ is the area of intersection of all the flaws with the plane defined by the normal $\vec{n}$ and abscissa $x$; $\delta S$ is the total area at the intersection plane.

For a simple one-dimensional case of homogeneous damage distribution of Figure 1.8, simple definition of damage as the effective surface density of microdefects is:

$$D = \frac{S_D}{S} \tag{1.6}$$

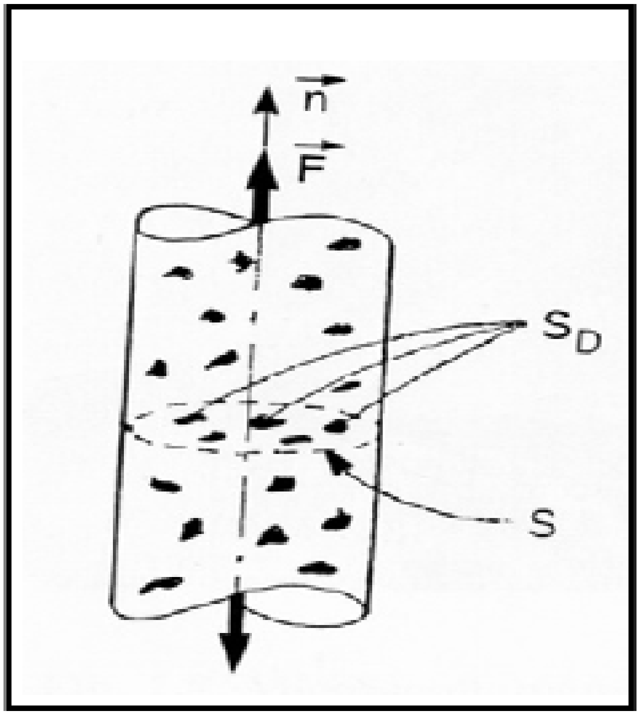

Figure 1.8: Damaged RVE in a
damaged body (Lemaitre and Lippmann, 1996).

Damage D is bounded as:

$$0 \leq D \leq 1 \tag{1.7}$$

where $D = 0$ represents the undamaged RVE material and $D = 1$ represents fully broken RVE material in two parts. In fact, the failure occurs for $D < 1$ through a process of instability, which suddenly induces the decohesion of atoms in the remaining resisting area. This rupture corresponds to a critical value of damage $D_c$, which depends upon the material and the conditions of loading:

$$0 \leq D \leq D_c \tag{1.8}$$

The most important methods to measure damage are classified as follows:

a) Direct measurements: This is done by observing microcrack pictures.

b) Variation of the elasticity modulus: This is an indirect measurement based on the influence of damage on elasticity:

$$\varepsilon_{eq} = \frac{\sigma}{E(1-D)} \tag{1.9}$$

This method requires accurate strain measurements. Strain gauges are commonly used and $\bar{E}$ is most accurately measured during unloading. If $\bar{E} = E(1-D)$ is considered as the effective elasticity modulus of the damaged material, the value of damage may be derived as:

$$D = 1 - \frac{\bar{E}}{E} \tag{1.10}$$

c) Variation of the microhardness: This is an indirect measurement based on the influence of damage on plasticity.

Rabotnov introduced the effective stress concept in 1968 as follows (Kachanov, 1986): If the RVE of Figure 1.8 is loaded by a force $\vec{F} = F\vec{n}$, the effective stress is:

$$\bar{\sigma} = \frac{F}{S} \tag{1.11}$$

If all microcracks or microcavities are represented by $S_D$ , it is convenient to introduce a definition for effective stress in tension state, $\overline{\sigma}_t$ related to the surface that effectively resists the load:

$$\bar{\sigma} = \frac{F}{S - S_D} \tag{1.12}$$

Introducing the damage variable, $\frac{S_D}{S}$, :

$$\bar{\sigma} = \frac{F}{(1 - D)} \tag{1.13}$$

The fracture of ductile solids has been observed to result from the large growth and coalescence of microscopic voids. This dependence guided McClintock to assume that fracture is reached when the spacing between voids in a material reaches a critical value. The fracture criterion derived from this assumption can be written as follows (McClintock, 1968):

$$\int \left[ \frac{\sqrt{3}}{2(n-1)} sinh \left\{ \frac{\sqrt{3}(1-n)}{2} \frac{\sigma_a - \sigma_b}{\bar{\sigma}} \right\} + \frac{3}{4} \frac{\sigma_a - \sigma_b}{\bar{\sigma}} \right] d\bar{\varepsilon} = C_6 \tag{1.14}$$

where the symbol n represents the strain-hardening coefficient of the Ludwik, Holomon, Voce or etc stress–strain relationship and $\sigma_a$ , $\sigma_b$ are the principal stresses in the direction of the greatest and smallest void deformation.

Most decoupled criterion were used for extrusion and forging (bulk forming), more recently (Chen, Zhou and Chen, 2010; Han and Kim, 2003; Korhonen and Manninen, 2008; Liu et al., 2009; Ozturk and Lee, 2007) developed these models for sheet forming and in some models they consider strain path, shear stress and etc.

#### 1.1.7.3 Coupled damage

Ductile fracture is a mode of material failure in which voids, either already existing within the material or nucleated during deformation, grow until they link together, or coalesce, to form a continuous fracture path. The existence of distributed microscopic voids, cavities, or cracks of the size of crystal grains is referred as material damage, whereas the process of void nucleation, growth and coalescence, which initiates the macro cracks and causes progressive material degradation through strength and stiffness reduction, is called damage evolution. Figure 1.9 and Figure 1.10 shows the stages of damage.

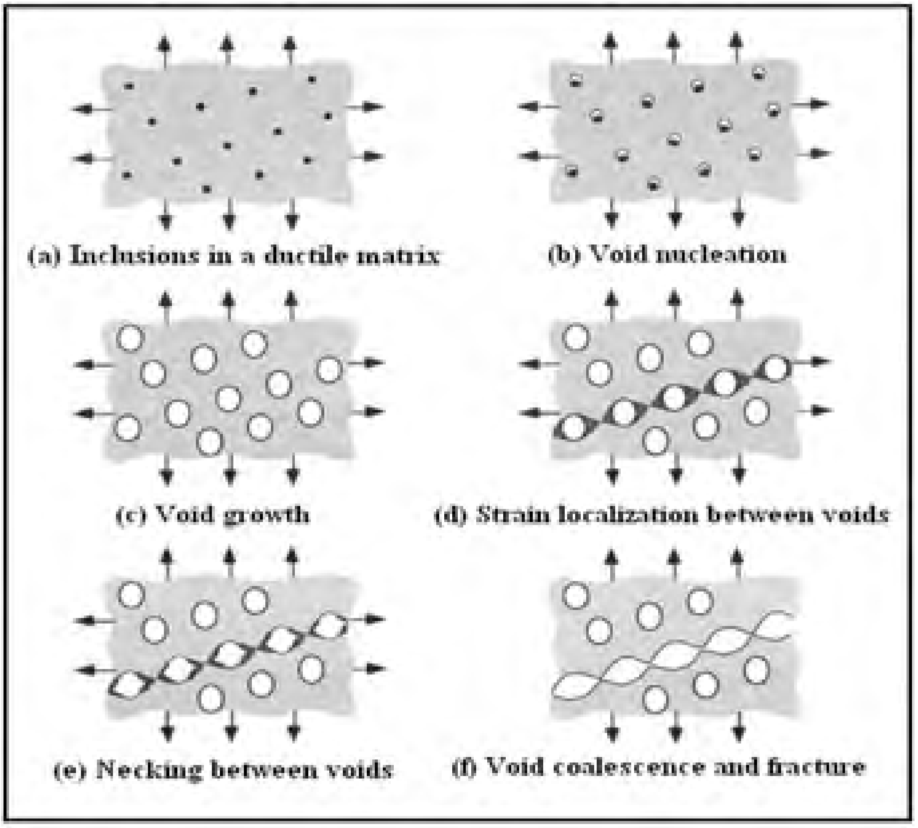

Figure 1.9: Stages in void nucleation, growth and coalescence in ductile metals (Anderson, 2005).

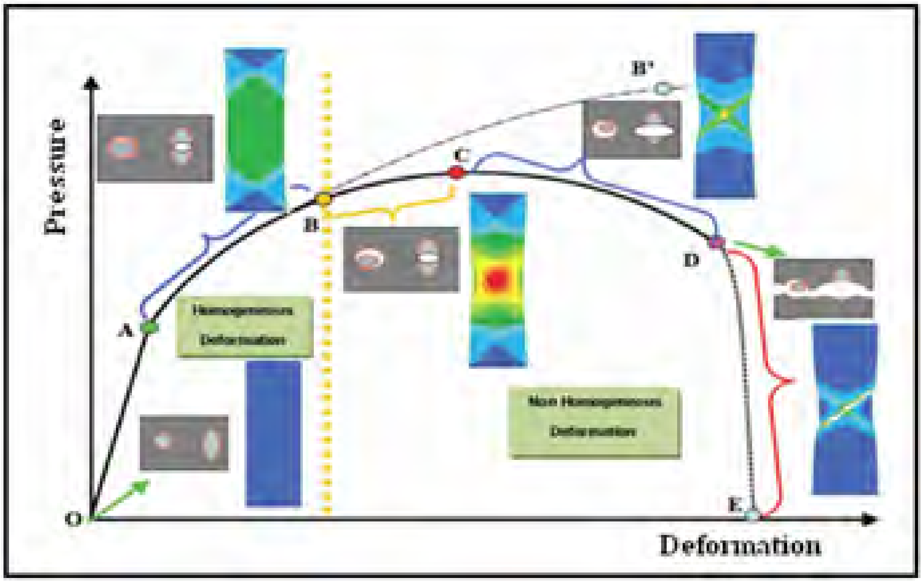

Figure 1.10: Damage stages in a tensile specimen (Mariage, 2003).

In Figure 1.10 deformation decomposed into domains which connect with three stages of the ductile damage:

OA: homogeneous linear elastic deformation of the specimen.

AB: homogeneous plastic deformation of the specimen. In this stage void nucleation with small size could not modify the plastic response.

The curve ABB' is the homogeneous answer of the specimen if no defect developed.

BC: voids grow and their effect begins gradually be effected on the plastic and elastic response of the material. The internal constraints begin to decrease leading to indubitably the acceleration of the fall of the tangent module which reached zero the point *C*. In this stage voids growth and damage behavior cannot be any more neglected.

CD: the mechanism of coalescence of the voids begins in the point *C*, with the beginning of the localized plasticity. In fact the distance between voids is small, therefore, localization of the plastic flow occurs, this leads to the breaking of these bonds by instability plastic so connecting between them to cause a macroscopic crack in *D*.

OE: this stage corresponds to the distribution of the macroscopic crack leading to final break of sample.

Figure 1.11 gives some micro graph depicting the phenomenon of damage on micro scale.

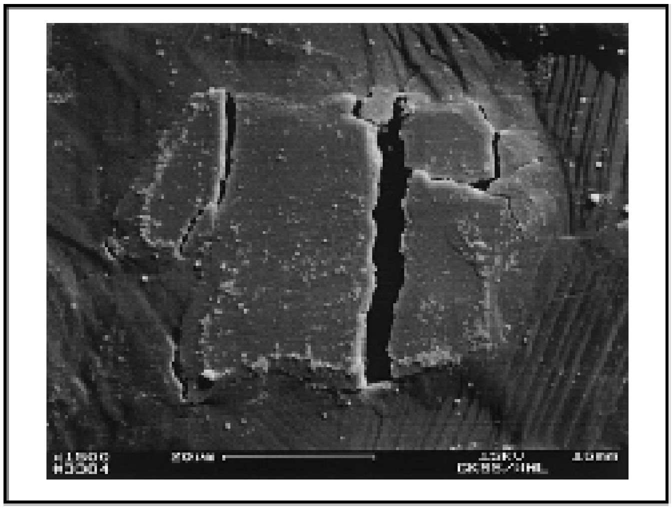

Figure 1.11: CrackedAl3Ti-particlein a tensile test specimen (Gänser, Werner and Fischer, 1998).

Micro mechanics of damage can be divided into three phenomena: void nucleation, void growth and void coalescence.

### a) Void Nucleation

It is well established at low temperatures plasticity dominates the phenomenon of nucleation and growth (Goods and Brown, 1979). At room temperature the cavities are nucleated either by second phase cracking or second phase debonding from matrix material (with the exception of titanium alloy), whereas in the case of creep (elevated temperatures), cavities can be nucleated at the grain boundaries as well (Goods and Brown, 1979).

Even if the material contains only one type of second-phase particle, void initiation will not occur simultaneously at all of the particles. Typically voids nucleate at the larger particles first. As the fracture process continues, voids nucleated at the larger particles grow while voids are nucleated at the smaller particles. The process becomes even more complicated for materials that contain several types of second-phase particles. In these materials, voids will often nucleate first at a particular particle type, and then in the fracture process at another set of particles.

It is often the case that some of the particles may never initiate voids at all, but may affect the fracture process only indirectly by in fluencing the flow characteristics of the matrix (Needleman, 1987).

### b) Void Growth

McClintock is the pioneer in modeling void growth for rigid non-hardening and linear hardening materials. McClintock obtained equations for growth of cylindrical voids under axisymmetric stress. The equations were based on the stress triaxiality. Then he formed equations for moderately hardening materials by interpolating between the two extremes (McClintock, 1963; 1968). Perra (Perra and Finnie, 2013) in his experiments on one hand found that the equations formed by McClintock underestimates the void growth and the other hand he confirmed the importance of stress triaxiality on void growth.

### c) Void Coalescence

Void coalescence is the final stage in the failure mode of ductile materials. It consists in the localization of plastic deformation at the micro scale inside the inter void ligament between neighboring voids, with material outside the localization plane usually undergoing elastic unloading. As shown in Figure 1.12, two coalescence mechanisms were reported using model materials (Weck et al., 2008):

i) The necking of the ligaments between voids caused by the highest principal stress.
ii) Shear-linking up of voids along the direction of the maximal shear stress.

These two mechanisms were also observed from the SEM fractographies of upsetting tests, shear tests, tensile tests of smooth and notched round bars (Bao and Wierzbicki, 2004; Li et al., 2011). The necking of the ligaments between voids is referred as dimple-dominant fracture while the linking up of voids is named as shear fracture (Li et al., 2011).

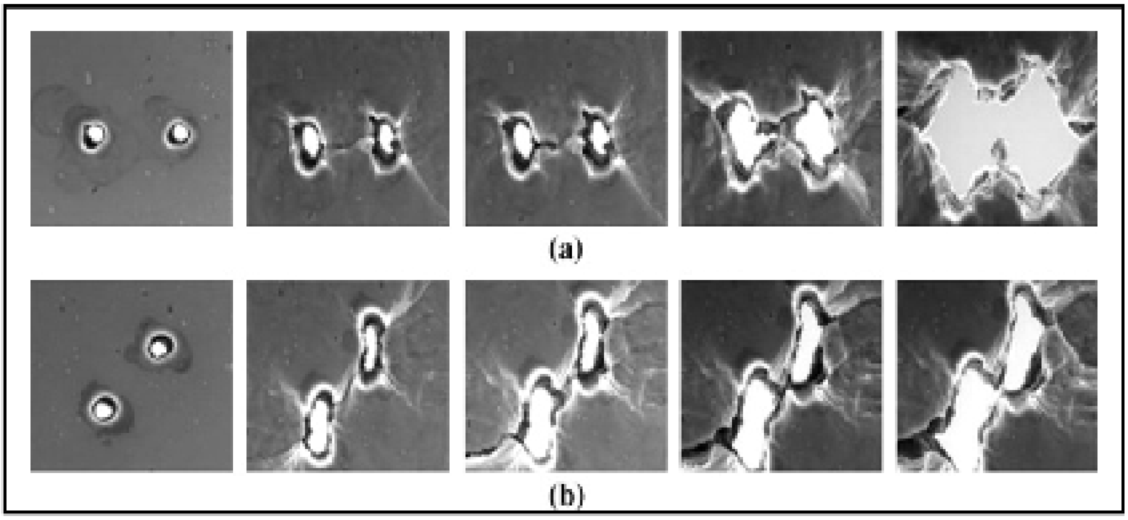

Figure 1.12: Two kinds of mechanisms for coalescence of voids:
(a) necking of inter-void ligaments; (b) shear-linking up of voids
(Weck et al., 2008).

### 1.1.8 Forming limit diagrams

In sheet and tube metal forming operations, the amount of useful deformation is limited by the occurrence of unstable deformation, which mainly takes the form of localized necking, wrinkling and facture or bursting in hydroforming. Failure by wrinkling occurs when the dominant stresses are compressive, tending to cause material thickening. Localized necking occurs when the stress state leads to an increase in the surface area of the sheet while the thickness is reduced and it is a very important phenomenon in determining the amount of useful deformation that can be imposed on a specimen.

The forming limit diagram is a constructive concept for characterizing the formability of sheet or tube metals. It was proved to be an essential tool for material selection, design and try out of the tools for sheet and tube forming operations such as deep drawing and THF. Since the experimental determination of FLDs requires a wide range of sheet or tube forming tests, consequently a large variety of expensive equipment and tremendous experimental effort, have been made to predict the FLDs, taking into account the theory of plasticity, material parameters and instability conditions.

#### 1.1.8.1 Forming limit diagram concept

Stretch forming is a significant component in many sheet metal manufacturing processes. Simultaneously with the progressively thinning of a sheet, two models of plastic instability are possible, a diffuse necking followed by a localized necking.

A study of failure in biaxial stretching of sheets by Keeler and Backofen (Keeler and Backofen, 1963) showed the existence of what is known as forming limit diagrams (FLDs). The main discovery was that the largest principal strain before any localized thinning in a sheet increased as the degree of biaxiality increased. Later, Keeler (Keeler, 1965) found the material properties have great effect on the strain distribution in biaxial stretching of sheet metal. He point out for higher exponent of the material work hardening, n, the strain distribution will be relatively homogeneous. On the contrary, materials having lower n values develop sharp strain gradients and the deformation concentrates in a very small region, then causing earlier failure. A map in principal strain space $(\varepsilon_1, \varepsilon_2)$, separates safe strain states that a material could provide. By definition, $\varepsilon_1$ is the major principal strain, and $\varepsilon_2$ is the minor principal strain. Therefore, FLDs show the combination of major and minor in-plane principal strains beyond which failure occurs. These strains can be represented as either engineering or true strains. With further development of the experimental techniques by Goodwin (Goodwin, 1968b), a FLD for mild steel was obtained. Figure 1.13 shows the Keeler-Goodwin diagram due of the contribution of both authors to the understanding of material formability.

The FLDs represent a wide range of forming limit strains that are predicted when sheet material is deformed along linear strain paths. These strain paths range from uniaxial tension to plane strain to equi-biaxial tension, as illustrated in Figure 1.14, which shows an example of a theoretical FLD plotted in terms of true strains, rather than engineering strains

(Holmberg, Enquist and Thilderkvist, 2004). These linear strain paths can be described by the ratio of minor true strain($\epsilon_2$) to major true strain($\epsilon_1$) where:
$\beta = \frac{d\epsilon_2}{d\epsilon_1}$ . A path where $-0.5 < \beta < 0$ results in drawing of the sheet material. When $\beta \approx 0$ a condition of plane strain is achieved and when $0 < \beta < 1$ the material is stretched in biaxial tension.

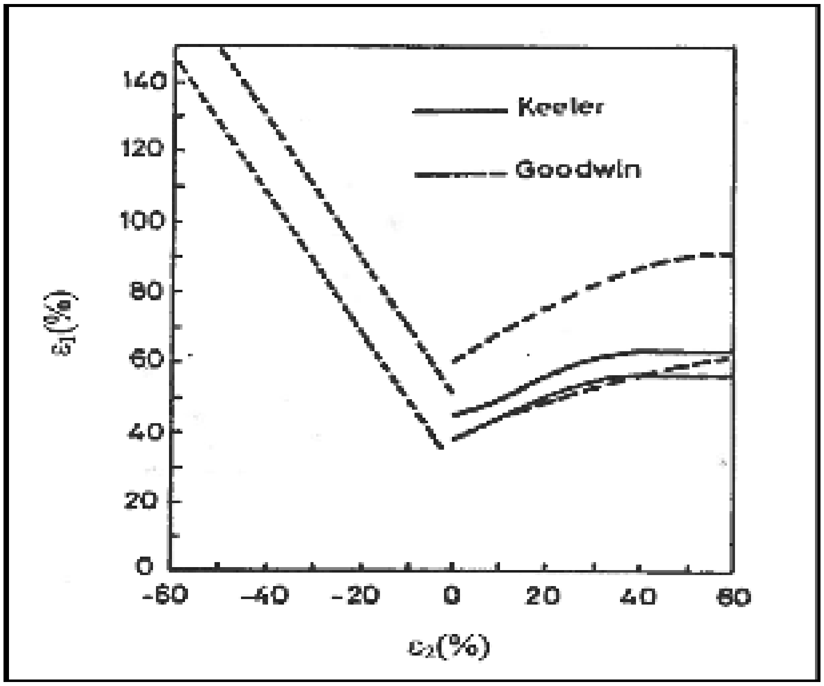

Figure 1.13: Keeler-Goodwin forming limit diagram.

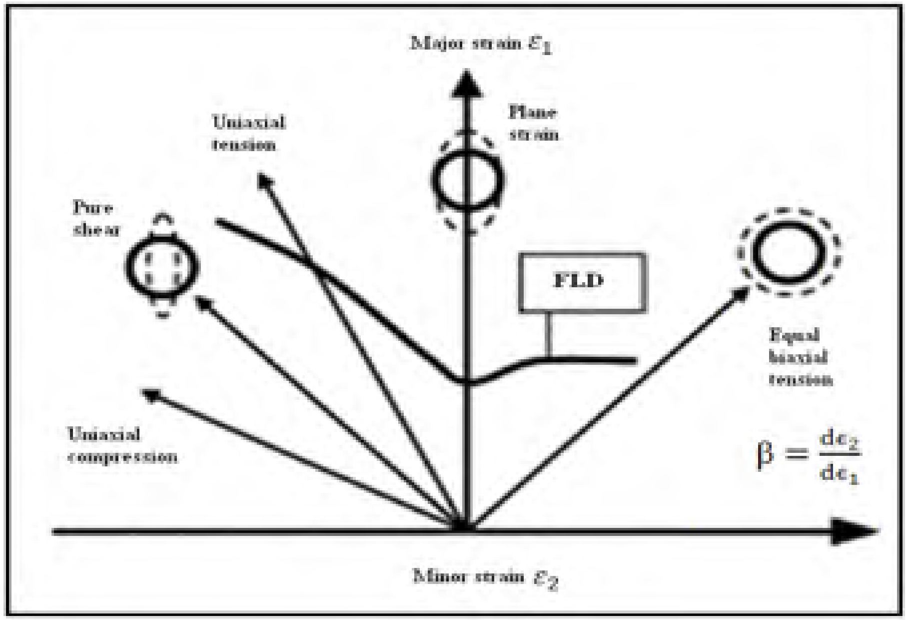

Figure 1.14: A typical Forming Limit Diagrams (FLD)
along with different strain states
(Holmberg, Enquist and Thilderkvist, 2004).

As shown in the figure, the strain combinations below the forming limit curve are considered to be safe while the one above it are considered to be associated with failure.

Although the FLD method has been proven to be a useful tool in the analysis of forming severity, it might not always be accurate in complicated forming operations because of different modes of deformation experienced by the part at different stages of a single forming operation. Even a change in lubrication can affect the path of deformation. It has also been reported that a criterion based on stress, instead of strain is better for evaluating forming limits (Doege and Dröder, 1997). In summary, the sheet and tube metal forming process can be limited by various factors like local necking, tearing, fracture before necking, wrinkling etc. Typically, a forming window (Hu, Marciniak and Duncan, 2002) in which plane stress sheet forming is possible is identified and shown in Figure 1.15.

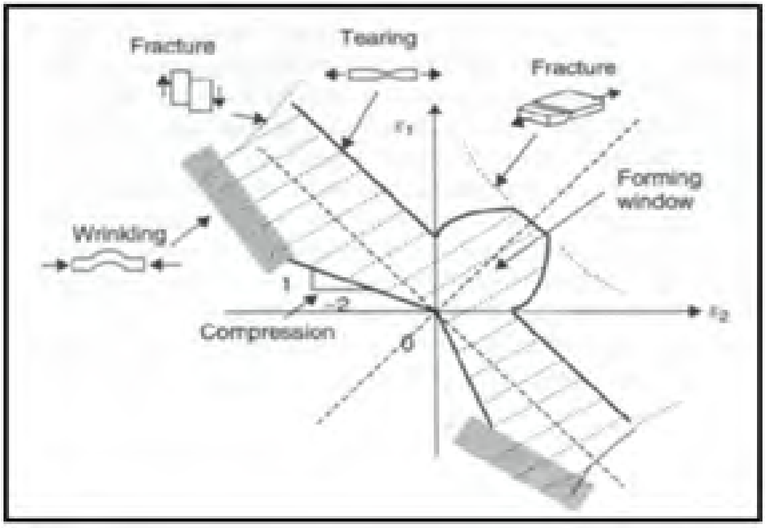

Figure 1.15: The forming window for forming of sheet
(Hu, Marciniak and Duncan, 2002).

For free expansion with end feeding as shown in Figure 1.16, it can see that depending on the relation of pressure and axial feed the final bulge can result in different part quality. Excessive pressure would result in excessive part thinning leading to bursting; excessive axial feed would result in a wrinkled part (dead wrinkle as defined earlier). The bulges in these two extreme cases can be mapped onto the two-dimensional strain space, Figure 1.16.b, as being in the neighborhood of plane strain to balance bi-axial state for the bursting case and pure shear state for the wrinkled.

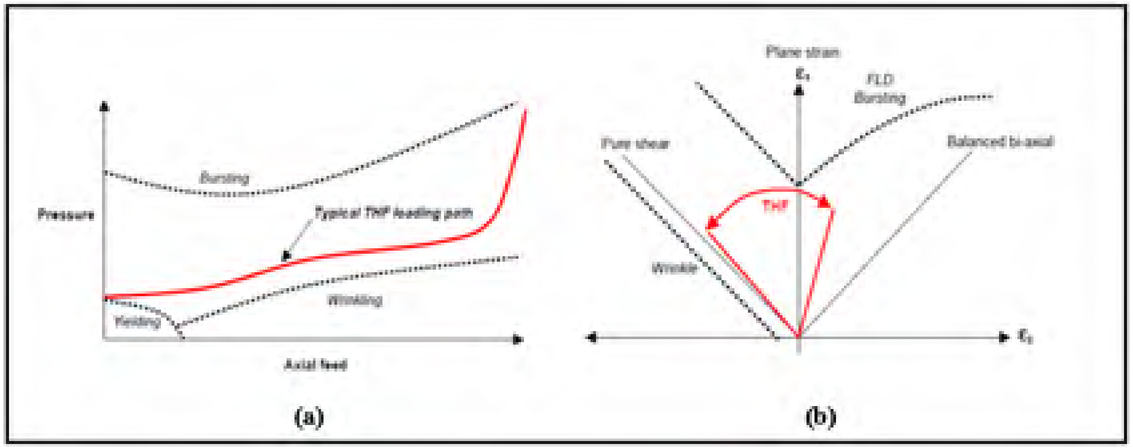

Figure 1.16: (a) Loading path in the THF forming window, (b) in-plane strain plot.

#### 1.1.8.2 Theoretical models for calculation LFD's

Forming limits of tube metals are influenced by several physical factors of which the most important ones are material work-hardening, strain rate sensitivity, plastic anisotropy, the development of structural damage and strain path. It is difficult to experimentally assess the influence of each parameter individually since it is virtually impossible to change only one at a time. The theoretical analysis of plastic instability and flow localization may supply relevant information to prevent the failure on the THF. Therefore, extensive efforts have been devoting to the development mathematical models that capable to predict accurately the plastic flow localization of hydroforming processes.

The first one, which is a linear method for sheet, is based on the plastic instability of homogeneous sheet metals and describes the initiation of localized band of straining in an uniform sheet (Hill, 1952; Stören and Rice, 1975).

The second one, which is a non-linear method, is based on the plastic instability of heterogeneous sheet. It is assumed an initial weakness, imperfection or inhomogeneity in the sheet which gradually develops into a neck as straining proceeds (Marciniak and Kuczyński, 1967).

In the following, a review of the most important theoretical models developed for FLDs at necking (FLDn) predictions are presented.

##### a) Linear analysis

Giving explicit solutions for predicting limit strains, the linear analysis is easy to applied to the actual press shop. Since the 1950's, many studies on linear or bifurcation analysis have been preformed showing useful results through the use of linear analytical methods.

##### i) Swift diffuse necking

In 1952, based on the Considere's analysis, Swift (Swift, 1952) developed a criterion for predicting the onset of diffuse necking with the assumption that plastic instability occurs at a maximum load for proportional loading, calculating the critical major strain for diffuse necking as:

$$\varepsilon^* = \frac{2n(1+\beta+\beta^2)}{(\beta+1)(2\beta^2-\beta+2)} \tag{1.15}$$

where $\beta$ is the strain ratio, expressed by:

$$\beta = \frac{d\varepsilon_2}{d\varepsilon_1} \tag{1.16}$$

Figure 1.17 shows the forming limit curve obtained through the swift criterion, being known as so called Swift diagram or diffuse necking curve. It interesting to observe that the diffuse necking occurs in uniaxial tension, plane strain and biaxial stretching when the critical major strain reach the same value, specifically equals to the work hardening coefficient when a power hardening law is used.

Swift's analysis can applied to the whole range or deformation, i.e. from uniaxial tension to equibiaxial stretching but the predicted limit strains are much lower than the experimental data when the strain ratio is negative.

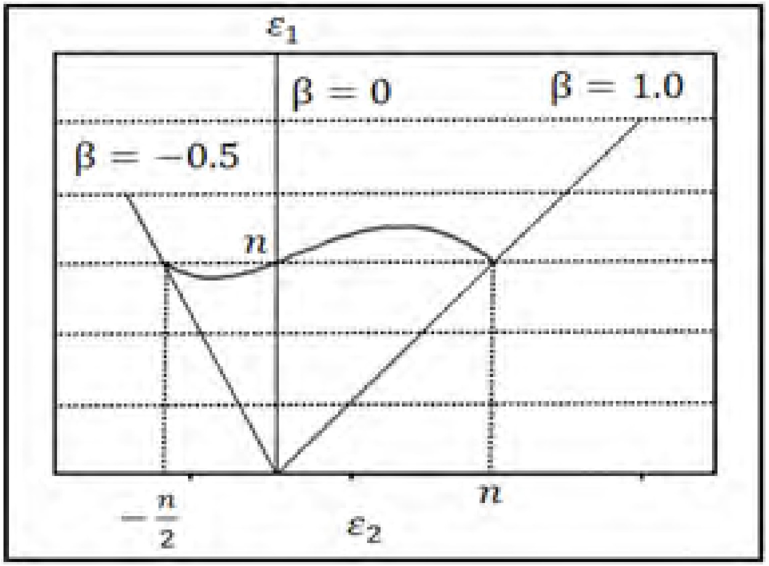

Figure 1.17: The Swift forming limit curve predicting the diffuse necking.

### ii) Bifurcation method with flow theory (Hill)

With the assumption that the onset of failure, or discontinuity of stress and velocity, leads to localized necking, Hill (Hill, 1952) described the restriction on the flow stress and rate of work hardening for the growth of localized necking. Hill observed that, during uniform deformation of a sheet, a localized sheet zone can develop along the zero-extension direction, specifically when the plastic work increment within the zone becomes less than that for uniform deformation. The criterion for the occurrence of instability is given by:

$$\frac{d\sigma}{d\varepsilon} = \frac{\sigma}{1+R} \tag{1.17}$$

where $R$ is the plastic anisotropy parameter.

From Hill's analysis, the localized band angle $\theta$, which is measured between the normal to the band and the major strain direction is expressed by:

$$\theta = arctan(-\beta)^{\frac{1}{2}} \tag{1.18}$$

where β is the strain ratio.

Thus, it is obviously that the angle has a real value only if the strain ratio is negative. In consequence, Hill's analysis predicts that the localized necked cannot from under stretching conditions (when the strain ratio is positive).

Using a power law stress-strain relation,

$$\sigma = K\varepsilon^n \tag{1.19}$$

The critical condition for localized necking for the negative strain ratio becomes:

$$\varepsilon_1{}^* = \frac{n}{1+\beta} \tag{1.20}$$

Consequently, the Hill predicted maximum principal strain $\varepsilon_1{}^*$ prior to localized has a magnitude of $\epsilon_1{}^* = \mathrm{n}$ under a plane strain condition and increase to a value of $\epsilon_1{}^* = 2\mathrm{n}$ in uniaxial tension.

Figure 1.18 shows the diffuse and local necking theories predicted by Hill compared to an experimental FLC.

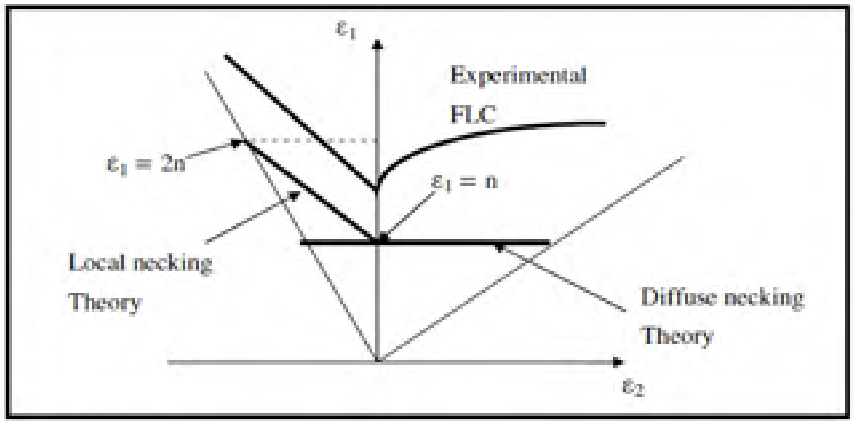

Figure 1.18: A FLD predicted limits given from both the diffuse and local necking theories proposed by Hill compared to an experimental FLC (Kilfoil, 2007).

### iii) Bifurcation with vertex theory (Storen and Rice)

The physical theory of plasticity, based on simple crsrtallographic slip models, predicts the development of a sharp vertex at the loading point on the yield surface of a polycrystalline.

Storne and Rice (Stören and Rice, 1975) incorporated the *J2* deformation theory of plasticity, which is a simplified model of the corner theory, into the classical bifurcation analysis to predict the localized necking over the entire range of the FLD.

Recently, Jie (Jie et al., 2009) proposed a modified bifurcation analysis for strain-rate-dependent sheet metal forming limits, by including the a quasi-linear stress–strain relation in addition to the force equilibrium condition.

Chow (Chow, Hu and Jie, 2003) developed a generalized method to predict forming limits, by considering Hosford's high-order yield criterion, Hill's quadratic yield criterion and the von Mises yield criterion.

### b) Marciniak- Kucyzynski method

Marciniak- Kucyzynski (M-K) (Marciniak and Kuczyński, 1967) have developed a theory based on the assumption that necking develops from local regions of initial heterogeneity. They introduced thickness imperfection in the sheet, perpendicular to the principal stress and strain direction as a groove simulating pre-existing defects in the material.

Necking was considered to occure when the ratio of the thickness in the groove to the nominal thickness is below a critical value. The two zones in the material: uniform region 'a' having a thickness $t_a$and the groove region 'b' having the thickness $t_b$ are shown in Figure 1.19 (Graf and Hosford, 1990).

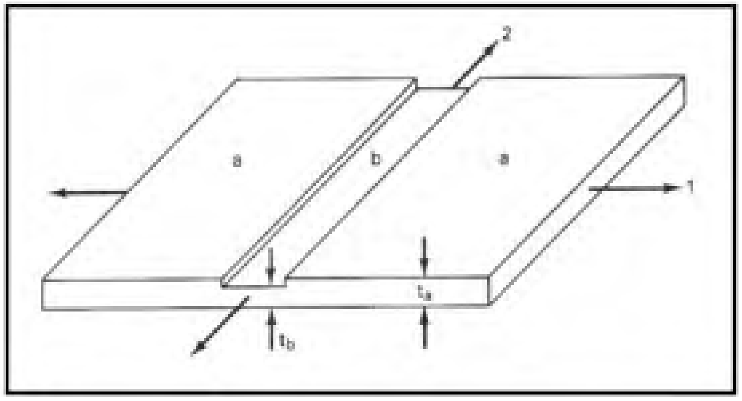

Figure 1.19: Schematic of sample with groove 'b' and uniform region 'a'(Graf and Hosford, 1990).

The coefficient of geometrical non-homogeneity is expressed as $f = \frac{t_b}{t_a}$. The strains parallel to the groove in both regions are assumed to be same. Deformation outside the groove is assumed to occur such that the ratio of stresses and strains remain constant. M-K showed that deformation within the groove occurs at a much faster rate than the rest of the sheet and the concentration of strain in the groove eventually approaches plane strain. Failure is taken to occur when the ratio of strain in the groove to the strain in the uniform region becomes too high (infinity in theory, about 10 in practice) (Ahmadi, Eivani and Akbarzadeh, 2009; Butuc, Gracio and Barata da Rocha, 2003).

Thus the inhomogeneity leads to an unstable growth of strain in the weaker regions subsequently leading to localized necking and failure. The principal strains in the uniform region when the strain in the groove is localized represent the limit strains and define a point in the forming limit curve. By varying the strain ratio different points on the FLD can be obtained. The level of the predicted FLD is fairly sensitive to the assumed value of the initial imperfection f, which is an adjustable fitting parameter in the theory.

In the M-K analysis, a linear imperfection of infinite length is assumed. Some works have challenged this assumption. Burford and Wagoner (Burford and Wagoner, 1989), with the help of finite element analysis showed that both the size and aspect ratio (length/width) of the imperfection affect the localized necking process. The rate of strain localization decreased for a reduced aspect ratio defect (thus higher limit strains) and this influence was found to be of comparable magnitude to the inhomogeneity factor f. It has also been stated (Narasimhan and Wagoner, 1991) that the simplifications made in the M-K model of a defect of infinite length contribute to overstating the impact of a real material defect and thus the M-K curve represented a more severe forming condition than the finite-length notch.

Ávila and Vieira (Ávila and Vieira, 2003) developed an algorithm for prediction of the right-hand side of FLDs based on the M-K model. Five different yield criteria (von Mises', Hill's 1948, Hill's 1979, Hosford's and Hill's 1993) were implanted into this algorithm to analyze their influence on FLDs.

#### 1.1.8.3 Sensitivity of theoretical models for calculation LFD's

Research has shown that the calculated forming limit strain using theoretical models depend sensitively on several factors, such as the material anisotropy, the material hardening, the material texture and microstructure and the strain paths. Based on this fact, numerous authors tried to increase the performance of theoretical methods.

### i) The effect of plastic anisotropy

Plastic anisotropy is related to the crystallographic texture of a material's microstructure after it has under gone processing (e.g., rolling or annealing). It is a measure of the preferred grain orientations in the material and how they react under deformation. It can be represented as either normal or planar anisotropy. Normal anisotropy measures a material's ability to resist thinning during a uniaxial tension test using the Lankford parameter:

$$R = \frac{\varepsilon_w}{\varepsilon_t} \tag{1.21}$$

where $\varepsilon_w$, $\varepsilon_t$, are the strains in the width and thickness directions, respectively. The $R$ value is typically measured in the 0º, 45º and 90º sheet directions. Planar anisotropy is a measure of how the R-value varies with respect to the different sheet or tube directions.

More recently necking has been described based on anisotropy material properties for tube metal forming (Assempour, Nejadkhaki and Hashemi, 2010; Banabic et al., 2010; Hwang, Lin and Chuang, 2009).

### ii) The effect of material hardening

Beside the plastic anisotropy, the material hardening behavior also plays an important role on the prediction of theoretical forming limits.

In the theoretical models an empirical strain hardening law adopted, as follows:

$$\bar{\sigma} = k(\varepsilon_0 + \bar{\varepsilon})^n \tag{1.22}$$

where $\bar{\sigma}$ is the effective stress, $\bar{\varepsilon}$ the effective strain, $\varepsilon_0$ the prestrain, *n* the strain hardening exponent and k is the strength constant.

Barata da Rocha (BARATA DA ROCHA, 1985) and Butuc, Gracio et Barata da Rocha (Butuc, Gracio and Barata da Rocha, 2003; 2006; Yoshida and Kuwabara, 2007) showed that the anisotropic hardening and transient work hardening are important influential factors in predicting FLD sheet and tube and he concluded that more accurate constitutive laws should be used.

#### iii) The effect of strain path

During an actual forming operation, a material element may undergo considerably large changes in strain path, and these changes can significantly later the forming limits (Graf and Hosford, 1993; 1994; Kuwabara, 2007; Yao and Cao, 2002).

### 1.1.8.4 Conclusion

Although all strain path methods could be easily utilized directly on the press-shop floor for die and process optimization, it suffered from a number of issues. When applied to secondary forming operations involving pre-strain and non-linear loading paths, it failed to predict failure (Ghosh and Laukonis, 1977; Graf and Hosford, 1993) .This often resulted in premature failure of the part far below the FLD. In other cases, strains far above the FLD were attained without necking. The stress based FLD method, proposed by Stoughton (Stoughton, 2000), offered a common forming limit curve in stress space, which was independent of the amount of pre-strain and appeared to be a universal characteristic of the material behavior. It was expressed in terms of principal major and minor in-plane components of stress. This criterion helped to overcome the limitations of the conventional strain based FLD and could be used in the analysis of non-proportional paths and multi-stage forming processes.

More recently Yoshida (Yoshida, Kuwabara and Kuroda, 2007) has studied the influence of different strain path for stress based forming limit diagram, two types of combined loading: a combined loading consisting of two linear stress paths in which unloading is included between the first and second loadings (combined loading A), and combined loading in which the strain path is abruptly changed without unloading (combined loading B). Yoshida concluded that it is premature to conclude that the forming limit stress is path-independent.

#### 1.1.8.5 Forming limit diagram for tube hydroforming

The strain and stress based FLD were derived according to through-thickness plane stress assumptions. When a straight or pre-bent tube is expanded within a hydroforming die, the through-thickness component of cannot be neglected, making the stress state three-dimensional and invalidating application of strain and stress based FLDs. Simha (Simha, Grantab and Worswick, 2007; Simha et al., 2005; Simha et al., 2007) suggested the extended stress-based FLC (XSFLC), which was applicable to the prediction of necking under three-dimensional stress states.

Also, limited number of published data on tube FLD by Groche (Groche, 2004; Groche, Breitenbach and Steinheimer, 2003; GUTIERREZ et al., 2007), Green (Green and Stoughton, 2004), Chu (Chu et al., 2006) and Chen (Chen, Soldaat and Moses, 2004) revealed no consensus as to how strain-based FLD should be obtained and applied to the prediction of the onset of necking in THF. The approaches range from the application of sheet FLC and the Keeler-Brazier approximation in THF (Chen, Soldaat and Moses, 2004; Green and Stoughton, 2004) to the determination of a special tube FLD, different from the sheet FLD, using the tube free expansion test (Chu et al., 2006; Groche, 2004; Groche and Breitenbach; GUTIERREZ et al., 2007). The tube free expansion test with various ratios between the axial load and internal pressure provided different strain paths in strain space (Figure 1.20) and could be used both for validation of FLD for tube applications and for establishing original tube FLD. To obtain plane strain conditions in the middle cross-section of the tube, a tube with fixed ends and zero axial load should be pressurized, while for the left and right sides of the FLD compressive and tensile axial loads should be applied to the tube ends, respectively (Figure 1.21).

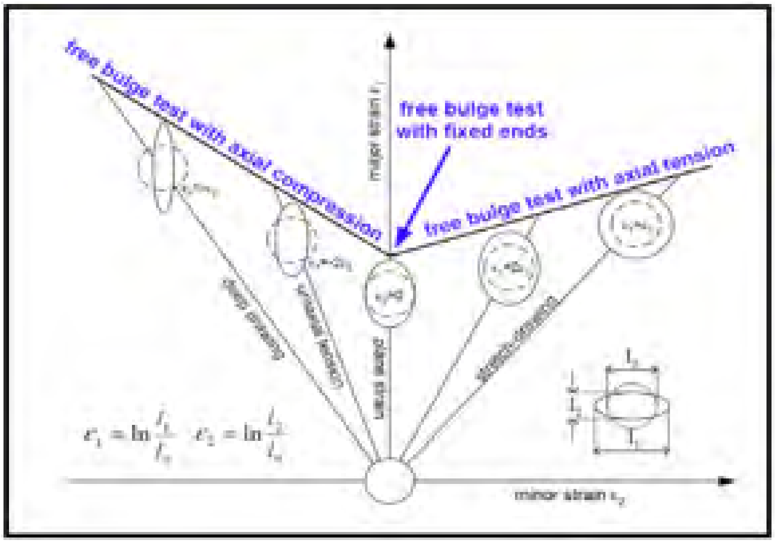

Figure 1.20: Forming limit diagram with characteristic regions (Chu et al., 2006).

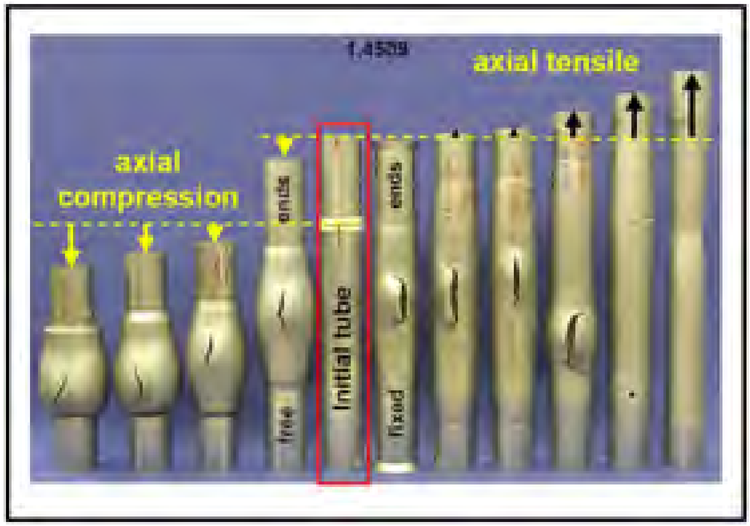

Figure 1.21: Tube specimens tested to obtain tube FLD (Groche, 2004).

Also, the sheet FLD concept implied that the strain in the region near to the neck at the onset of necking be utilized as the necking strain of the material for a given loading path. But If such approach was utilized for THF, the obtained FLD would have limited or no application to failure prediction using FE simulations. This can be illustrated by the results presented by Groche (Groche, 2004) and Green (Green and Stoughton, 2004). Groche utilized the strain next to the failure location to determine the FLC of 1.4301 stainless steel tube using the tube free expansion test. The tube FLD is shown in Figure 1.22. As it can be seen the local strain approach produced higher predictions for the tube expansion at the onset of necking. The sheet FLD for the same material, shown in Figure 1.22 was higher than tube FLD and would produce even higher over-prediction of the tube expansion if utilized for the prediction of the onset of necking in the tube free expansion test.

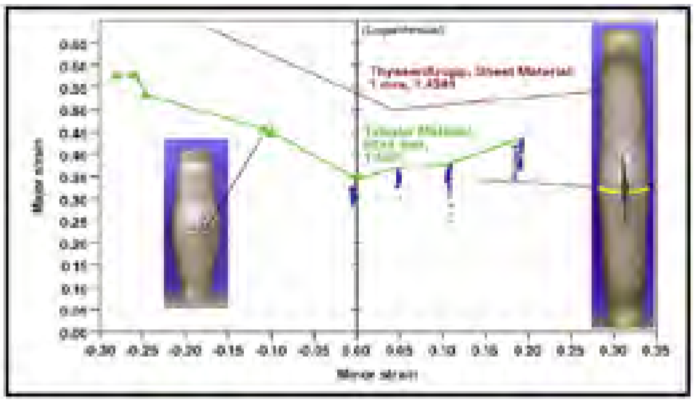

Figure 1.22: 1.4301 stainless steel sheet versus
tube FLDs (Groche, 2004).

Chen (Chen, Soldaat and Moses, 2004) conducted FE MODELING of an AKDQ steel tube free expansion test with the strain-based FLC obtained using Keeler-Brazier approximation, which resulted in 50% over-prediction of the experimental radial expansion at the onset of necking. This result confirmed that tube FLD should be lower than the one established using the Keeler-Brazier approximation or corresponding sheet FLD. Chu (Chu et al., 2006) showed both analytically and experimentally that for an aluminum tube the FLD should be one half of the sheet value (Figure 1.23).

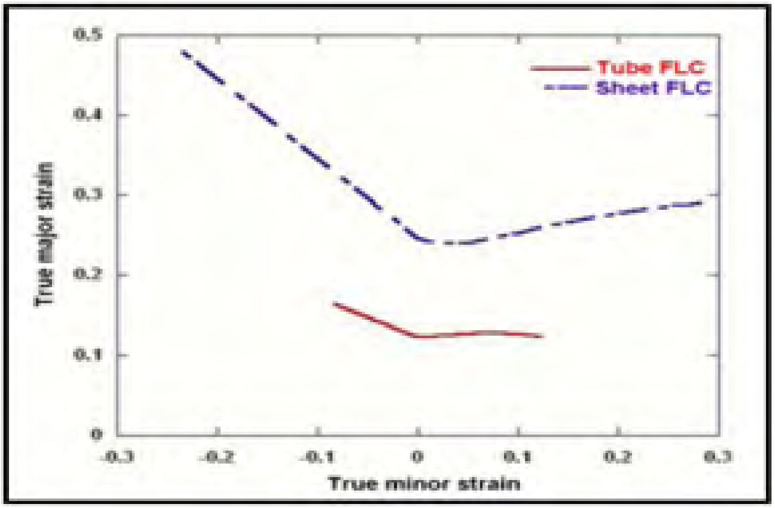

Figure 1.23: (a) analytically obtained aluminum sheet and tube FLDs; (b) experimental results for tube FLD (Chu et al., 2006).

As a result, some general guidelines for the tube FLD determination can be summarized: the sheet FLD leads to significant over-predictions of expansion if utilized in THF applications; over-prediction of tube expansion at the onset of necking might also be a result of use of a local strain approach in tube FLD generation, if the strain at the neck was utilized.

The last comment on tube FLD should be made regarding the determination of the moment of necking initiation in tube free expansion tests. The internal pressure vs. radial expansion curve, had a peak after which expansion continued to grow, while internal pressure decreased. Analytical solutions based on simple assumptions and FE simulations (Chen, 2002; Chen, 2001; Chen, Soldaat and Moses, 2004; Hu, Marciniak and Duncan, 2002; Kim and Kim, 2002; Xia, 2001) confirmed the existence of the peak and subsequent decrease of internal pressure required to continue the expansion. The relationship between the internal pressure and radial expansion was shown to be nonlinear according to the analytical solution (Hu, Marciniak and Duncan, 2002). The non-linearity was the source of the peak on the curve. At the same time, Chen (Chen, 2002), Xia (Xia, 2001) and Marciniak (Hu, Marciniak and Duncan, 2002) utilized this peak as an indicator of instability and necking initiation, regarded as maximum pressure criterion. Such assumption would be desirable due to its apparent simplicity, while its nature was wrong. Chen (Chen, Soldaat and Moses, 2004) experimentally showed that in free expansion testing, tubes did not neck at the maximum pressure. This occurred between the point of maximum pressure and the point of burst on the internal pressure versus radial expansion curve.

## Conclusion of literature review and enlightening of problematic

In this chapter various major aspects of THF were presented. The material behavior and failure behavior were analysed. Furthermore, some important process parameters were described.

This work has led us to conclude that:

- There is a substantial need to reduce the number of unknown parameters to predict material behavior more accurately. The main benefit is to reduce the needs of trial and error design. However, the use of trial and error redesign steps in some cases is mandatory.
- There is no general formability model before and after onset of instability that can be used for all sheet and tube forming processes. Amongst forming process, tube hydroforming has a highly complex mechanism due to different process parameters that can influence the process. Thus, more attention should be paid to understand, predict and optimize the process parameters for this advanced metal forming process.
- A few studies have focused on the influence of formability methods to measure formability of tubes before the one set of instability. Therefore, extensive investigations to discover the factors governing formability of seamless tubes.
- Very limited analytical models have been reported for burst prediction. Most of existing analytical models are constructed based on damage models were developed for sheet and bulk forming processes. Furthermore, no analytical model was found to predict failure or bursting for aerospace materials.
- FE modeling is the most prominent numerical method for THF simulation. However the FE results are relevant to the accuracy of implemented input parameters in the model.

- Most of the existing research works in literature are useful to measure formability and predict the failure roughly, while in a real THF process of aerospace alloys accurate formability parameters can be used for accurate FE modeling.
- Amongst reported damage models in literature, special attention has been paid to decoupled damage models. However the original decoupled damage models are designed to predict failure in sheet or bulk metal forming. Therefore, certain levels of modifications should be incorporated to decoupled damage criteria for applying them to tube materials

# CHAPTER 2

## EVALUATING THE FLOW STRESS OF AEROSPACE ALLOYS FOR TUBE HYDROFORMING PROCESS BY FREE EXPANSION TESTING

* This section has been published: M. Saboori, H. Champliaud, J. Gholipour, A. Gakwaya, J. Savoie, P. Wanjara, Evaluating the flow stress of aerospace alloys for tube hydroforming process by free expansion testing, International Journal of Advanced Manufacturing Technology, (2014) VOL 28 NO 4 437

In order to obtain accurate tube hydroforming (THF) simulation results, one of the important inputs in the FE modeling of the process is the mechanical response of the material during THF. Generally, the mechanical response is defined by the stress-strain behavior that can be determined from tensile testing of the specimens extracted either from the sheet used for roll forming of the tubes or directly from the tubes. More recently, free expansion testing has been used to characterize the mechanical response of the material for hydroforming applications. The free expansion test can emulate process conditions similar to those found during THF, and, as such, can be used to obtain reliable and accurate information on the mechanical response/properties of the tubular material. The aim of this section is to present an approach for evaluating the stress–strain behavior of different materials using a 3D deformation measurement system in conjunction with an analytical model. Here, to characterize the mechanical response of the materials, free expansion (bulge) testing and tensile testing were used for austenitic stainless steel types 321 (SS 321) and 304L (SS 304L), INCONEL® alloy 718 (IN 718) and aluminum alloy 6061 in the annealed “0” temper condition (AA 6061-0). The mechanical response of each material, measured through free expansion testing of tubular forms, was compared to the respective stress-strain behavior determined from the uniaxial tensile test using ASTM E8 geometry specimens extracted from the tubes. For each material studied in this work, the two flow stress behaviors were distinct, indicating that the test method can have a noticeable effect on the mechanical response. Finite element modeling of the free expansion of each material was also utilized to simulate the THF process with the flow stress curves obtained experimentally; the predicted expansion and burst pressure results were close to the experimental data indicating that the approach developed and described in this work has merit for characterizing the mechanical response of aerospace alloys for hydroforming applications.

## Introduction

Over the last decade, THF has become a popular technology in the automotive industry due to its capacity to manufacturing complex shapes with fewer steps than traditional stamping and welding processes. However, the application of the THF process in the aerospace sector is comparatively recent with many challenges due to the high strength and/or limited formability of aerospace materials. Compared to the other forming processes, hydroforming has many advantages such as weight reduction through more efficient section design and manufacturing, improved structural strength, tighter manufacturing tolerances and lower tooling cost, mainly due to fewer die components, as described by Hartl (Hartl, 2005) for tubular products and Lang (Lang et al., 2004) for both tube and sheet metal forms. The success/failure of the THF process largely depends on many factors; Ahmed and Hashmi (Ahmed and Hashmi, 1997) considered the importance of, such as the mechanical properties of the material, while Vollertsen and Plancak (Vollertsen and Plancak, 2002) deliberated the loading path during the process, tool geometry and friction condition. Koç and Altan (Koc and Altan, 2002) examined the effect of loading path on wrinkling, bulking and bursting during the THF process of a T- shape geometry. Later, Yang and Zhang (Yang, Zhang and Li, 2006) studied these effects on the free expansion process. Among the above-mentioned factors, the mechanical properties (yield strength, ultimate tensile strength and elongation) and flow characteristics of the material play a critical role in the process design for THF. In general, the material parameters and mechanical properties for FE modeling applications are determined by different methods such as tensile testing and/or free expansion/bulge testing. Conventionally, tensile test data have been determined from flat sheet products (i.e. materials used to manufacture the tube by roll forming, welding and sizing) to determine the properties of the tubular forms. However the tube manufacturing process changes the mechanical response/properties of the material from that in the initial sheet condition; for instance Koç

(Koç, Aue-u-lan and Altan, 2001) reported a difference in the flow behavior of tubular products from that of the blank sheet and Sokolowski (Sokolowski et al., 2000) confirmed this difference by performing interrupted free expansion and tensile tests for SS 304. This discrepancy in the mechanical response may be even more prominent for seamless tubes that are manufactured from billet forms that undergo substantial changes in the microstructure and, thus, the mechanical response.

In order to perform the pertinent numerical simulations of the THF process, designers need more realistic and/or more accurate information on the mechanical properties of the tube. In this regard, tensile testing of the specimens extracted from the tube material as well as free expansion testing of the tube were performed by different researchers in order to determine the mechanical properties for accurate simulating the THF process. Song (Song, Kim and Kang, 2007) calculated analytically the flow stress of tubular material using the free expansion process with end feeding and considered the effect of friction. More recently, Song (Song et al., 2010) evaluated the flow stress characteristics of a steel with 0.09% carbon and 0.52% manganese using tensile samples extracted from sheet and tube geometries. Hwang and Wang (Hwang and Wang, 2009) evaluated the stress–strain characteristics of annealed C26800 zinc copper tubes and AISI 1215 carbon steel tubes by the free expansion process and considered their anisotropic properties. Later, Saboori (Saboori et al., 2013b) studied the effect of different material models on predicting the expansion behavior of SS 321 during the free expansion process. Several analytical methods have been proposed to improve the accuracy of the flow stress curves for FE modeling of the THF process. For instance, Fuchizawa and Narazaki (Fuchizawa and Narazaki, 1993) developed an analytical model in which the profile at the free expansion region was assumed to be a circular arc and its radius of curvature was determined experimentally. Koç (Koç, Aue-u-lan and Altan, 2001) proposed a combination of an online and offline measurement procedure to determine the necessary parameters (longitudinal and circumferential radius of curvature, as well as the expansion and thickness at the maximum bulge height) to calculate the stress-strain curve. Hwang and Lin (Hwang and Lin, 2002) assumed that the profile of the bulged zone was elliptical. More recently, Hwang (Hwang, Lin and Altan, 2007) calculated the stress-strain curve from the experimental data using online measurement of the bulge height by assuming an elliptical bulge profile and measuring the thickness by cutting the tubes at different stages of the hydroforming process. In contrast, Bortot (Bortot, Ceretti and Giardini, 2008) developed an offline analytical approach using a coordinate measuring machine (CMM) to measure the bulge profile and the tube thickness at different stages of the process. Lately, Aguir (Aguir, BelHadjSalah and Hambli, 2011) used an artificial neural networks-genetic algorithm method to identify material parameters and Zribi (Zribi, Khalfallah and BelHadjSalah, 2013) proposed an inverse method to calculate constitutive parameters in the free expansion process.

Presently for THF applications, knowledge of the formability of aerospace materials is quite limited and one of the objectives of this section is to understand how to accurately determine the mechanical properties of some aerospace alloys, such as SS 321, SS 304L, IN 718 and AA 6061-0, utilizing both the uniaxial tensile test and the free expansion test. The tensile testing was performed using specimens extracted from the tubes instead of sheets. The generated pool of data presented in this section provides then a valuable data base for these alloys. Specifically, to determine the stress-strain curve by the free expansion test, a novel online measurement approach was developed using a 3D automated deformation measurement system (Aramis®) to extract the coordinates of the bulge profile during the test. These coordinates were used to calculate the circumferential and longitudinal curvatures, which were then utilized to determine the effective stresses and effective strains at different stages of the THF process. It is noteworthy that with this approach all the data is generated through a single test in contrast to the conventional methods that use multiple tests to generate the same type of data. In addition, as the curvatures are calculated with the experimental coordinates, there is no assumption (circular, elliptical, etc.) associated to the shape of the section, thus resulting in more accurate analytical results with the methodology presented in this section. The flow stresses obtained from the free expansion tests were compared with those obtained from tensile testing of the specimens extracted from the tubes for the materials considered in this work, i.e. SS 304L, SS 321, IN 718 and AA 6061-0.

### Characterizing the flow stress of tubular materials in the THF process

In the free expansion test, the tube is first clamped between the two halves of the die as shown in Figure 2.1.a. The tube ends are then sealed using two plungers. Pressurized fluid is then applied into the tube through the end plungers. With increasing internal pressure, expansion (bulging) of the tube occurs, and at its limit the tube will burst. It is noteworthy that the movement of the tube ends was restricted; hence end feeding, which could push the tube material towards the expanding zone during the process, was prohibited.

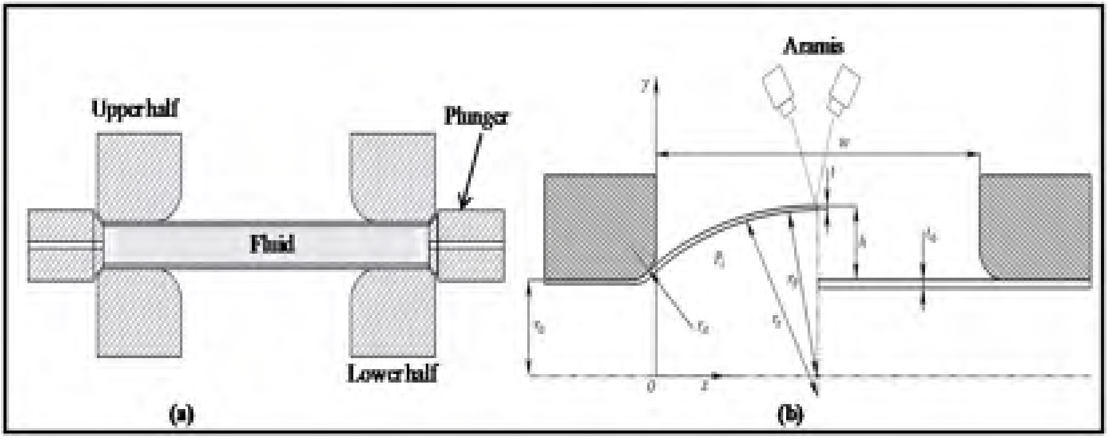

Figure 2.1: Schematic diagrams of (a) the tube free expansion tool and (b) the test setup with the 3D deformation measurement system.

Two sets of parameters, constant and variable, are involved in this process. The constant parameters comprise the length of the expansion zone (w), the die radius at the entrance of this zone (r), and the initial thickness of the tube ($t_0$). The variable parameters describe the tube bulge profile evolving with increasing internal pressure (p) and include the bulge height (h), thickness at the maximum bulge height or pole (t), bulge circumferential radius ($r_\theta$), and bulge longitudinal radius ($r_z$). In this work, these variable parameters were measured online during the hydroforming process using an Aramis® 3D deformation measurement system, as shown in Figure 2.1.b. The Aramis® system consists of two CCD cameras that can capture a predetermined number of frames per second (or steps) and uses a random dot pattern applied to the surface of the sample for measuring the deformation during the test.

In order to develop an accurate and efficient method to generate the flow stress curves for each material, a systematic and methodological approach in data acquisition from the hydroforming press and the Aramis® system was established. Using the membrane theory and considering equilibrium conditions, the following equation can be written for an element of the tube at the maximum bulge height Fuchizawa and Narazaki (Fuchizawa and Narazaki, 1993):

$$\frac{\sigma_\theta}{r_\theta} + \frac{\sigma_z}{r_z} = \frac{p_i}{t_i} \tag{2.1}$$

where $p_i$ is the internal pressure and $ti$ is the wall thickness at stage $"i"$ with $\sigma_\theta$ and $\sigma_z$ being the circumferential and longitudinal stress components, respectively. From the force equilibrium at the maximum bulge height, the following equations have been derived for $\sigma z$ and $\sigma_\theta$ (Fuchizawa and Narazaki, 1993):

$$\sigma_z = \frac{p_i(r_{\theta_p} - t_p)^2}{2t(r_{\theta_p} - t_p/2)} \tag{2.2}$$

$$\sigma_\theta = \frac{p_i(r_{\theta_p} - t_p/2)}{t_p} \times \left\{\left[1 - \frac{t_p}{2(r_z - t_p/2}\right]\left[1 - \frac{t_p}{2(r_{\theta_p} - t_p/2)}\right] - \frac{(r_{\theta_p} - t_p)^2}{2(r_z - t_p/2)(r_{\theta_p} - t_p/2)}\right\} \tag{2.3}$$

where $r_{\theta p}$ is the maximum circumferential radius of curvature and *tp* is the wall thickness at the maximum bulge height (i.e. at the maximum pressure).

In the free expansion process, the tube is sufficiently thin so that a plane stress state ($\sigma_t \cong 0$) can be assumed. According to Hill's yield criterion and its associated isotropic hardening law (Hill, 1979), the effective stress ($\bar{\sigma}$) is a function of the principal stresses as follows:

$$\bar{\sigma} = \frac{1}{2(1+R)}\left[(1+2R)(\sigma_\theta - \sigma_z)^m + (\sigma_\theta + \sigma_z)^m\right]^{\frac{1}{m}} \tag{2.4}$$

where $\sigma_\theta$ and $\sigma_z$ are the principal stresses in the circumferential and longitudinal directions, respectively, *R* refers to the anisotropic parameter and m refers to the stress exponent. The value of m is determined by the degree of anisotropy of the material and must be greater than 1 to ensure convexity of the yield surface. For different *R* values, the loci are ellipses when $m = 2$. In the case of $R = 1$, the Hill yield function abridges into the von Mises yield function. The effective strain can then be calculated as a function of the principal strains as follows (Hill 1979):

$$\bar{\varepsilon} = \frac{1}{2}\left[2(1+R)\right]^{\frac{1}{m}}\left[(\varepsilon_\theta + \varepsilon_t)^{\frac{m}{m-1}} + (1+2R)^{\frac{-1}{m-1}}(\varepsilon_\theta + \varepsilon_t)^{\frac{m}{m-1}}\right]^{\frac{m-1}{m}} \tag{2.5}$$

where $\varepsilon\theta$ and $\varepsilon t$ are the strains in the circumferential and thickness directions, respectively. The circumferential strain and longitudinal strain ($\varepsilon_z$) can be extracted from the Aramis® system, so that the principal strain in the thickness direction at the maximum bulge height can be obtained through the volume constancy assumption (plastic incompressibility condition):

$$\varepsilon_t = -(\varepsilon_\theta + \varepsilon_z) \tag{2.6}$$

By studying the influence of different hardening laws, it was found that the Swift hardening law (Equation 2.7) can be fitted best to the experimental data for austenitic stainless steels Saboori (Saboori et al., 2013a; 2013b) for IN 718 Anderson (Anderson, 2010) and for SS 304 Koç (Koç, Aue-u-lan and Altan, 2001) while for aluminum alloys the Hollomon hardening law (Equation 2.8) was reported to give the best fit Abrantes (Abrantes, Szabo-Ponce and Batalha, 2005):

$$\bar{\sigma} = k_s(\varepsilon_0 + \bar{\varepsilon}_p)^{n_s} \tag{2.7}$$

$$\bar{\sigma} = k_h(\bar{\varepsilon}_p)^{n_h} \tag{2.8}$$

In the above equations, $\varepsilon_0$ is the initial plastic strain, $\bar{\varepsilon}_p$ is the effective plastic strain, $k$ is the strength coefficient and $n$ is the strain hardening exponent of the material (s and h indexes correspond to Swift and Hollomon law, respectively). In Equations 2.7 and 2.8, in order to determine the flow stress curves, continuous and accurate measurements of the thickness ($t$), the maximum circumferential radius ($r_{\theta_p}$) and the bulge curvature or longitudinal radius ($r_z$) are required.

In this study, to eliminate any assumption related to the bulge geometry, an Aramis® system was used to collect the data on the bulge curvature, tube thickness, bulge height and the three principal strains at every stage of the free expansion test. To generate the bulge profile, several coordinates ($z_i$, $y_i$) were extracted along the tube length at the bulge zone from the Aramis® system and the profile was generated by fitting a piecewise polynomial (a spline). A mathematical function of a generic form $y = f(z)$ was thus considered for defining the bulge profile at different levels of internal pressure. This function can be written as:

$$y = az^3 + bz^2 + cz + d \tag{2.9}$$

where $a$, $b$, $c$ and $d$ are the constants that define the profile and must be determined during the test at each step. After taking the first and second derivatives of this function, the curvature ($\kappa$) and the value of $r_z$ at the maximum bulge height can be determined as follows:

$$\kappa = \frac{d^2y/dz^2}{\left[1 + (dy/dz)^2\right]^{3/2}} \tag{2.10}$$

$$r_z = \left[\frac{1}{\kappa}\right]_{z={}^{w}/_{2}} \tag{2.11}$$

By determining the values of the effective stress and effective strain at each Aramis® step, the biaxial flow stress curve of the tube material can be generated. At this stage, a curve fitting algorithm based on the least squares method was used to find the constants in the different work hardening equations, such as the k and n values in Equations 2.7 and 2.8. When compared to the current state-of-the-art, the innovative contribution of the methodology developed in this study is the elimination of geometric assumptions for the bulge profile (e.g. circular or elliptical), which then leads to a more reliable and accurate determination of the flow stress curves for FE modeling of the THF process. In addition, the continuous or online measurement capability with the Aramis® system (i.e. no interruptions for measuring the profile and/or sectioning the tubes to measure the thickness) considerably minimizes the required experimentation effort and, thus, the costs related to the tube materials, labor and facility operation.

## Experimental procedure

### 2.1.1 Free expansion tests

In this work, two sets of dies, for different tube diameters, were used. Figure 2.2 illustrates the 3D CAD model of one of the dies used for the free expansion tests. Figure 2.3 shows the setup used for THF trials, which involved the use of a 1000 ton fully instrumented hydroforming press capable of applying 400 MPa of internal pressure and equipped with the Aramis® system as well as the two die sets. During the process, the ends of the tubes were maintained fixed in place and sealed using two end plungers. The experimental conditions for the two sets of free expansion experiments are given in Table 2.1. It is noteworthy that the first set of experiments was conducted on SS 321, IN 718 and SS 304L, while the second was performed only for AA 6061-0. To ensure the consistency of the data, each condition was repeated at least two times.

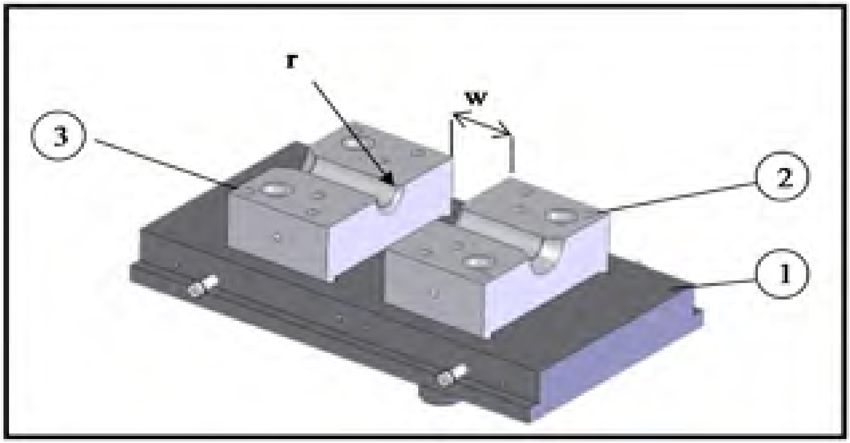

Figure 2.2: CAD of the die-set: showing (1) the lower shoe, (2) the lower right cavity and (3) lower left cavity.

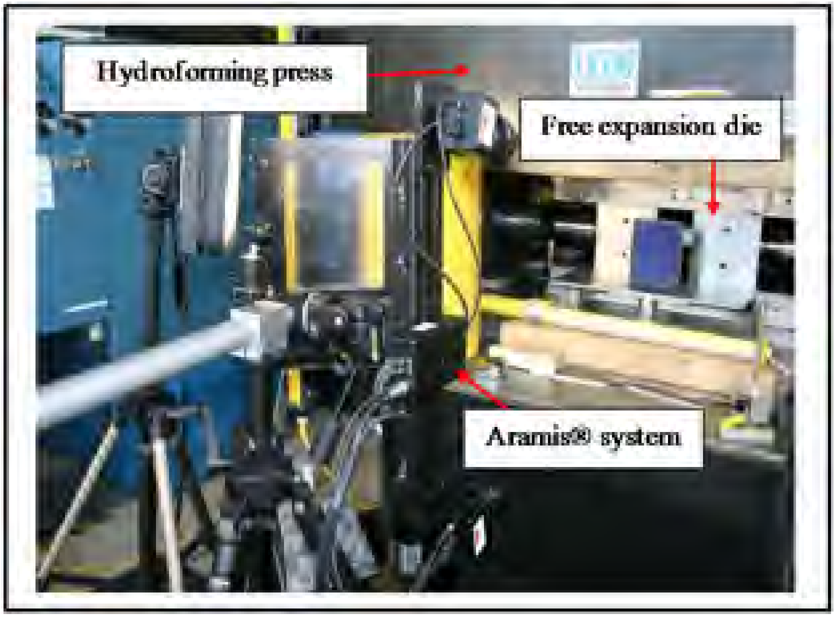

Figure 2.3: Experimental setup for the free expansion tests.

Table 2.1: Experimental conditions for the first and second set of the free expansion trials.

| Materials | $L_0$ (mm) | $D_0$ (mm) | w (mm) | r (mm) |
|---|---|---|---|---|
| SS 321<br>0.9 mm and 1.2 mm thick | 228.6 | 50.8 | 101.8 | 7.5 |
| IN 718<br>0.9 mm and 1.2 mm thick | 228.6 | 50.8 | 101.8 | 7.5 |
| SS 304L<br>1.6 mm thick | 228.6 | 50.8 | 101.8 | 7.5 |
| AA 6061-0<br>3 mm thick | 381.0 | 88.9 | 165.0 | 7.5 |

### 2.1.2 Tensile tests

Tensile specimens having a standard geometry of 50 mm in gauge length and 12.7 mm in width were machined in accordance to ASTM E8/E8M-11 (E8, 2011) from the tubular material used for the free expansion tests. Specifically, the specimens were cut longitudinally from each tube, as shown in Figure 2.4. With the exception of the SS 304L tubes that were seam welded, the tubes for SS 316L, IN 718 and AA 6061-0 were seamless. For the welded SS 304L tube, the specimens were extracted from three positions relative to the seamed joint (i.e. 90°, 180° and 270°, considering the weld seam being at 0°), as shown in Figure 2.4. In contrast for the seamless tubes, tensile specimens were extracted from the tube at 90° intervals (i.e. 0°, 90°, 180° and 270°). It is noteworthy that the deformation direction during hydroforming is biaxial and the extraction of these tensile specimens from the tubes allows the measurement of the mechanical response of the material only along the longitudinal direction. All the tensile specimens were tested at room temperature and a constant crosshead rate of 2 mm/min using a 250 kN MTS testing frame equipped with a laser video extensometer and ARAMIS® system. At least three tensile specimens for each tube material were tested to ensure test data reproducibility. The effective true stress–true strain curves were obtained by averaging the tensile test data for each tubular material.

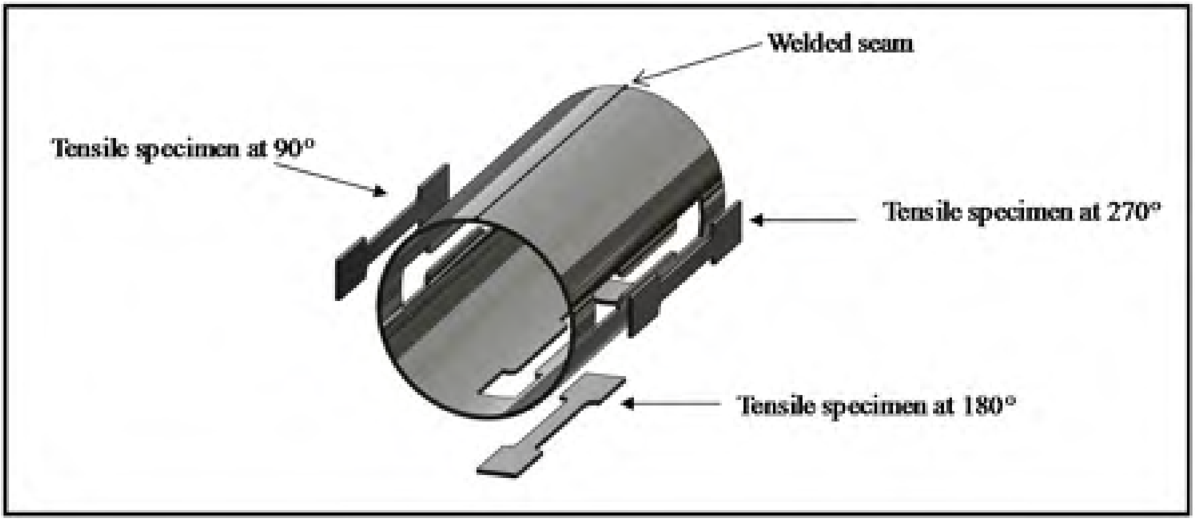

Figure 2.4: Location of the tensile specimens extracted from seam welded SS 304L.

## Results and discussion

As mentioned previously, the free expansion tests were performed without end feeding up to the rupture/burst of the tube for each aerospace material examined in this work (i.e. SS 321, SS 304L, IN 718 and AA 6061-0) in order to determine the true stress-true strain relationships under biaxial testing conditions. Figure 2.5 shows examples of the free expanded tubes after bursting.

A code was developed in Matlab based on the flowchart presented in Figure 2.6 (see ANNEX I). As indicated in the flowchart, the values of $w$, $t_0$, $D_0$, $R$ and m were taken as the initial input. The parameters affecting the accuracy of the calculation, $h_p$, $t_p$, $r_\theta$ and the profile coordinate points ($z_i$, $y_i$), were extracted from the Aramis® system at different steps during the free expansion process. Then, a 3rd order spline was fitted through the extracted coordinates, as shown in Figure 2.7. It should be mentioned that higher order splines (4th and 5th orders) for fitting to the longitudinal profile were also considered, but the resulting effect on the accuracy of the fitted curve was negligible (less than 2% at low pressures and almost zero at high pressures). For each material, the hydroforming pressure versus bulge height was then extracted from the experimental data to calculate the variables ($\varepsilon_t$, $\varepsilon_\theta$, $\varepsilon_z$, $\sigma_z$ and $\sigma_\theta$) needed to evaluate the biaxial true stress-true strain curves. Once the stress-strain response of the material was obtained, the related hardening constants for the Swift or Hollomon laws were determined numerically using the nonlinear least squares function available in the Matlab software (see ANNEX II). In this way, the associated error related to the bulge profile assumption was minimized, as the profile was determined from the real geometry of the bulge during the process.

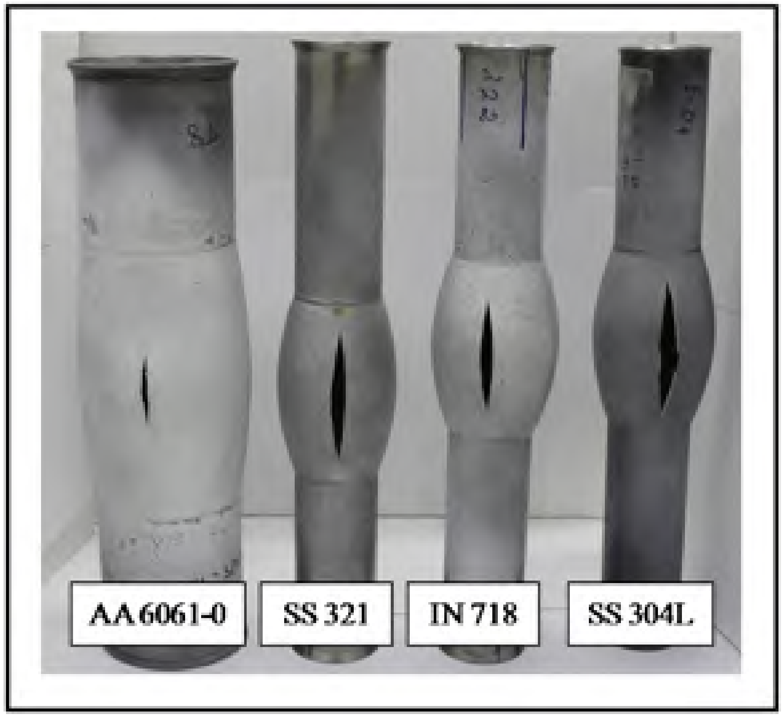

Figure 2.5: AA 6061-0, SS 321, IN 718, and SS 304L
and tubes after free expansion testing.

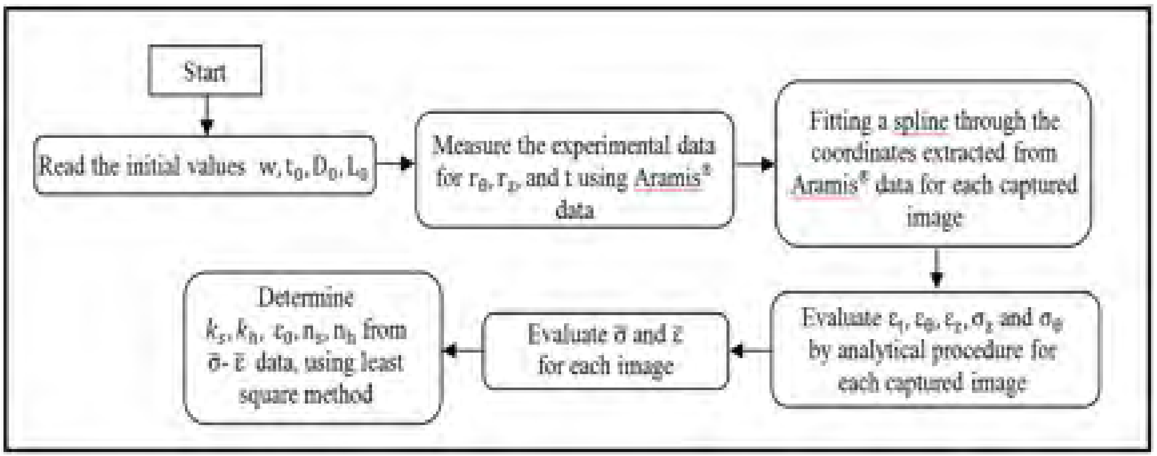

Figure 2.6: Flow chart for determining the flow curves.

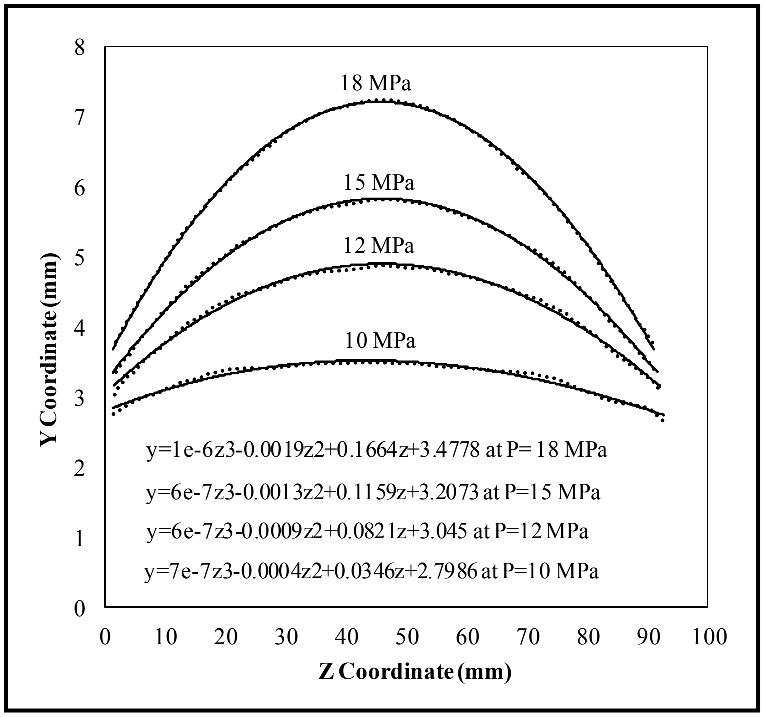

Figure 2.7: Tube profile coordinates and 3rd order spline fitted at different pressures during the free expansion process.

### 2.1.3 Comparison of the tube free expansion and tensile test results

Using the methodology described above, the flow stress curves obtained under different loading conditions (biaxial from free expansion and uniaxial from tensile testing) were determined for the different aerospace alloys, including SS 321, IN 718, SS 304L and AA 6061-0, as presented in Figure 2.8. It is noteworthy that in the case of the free expansion test data, the true stress-true strain curves plotted in Figure 2.8 were determined using a spline profile (present work) and an elliptical profile (as described by Hwang (Hwang, Lin and Altan, 2007)). For AA6061-0 and SS 304L, the true stress-true strain curves determined using the free expansion test data with a spline and elliptical profiles as well as the tensile test data indicated similar flow stress behaviors; the maximum strain was greater by 0.038 for AA6061-0 and by 0.054 for SS 304L under biaxial (spline) as compared to uniaxial loading conditions. In contrast, for both IN 718 and SS 321 (0.9 mm and 1.2 mm thick), the loading condition and bulge profile assumptions (spline, elliptical, etc.) have an effect on the flow stress curve.

The relative differences in the stress-strain curves generated for the AA 6061-0 and SS 304L by means of tensile testing and free expansion testing based on the spline profile are in accordance with that expected from a fundamental perspective that the biaxial behavior is an extension of the uniaxial condition. However, for IN 718 and SS 321, the uniaxial stress-strain curve deviates from that of the biaxial and this may be explained from a perspective of the influence of anisotropy and material microstructure (including texture) on the mechanical response. Specifically, in the case of tensile testing, the uniaxial stress-strain curve is highly dependent on the direction of sampling. Thus depending on the relative direction of the deformation to the anisotropic property of the material, the uniaxial true stress-strain curves may then be representative or atypical of the hydroforming process. In contrast, in the case of free expansion, the average anisotropy contributes to generate the stress-strain curve, which then well represents the mechanical response of the material during the hydroforming process. Nevertheless, the material response appears to be dependent on the assumptions applied to the bulge profile (spline or elliptical), as illustrated in Figure 2.8. Since the evolving tube geometry during the free expansion process is calculated more accurately by the online approach adopted in the present model using a spline profile approximation, it is expected that the thickness as well as the longitudinal and circumferential strains would better represent the actual conditions during THF as compared to assuming a fixed geometry (e.g. elliptical or circular) throughout the process. The work hardening constants of the Swift or Hollomon laws for the different materials were ascertained by the free expansion based on the spline profile and tensile tests, as shown in Table 2.2 and Table 2.3, respectively. In addition, Table 2.4 gives the work hardening constants of the Swift or Hollomon laws for the free expansion test data obtained in the present work for the different materials but using an elliptical bulge profile. In particular, two averaged curves were generated, one from the two repetitions of the free expansion test and another from the three repetitions of the tensile test, so as to calculate the respective material constants for each alloy examined in this work. Of course, for the free expansion test data, a spline or elliptical profile was included as a variant. Typically, since the loading condition in free expansion is different from that in tensile testing, the material constants obtained from the mechanical response of the material during free expansion are different from those calculated from the uniaxial tensile behavior. Interestingly, as an example, the values presented in Table 2.2 for 0.9 mm thick SS 321 are different from the those reported previously ($k_s$= 1890.85, $n_s$= 0.84, $\varepsilon_0$= 0.086), which were based on the assumption that the bulge profile was part of an ellipse (Saboori (Saboori et al., 2013b)). Using the material constants in Table 2.2 (calculated with online measurements of the real bulge profile) and the ones presented here from previous work (with the bulge geometry assumed to be elliptical), at 0.3 strain, the effective stresses are 800 MPa and 850 MPa, respectively. Similarly, at 0.4 strain, the effective stress values are 918 MPa and 1031 MPa, respectively. Hence, between the two methods, at an effective strain of 0.3 and 0.4, the difference in the effective stress is 6% and 12%, respectively, and alludes to the impact of the bulge geometry on the mechanical response of the material.

Table 2.2: True stress–true strain relations based on the free expansion test results using a spline profile.

| Material | Thickness (mm) | Swift model $\bar{\sigma} = k_s(\varepsilon_0 + \bar{\varepsilon}_p)^{n_s}$ | Hollomon model $\bar{\sigma} = k_h(\bar{\varepsilon}_p)^{n_h}$ |
|---|---|---|---|
| SS 321 | 0.9 | $\bar{\sigma} = 1427.45(0.035 + \varepsilon_p)^{0.53}$ | - |
| SS 321 | 1.2 | $\bar{\sigma} = 1397.81(0.052 + \varepsilon_p)^{0.63}$ | - |
| IN 718 | 0.9 | $\bar{\sigma} = 1880.6(0.072 + \varepsilon_p)^{0.59}$ | - |
| IN 718 | 1.2 | $\bar{\sigma} = 1980.2(0.07 + \varepsilon_p)^{0.62}$ | - |
| SS 304L | 1.6 | $\bar{\sigma} = 1413(0.05 + \varepsilon_p)^{0.47}$ | - |
| AA 6061-0 | 3.0 | - | $\bar{\sigma} = 267.5(\varepsilon_p)^{0.33}$ |

Table 2.3: True stress–true strain relations based on the tensile test results.

| Material | Thickness (mm) | Swift model $\bar{\sigma} = k_s(\varepsilon_0 + \bar{\varepsilon}_p)^{n_s}$ | Hollomon model $\bar{\sigma} = k_h(\bar{\varepsilon}_p)^{n_h}$ |
|---|---|---|---|
| SS 321 | 0.9 | $\bar{\sigma} = 1458.29(0.026 + \varepsilon_p)^{0.49}$ | - |
| SS 321 | 1.2 | $\bar{\sigma} = 1461.54(0.048 + \varepsilon_p)^{0.62}$ | - |
| IN 718 | 0.9 | $\bar{\sigma} = 2053.36(0.071 + \varepsilon_p)^{0.62}$ | - |
| IN 718 | 1.2 | $\bar{\sigma} = 2063.85(0.08 + \varepsilon_p)^{0.64}$ | - |
| SS 304L | 1.6 | $\bar{\sigma} = 1350.6(0.065 + \varepsilon_p)^{0.47}$ | - |
| AA 6061-0 | 3.0 | - | $\bar{\sigma} = 239.98(\varepsilon_p)^{0.28}$ |

Table 2.4: True stress–true strain relations based on the free expansion test results using an elliptical profile.

| Material | Thickness (mm) | Swift model $\bar{\sigma} = k_s(\varepsilon_0 + \bar{\varepsilon}_p)^{n_s}$ | Hollomon model $\bar{\sigma} = k_h(\bar{\varepsilon}_p)^{n_h}$ |
|---|---|---|---|
| SS 321 | 0.9 | $\bar{\sigma} = 1890.85(0.086 + \varepsilon_p)^{0.84}$ | - |
| SS 321 | 1.2 | $\bar{\sigma} = 1800.6(0.0081 + \varepsilon_p)^{0.81}$ | - |
| IN 718 | 0.9 | $\bar{\sigma} = 2320.22(0.124 + \varepsilon_p)^{0.79}$ | - |
| IN 718 | 1.2 | $\bar{\sigma} = 2354.4(0.114 + \varepsilon_p)^{0.77}$ | - |
| SS 304L | 1.6 | $\bar{\sigma} = 1399.84(0.11 + \varepsilon_p)^{0.5}$ | - |
| AA 6061-0 | 3.0 | - | $\bar{\sigma} = 263.9(\varepsilon_p)^{0.31}$ |

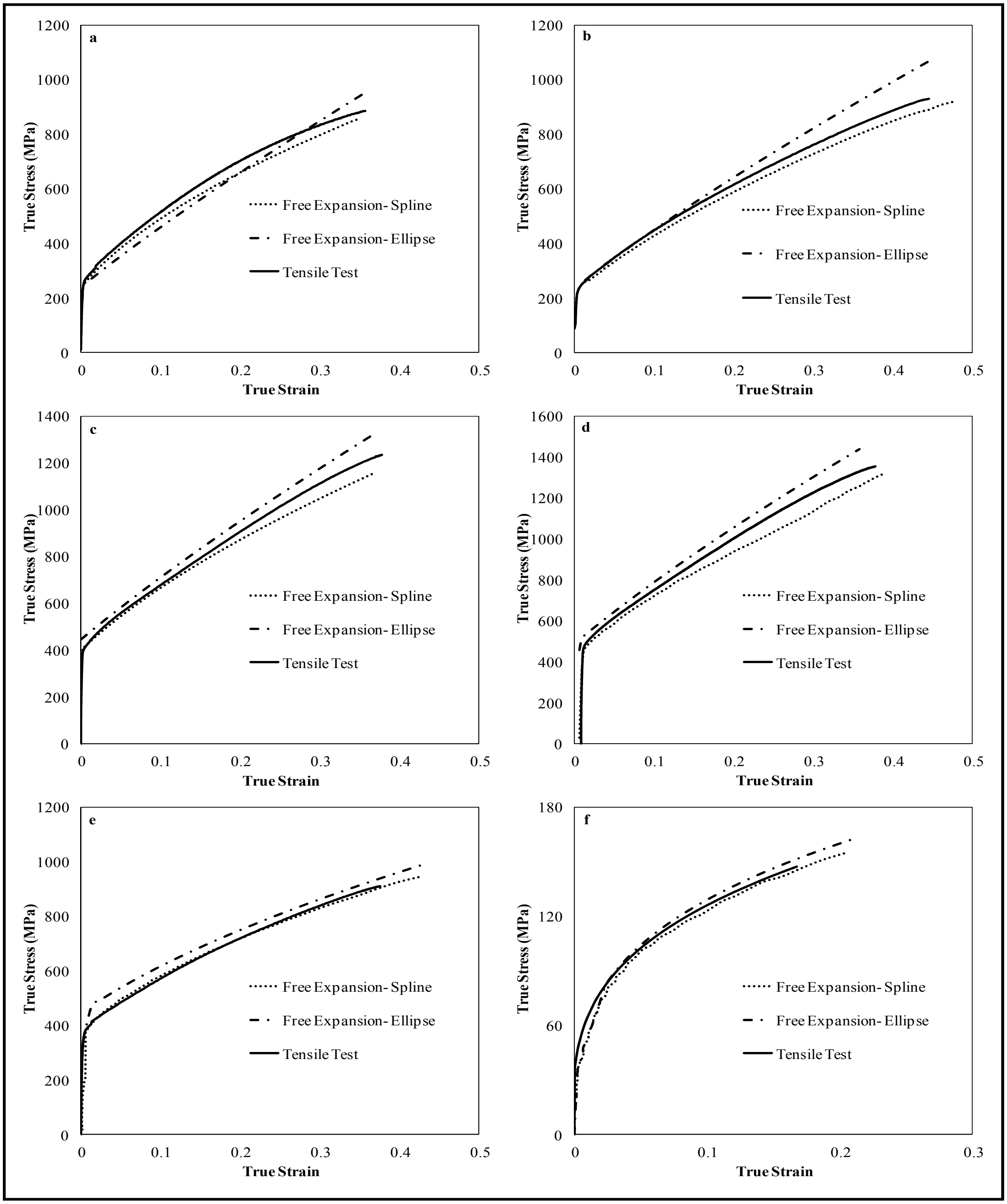

Figure 2.8: Comparison of the flow stress curves for (a) SS 321, 0.9 mm thickness, (b) SS 321, 1.2 mm thickness, (c) IN 718, 0.9 mm thickness, (d) IN 718, 1.2 mm thickness, (e) SS 304L, 1.6 mm thickness and (f) AA 6061-0, 3 mm thickness.

## Numerical validation

With the objective of verifying the accuracy of the proposed approach for obtaining the true stress-true strain curve of each material, results from the FE analysis of the free expansion test were compared to the experimental data. Specifically, a FE model of the free expansion test was developed and used to simulate the process for each material using the same geometrical dimensions and loading conditions applied during experimentation. Using the existing symmetry boundary conditions in the geometry, only one eighth of the die and tube materials were used in the model. Meshing was performed in ANSYS 12 software and the model was solved using LS-DYNA (V971 R6.1.2). Figure 2.9 shows the mesh used for the die and a tube in the FE analysis. A quadrilateral shell element with 5 integration points through the thickness was used for the model. The fully integrated advanced Belytschko (Belytschko (Belytschko, Lin and Chen-Shyh, 1984)) with the shell thickness change option activated was utilized as the shell element formulation. By varying the mesh size, it was found that 12,446 elements, with an aspect ratio of one for the initial (undeformed) tube, were sufficient to obtain a nearly mesh-independent solution with accurate results. The die was modeled as a rigid body and the tube as a deformable material. In the model, a surface-to-surface contact algorithm was applied to the interface between the tube and the die with Coulomb's friction set to 0.1 in accordance with different reported values in the literature for an unlubricated condition (Vollertsen and Plancak (Vollertsen and Plancak, 2002) and Abrantes (Abrantes, Szabo-Ponce and Batalha, 2005)). To mimic the experimental loading conditions in the FE model, the internal pressure was applied on each element of the meshed tube and increased linearly, whilst fixing the end nodes of the tube to emulate the no end feeding condition used during the free expansion process. The simulation results for the bulge height versus internal pressure were computed up to the maximum bulge height obtained experimentally. It is noteworthy that in the present work, the effect of anisotropy and, in the case of SS 304L only, the effect of the welded seam, on the mechanical response was not considered in the FE model of the free expansion process. To this end, the effective true stress-true stain data employed in the FE model were based on the formulations given in Table 2.2 (spline profile) for the different alloys studied in this work. To understand the influence of different material models on the FE simulation results, the uniaxial true stress-true strain curves, as formulated in Table 2.3 were also implemented in the free expansion model. In addition the influence of the bulge profile on the FE simulation results was considered using the formulations in Table 2.4 (elliptical profile).

The bulge height (h) versus internal pressure results, extracted from the simulations using the three sets of material constants (Table 2-2-Table 2-4), are compared with the experimental data (obtained from Aramis® and the hydroforming press) in Figure 2.10 for each alloy and thickness studied in this work. Based on the free expansion data using spline profile, the simulation results for each material is in good agreement with the experimental data, with errors less than 4% for all the burst pressures, as demonstrated in Table 2.5. It is noteworthy that for 1.2 mm thick IN 718, the general behavior, calculated from the FE simulation, however, deviates somewhat from the experimental data. In the case of AA 6061-0, the bulge height behavior deviates at intermediate pressures and this may be an effect of anisotropy in the material, the different material model (Hollomon) and/or the higher impact of any error at the low pressures. Regardless, the use of the material constants from the free expansion test with a spline profile showed a better prediction of the burst pressure for the cases considered in this work as demonstrated in Table 2.5, where $P_E$ is the experimental burst pressure, $P_{Fs}$ and $P_{Fe}$ are the predicted burst pressure based on free expansion data with spline and elliptical profiles, and $P_T$ is the predicted burst pressure obtained using the tensile data.

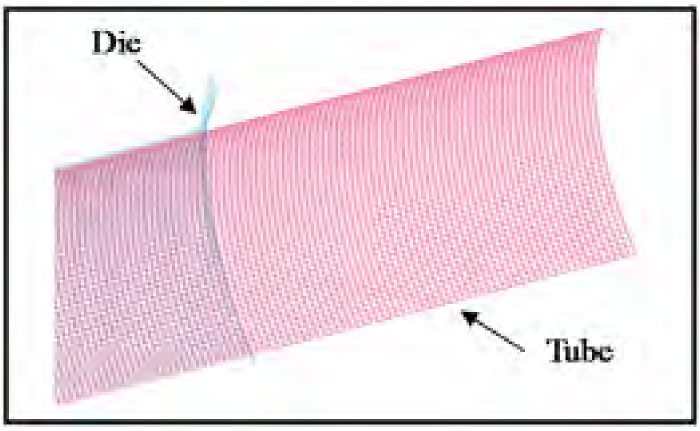

Figure 2.9: Mesh used in the FE modeling.

Table 2.5: Comparison of the predicted burst pressures calculated from the different material constants with the experimental data.

| Material | $P_E$ (MPa) | $P_{Fs}$ (MPa) | $P_{Fe}$ (MPa) | $P_T$ (MPa) | $Error_{Fs}$ (%) | $Error_{Fe}$ (%) | $Error_T$ (%) |
|---|---|---|---|---|---|---|---|
| SS 321 (0.9 mm) | 20.8 | 20.8 | 27.1 | 27.1 | 0.05 | 30 | 30 |
| SS 321 (1.2 mm) | 25.6 | 26.2 | 29.9 | 27.1 | 2.5 | 16.9 | 6 |
| IN 718 (0.9 mm) | 27.2 | 28.1 | 32.1 | 29.8 | 3.2 | 17.8 | 9.5 |
| IN 718 (1.2 mm) | 39.6 | 40.8 | 48.9 | 45.3 | 2.9 | 23.3 | 14 |
| SS 304L (1.6 mm) | 39.5 | 40.9 | 42.6 | 41.1 | 3.5 | 7.8 | 4 |
| AA 6061-0 (3 mm) | 8.7 | 8.9 | 9.1 | 8.53 | 2.5 | 4.9 | 1.6 |

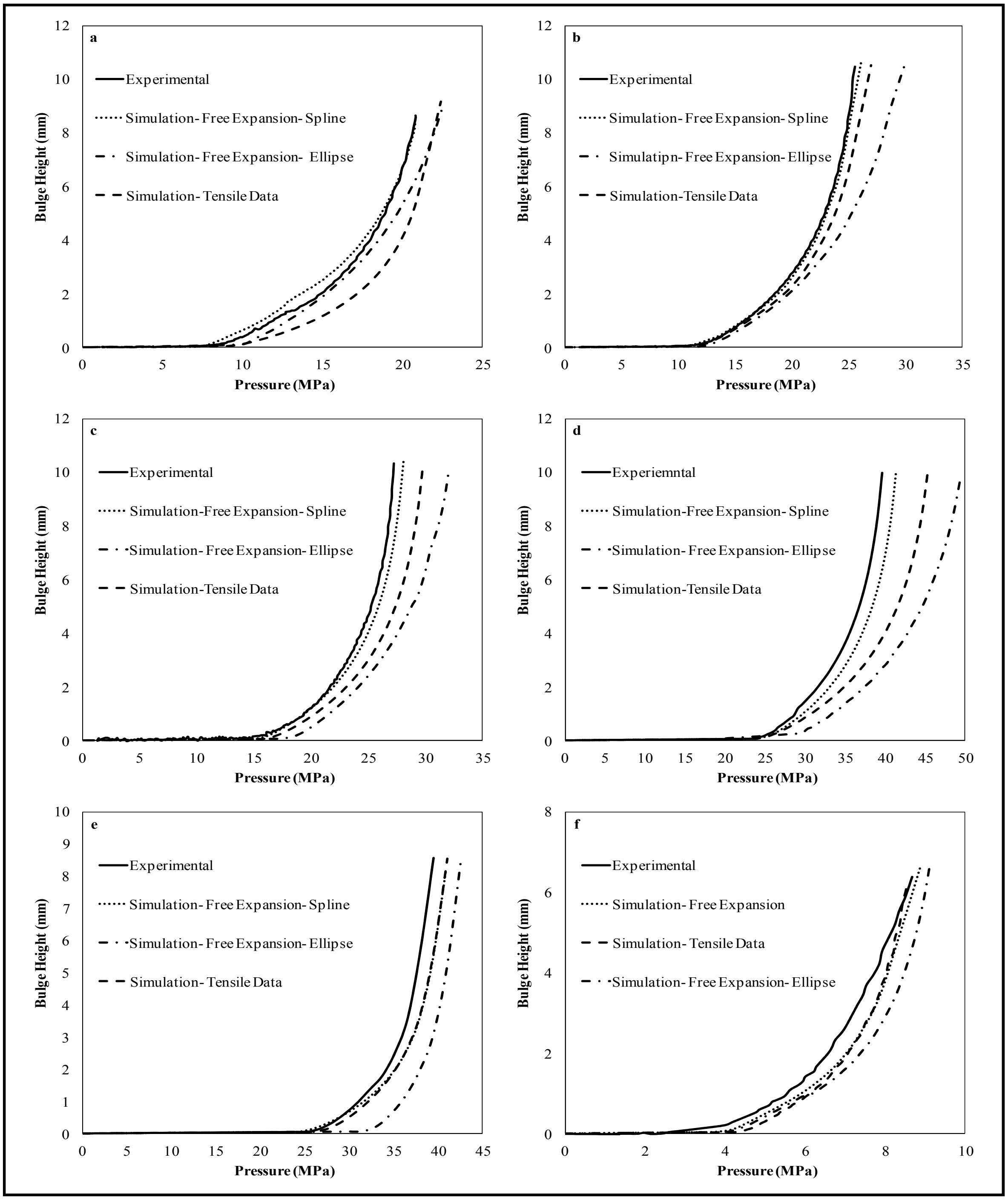

Figure 2.10: Maximum free expansion height versus internal pressure (a) SS 321, 0.9 mm thickness, (b) SS 321, 1.2 mm thickness, (c) IN 718, 0.9 mm thickness, (d) IN 718, 1.2 mm thickness, (e) SS 304L, 1.6 mm thickness and (f) AA 6061-0, 3 mm thickness.

## Conclusions

Based on the approach proposed in this work to determine the true stress-true strain curves of different aerospace materials using the free expansion test in conjunction with the Aramis® system, the following conclusions can be drawn:

- The true stress-true strain data was generated for different aerospace materials, and the data can help to design and FE model the THF process for aerospace applications.
- Compared to the interrupted test methods, online measurement of the curvature and the tube thickness at the maximum bulge height along with online calculation of longitudinal and circumferential strains highly reduced the experimentation required to calculate the true stress-true strain curves from free expansion testing.
- As observed from the response of the tested materials, the true stress-true strain curve generated using a 3rd order spline function definition for the bulge profile predicted better the material properties for the THF application.
- For each material, the simulation results of the internal pressure versus bulge height were within 4% of the experimental data when using the true stress-true strain curve from free expansion testing concomitantly with the approach proposed in this work.

# CHAPTER 3

## EXTENSION OF FLOW STRESS–STRAIN CURVES OF AEROSPACE ALLOYS AFTER NECKING

* This section has been submitted: M. Saboori, H. Champliaud, J. Gholipour, A. Gakwaya, J. Savoie, P. Wanjara, Extension of flow stress–strain curves of aerospace alloys after necking, Journal of Computational material science, Elsevier, submitted

To define accurately the expansion limits of aerospace materials, determination of the material behavior before and after the onset of necking, as well as the failure threshold are essential requirements. The plastic flow behavior before necking (pre-necking phase) has been fully identified by various mathematical models, such as Hollomon and Swift constitutive equations, but a criterion to satisfy the material behavior after necking (post-necking phase) is lacking. A suitable expression of the stress-strain model after necking can improve significantly the simulation results. A tool was developed to determine the true stress-strain curve for the post-necking regime of different aerospace alloys, such as inconel 718 (IN 718), stainless steel 321 (SS 321) and titanium (Ti6Al4V). Uniaxial tensile tests based on the ASTM E8M-11 standard were performed to determine the true stress-true strain behavior before necking. Two different methods, a weighted average method and a new hardening function were utilized to extend the true stress-true strain curve after necking. The two methods resulted in similar post-necking curves for the different materials, with consideration that the new hardening function could be used for more complicated hardening laws. The flow curves were employed in the simulation of the dome height test and then validated through experimentation. The simulation results were compared with the experimental data to verify the accuracy of the proposed methods in this work.

### Introduction

Application of finite element modeling in metal forming processes can reduce the lead time and the cost in the early phases of product development and can help to diagnose the possible manufacturing problems. The accuracy of the FE model depends on the accuracy of the input data, such as the material properties, friction condition and constitutive equations used in the finite element (FE) model. However, in the case of large plastic deformations, determination of the true stress-true strain curve is usually performed in the pre-necking phase of the tensile test. The post-necking phase is overlooked in most cases as the deformation becomes localized and occurs in a small region, i.e. the uniform stress state vanishes after the neck. The material behavior up to the onset of necking has been defined by different constitutive models, but a good knowledge of the material behavior after necking has not been fully addressed yet. Knowing the material behavior after necking is essential for performing accurate FE modeling of metal forming processes (Cooreman et al., 2007). Conventionally, two types of tests are used to determine the flow stress-strain curve for finite element (FE) modeling of hydroforming processes: (i) standard tensile testing and (ii) tube bulge testing. In both tests, the material behavior up to the onset of the neck is plotted, as plastic instability starts after this point. The work hardening behavior after necking is usually estimated by extrapolating the pre-neck stress-strain curve by considering the tangency condition at the neck point. However, this curve is not unique, as the slope of the extrapolated curve can change dramatically, resulting in a wide range of stress-strain behaviors after necking phase, which can highly affect the simulation results. Efforts to attain increased reliability for the material behavior after necking, either through tensile or bulge testing, is essential for increasing the accuracy of the FE modeling.

A pioneering theoretical model for determining the post-neck flow behavior was conducted by Bridgman (Bridgman, 1952) in 1952. Bridgman developed a method to calculate the true stress-true strain curve after necking for round specimens. This method required continuous measurement of the diameter and curvature changes at the neck region. More recently, Mirone (Mirone, 2004) and Boehme (Bohme et al., 1992) used an imaging technique to evaluate the neck curvature during tensile testing for the Bridgman method. This technique was based on measuring the evolving geometrical parameters of the neck profile, which required a significant amount of effort associated with the curve fitting procedure in the correlated images. It is noteworthy that these procedures cannot be applied to a flat specimen with a rectangular cross section. Later, an alternative analytical procedure was introduced by Zhang (Zhang et al., 1999) for flat tensile specimens. However, the validation of this method was limited to specimens with a cross-sectional aspect ratio (width/thickness) of greater or equal to eight. Ling (Ling, 1996) successively formulated the Zhang approach using a weighted average method with the Holloman hardening law for a copper alloy. Koç, and Zhang (Koc and Štok, 2004; Zhano and Li, 1994) combined FE modeling of the tensile test with experimental measurements to determine the material behavior after necking. In their approach, the material parameters were calibrated by iterative simulations of the tensile test, but, a significant amount of simulations were required to attain suitable stress-strain data after the neck. In a more recent work, Saboori (Saboori et al., 2012b) used a weighted average method in conjunction with the Swift and linear hardening laws to simulate uniaxial tensile testing of SS 321 to extend the flow stress-strain curve after the necking point. In their work, the flow behavior of the material was derived from an iterative FE modeling methodology of the experimental procedure (tensile testing) and comparing the predicted load-displacement values with the experimental data.

Presently, the knowledge on formability of aerospace materials is quite limited. One of the objectives of this section is to address this issue through an understanding of how to accurately determine the mechanical properties of some aerospace alloys, such as IN 718, Ti6Al4V and SS 321, after the onset of necking by developing a methodology based on uniaxial tensile testing. Another objective of this section is to develop a procedure/method that can be applied to all types of uniaxial tensile specimens (flat and round). Two semi-analytical methods, weighted average and new hardening are proposed to determine the flow behavior after necking. As will be shown in the following sections, the application of the weighted average method in FE modeling is simpler, but this method cannot be used for an exponential hardening function due to the complexity of the analytical procedure. On the other hand, the new hardening approach can work with all types of hardening functions, and also with a pointwise stress-strain curve, to obtain the material behavior after necking. Both methods utilize FE modeling of tensile test as a tool to obtain the predicted load-displacement results, which are then compared with the experimental data. This comparison is also used to assess the accuracy of each method. In the following sections, a description of the analytical procedure for the weighted average method developed in this study is described and a new hardening equation is also introduced. Then, the experimental procedure and the FE simulation results are presented. To this end, the new hardening approach was utilized in a case study of the dome height test followed by a discussion and conclusions.

## Analytical Procedure

### Weighted average method

In conventional tensile testing, plastic instability occurs just after the maximum load. At this point, strain localization starts by diffuse necking that may continue up to fracture (Korhonen and Manninen, 2008) or until the development of a localized neck, which then leads to fracture. Up to the maximum load, the load-displacement data can be converted into true stress-true strain. The most widely used constitutive equations for representing the material behavior in numerical or analytical models of a tube hydroforming process (THF) are Hollomon, Swift, Ludwik and Voce. Based on previous studies on IN 718 and SS 321 (Saboori et al., 2014a) for the pre-neck region, it was shown that the Swift hardening law (Eq. 3.1) can predict the experimental data better than the Holloman hardening law (Eq. 3.2).

$$\bar{\sigma} = k_s(\varepsilon_0 + \bar{\varepsilon}_p)^{n_s} \tag{3.1}$$

$$\bar{\sigma} = k_h(\bar{\varepsilon})^{n_h} \tag{3.2}$$

where $\bar{\varepsilon}$ is the effective strain, $\bar{\sigma}$ is the effective stress, $n_s$ and $nh$ are work hardening exponents for the Swift and the Hollomon constitutive equations, respectively, and $ks$, $kh$ and $\varepsilon_0$ are material constants that are determined from the experimental data. During tensile testing, as the material starts to deform plastically, the strain distribution is uniform up the onset of the neck at which point the tensile load reaches a maximum value. Beyond this point, the load bearing capacity of the specimen reduces and increasing strains cause higher stresses in a localized region. According to the Considère's criterion, the onset of diffuse necking is reached when the tensile load, *F*, reaches a maximum point and further small changes in the load, *dF*, can be calculated as follows (Considère, 1870):

$$dF = dA\bar{\sigma} + Ad\bar{\sigma} = 0 \tag{3.3}$$

So:

$$-\frac{d\bar{\sigma}}{\bar{\sigma}} = \frac{dA}{A} \tag{3.4}$$

with the assumption of volume constancy of the test piece:
$\frac{dA}{A} = -\frac{dl}{l} = d\bar{\varepsilon}$ (true strain) and Eq. 3.4 becomes: $-\frac{d\bar{\sigma}}{\bar{\sigma}} = \frac{dA}{A} = d\bar{\varepsilon}$ from which it can be

$$\frac{d\bar{\sigma}}{d\bar{\varepsilon}} = \bar{\sigma} \tag{3.5}$$

where $A$ is the cross sectional area of the sample at the gauge length. By applying Eq. 3.5 to the Swift hardening law the instability curve can be calculated as follows:

$$\frac{d\bar{\sigma}}{d\bar{\varepsilon}} = \frac{n_s\bar{\sigma}}{\varepsilon_0 + \bar{\varepsilon}} \tag{3.6}$$

at the neck, $\bar{\sigma} = \bar{\sigma}_{neck}$ and $\bar{\varepsilon} = \bar{\varepsilon}_{neck}$, where $\bar{\sigma}_{neck}$ and $\bar{\varepsilon}_{neck}$ are the effective stress and the effective strain at the neck, respectively. Swift's constants at the onset of necking are determined by Eq. 3.6 as follow:

$$n_s = \bar{\varepsilon}_0 + \bar{\varepsilon}_{neck} \tag{3.7}$$

$$K_s = \frac{\bar{\sigma}_{neck}}{(\bar{\varepsilon}_0 + \bar{\varepsilon}_{neck})^{\bar{\varepsilon}_0 + \bar{\varepsilon}_{neck}}} \tag{3.8}$$

After the onset of necking, strains and stresses no longer vary proportionally and additional strains concentrate in a narrow band. This is an ideal condition for localized necking, which can be followed by fracture. By substituting Eq. 3.7 and Eq. 3.8, in Eq. 3.1, the Swift law becomes:

$$\bar{\sigma} = \bar{\sigma}_{neck} \frac{(\bar{\varepsilon}_0 + \bar{\varepsilon})^{\bar{\varepsilon}_0 + \bar{\varepsilon}_{neck}}}{(\bar{\varepsilon}_0 + \bar{\varepsilon}_{neck})^{\varepsilon_0 + \bar{\varepsilon}_{neck}}} \tag{3.9}$$

Following the same procedure used for the Swift law, it is possible to find $n_h$ and $k_h$ for the Holloman law, and by substituting, Eq. 2, it becomes (Considère, 1870):

$$\bar{\sigma} = \bar{\sigma}_{neck} \frac{(\bar{\varepsilon})^{\bar{\varepsilon}_{neck}}}{(\bar{\varepsilon}_{neck})^{\bar{\varepsilon}_{neck}}} \tag{3.10}$$

Figure 3.1 illustrates the material behavior for 0.9 mm thick IN 718 that was extrapolated using the Swift and the Hollomon work hardening equations. As shown in this figure, the work hardening rate in the Hollomon curve decreases slightly beyond the neck in comparison with the Swift curve, which increases slightly; this condition is similar for all the other materials studied in this research. Saboori (Saboori et al., 2012b) have shown that these slight differences after necking influence the FE modeling results for free expansion of SS 321.

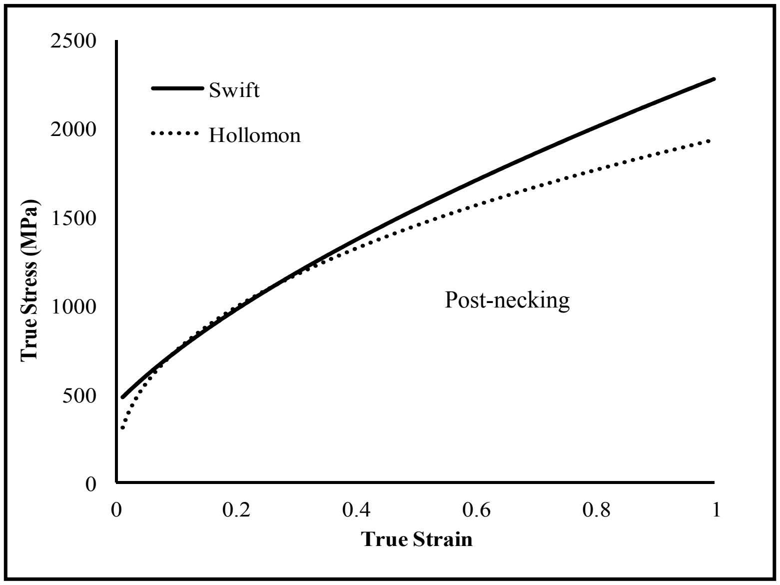

Figure 3.1: True stress-true strain curve for Hollomon and Swift work-hardening extrapolations.

In this study, to predict accurately the behavior of some aerospace materials, the extrapolation with the Swift law was considered as the upper bound and the Hollomon law was considered as the lower bound of the material response. Therefore, the plastic behavior of the material was derived based on the consideration that it was to be limited between these two bounds. The target material flow curve for post-necking can be given by combining equations (3.9) and (3.10) as follows:

$$\bar{\sigma} = \bar{\sigma}_{neck}\left[(1-\alpha)(\frac{\bar{\varepsilon}}{\bar{\varepsilon}_{neck}})^{\bar{\varepsilon}_{neck}} + \alpha\left(\frac{\bar{\varepsilon}_0+\bar{\varepsilon}}{\bar{\varepsilon}_0+\bar{\varepsilon}_{neck}}\right)^{\bar{\varepsilon}_0+\bar{\varepsilon}_{neck}}\right] \tag{3.11}$$

where $\alpha$ is a weight constant ($0 \leq \alpha \leq 1$). When $\alpha = 1$, Eq. 3.11 represents the Swift extrapolation and when $\alpha = 0$, it represents the Hollomon extrapolation. The weight constant $\alpha$ can be determined by minimizing the error between the experimental load and the load obtained from the FE model at the same displacement. Figure 3.2 illustrates the flowcharts used for both methods in this study. The solid lines in this figure present the flowchart for the weighted average method. Here, first the experimental load vs displacement $(F_i^{exp}, \Delta L)$ curve of the tensile test was extracted from the data acquisition system of the tensile equipment. Then, material constants for Swift and Hollomon were determined using the least squares curve fitting method available in the Matlab software. The simulation of the tensile test was performed in the LS-DYNA software for $\alpha = 0$ and $\alpha = 1$ to obtain the predicted load vs displacement for the lower and upper bounds, respectively. The program starts with $\alpha = 0$, which is the value for the Hollomon extrapolation. The program stops when the summation of square errors between the experimental and numerical loads, $\delta$, reaches a set value ($\delta \leq 10^{-3}$ in this study). If the condition for $\delta$ is not satisfied, the program goes through the next iteration by changing the value of $\alpha$, using the Lsqnonlin optimization function in the Matlab software.

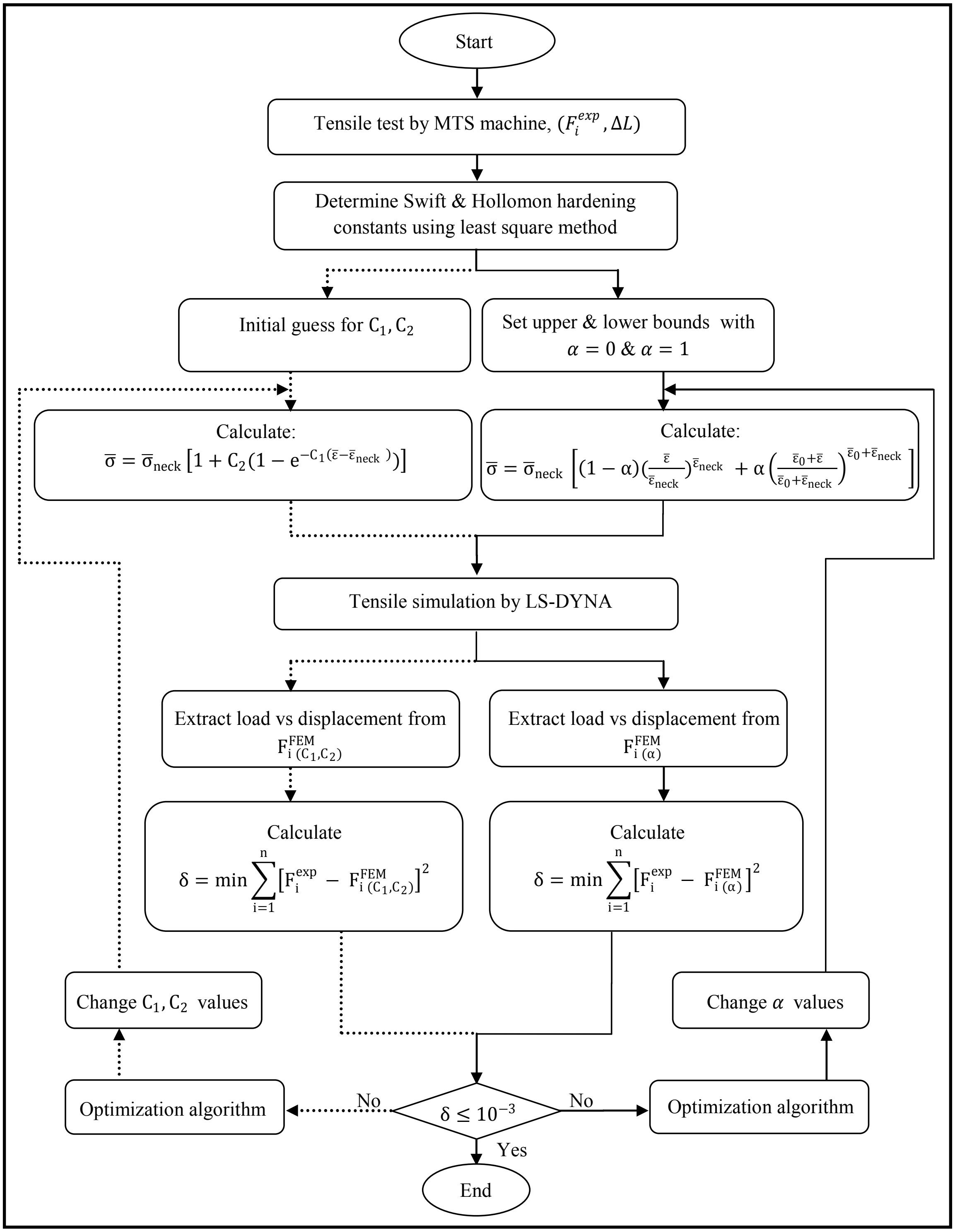

Figure 3.2: Flowchart for the weighted average method (solid line) and the new hardening function (dotted line).

### 3.1.1 New hardening function

Due to complexity in extracting the derivations required in the weighted average method for some exponential work hardening laws, such as Voce, the aforementioned method cannot be used to extrapolate the flow curve in the post-necking region. For this reason a second approach was developed based on the method proposed by Hockett-Sherby (Hockett and Sherby, 1975), Here, at large strains, the true stress-true strain curve has a steady-state condition. Furthermore, similar to other metallic alloys, in the region between the onset of necking and the steady-state condition, experimental results showed that the slope in the stress-strain curve ($\frac{d\bar{\sigma}}{d\bar{\varepsilon}}$) continuously decreases and reaches a state in which $\frac{d\bar{\sigma}}{d\bar{\varepsilon}} = 0$. Hence, to characterize this region, i.e. between the onset of necking and the steady-state condition of the stress-strain curve, the following relation can be considered (Hockett and Sherby, 1975; Saboori et al., 2013a).

$$\bar{\sigma} = \bar{\sigma}_s - \mu(\bar{\sigma}_s - \bar{\sigma}_{neck}) \tag{3.12}$$

where $\sigma_s$, is the steady-state flow stress and $\sigma_{neck}$ is the stress at the onset of necking. μ is a factor that is equal to unity at $\bar{\sigma} = \bar{\sigma}_{neck}$ or when $\bar{\varepsilon} = \bar{\varepsilon}_{neck}$ and that tends to zero at $\bar{\sigma} = \bar{\sigma}_s$ or when the strain approaches infinity (or relatively large values). A simple relation for μ that can satisfy these requirements at the onset of necking and for the regime beyond the neck is as follow:

$$\mu = \exp(-C_1(\bar{\varepsilon} - \bar{\varepsilon}_{neck})) \tag{3.13}$$

where $C_1$ is the material constant. It is noteworthy that in the above equation, when $\bar{\varepsilon} = \bar{\varepsilon}_{neck}$ the μ value is equal to unity and if $\varepsilon = \infty$ then μ is equal to zero.

If Eq. 3.12 is rewritten based on Eq. 3.13, then for the described boundary condition and the steady-state condition proposed by Hochett-Sherby (Hockett and Sherby, 1975), a new hardening function for determining the behavior of the material for post-necking can be developed as follows:

$$\bar{\sigma} = \bar{\sigma}_{neck}[(1 + C_2) - C_2\mu] \tag{3.14}$$

where $C_2$ is a material constant. By incorporating Eq. 3.13 into Eq. 3.14, the following exponential work hardening relationship can be obtained as:

$$\bar{\sigma} = \bar{\sigma}_{neck}\left[1 + C_2\left(1 - e^{-C_1(\bar{\varepsilon} - \bar{\varepsilon}_{neck})}\right)\right] \tag{3.15}$$

In the above equations, $C_1$ and $C_2$ are two constants that are calculated during the minimization process, as described by the dotted line in Figure 3.2. The advantage of this approach is that there is no requirement to start with a well known hardening law, such as Swift or Hollomon, as was the case for the weighted average method.

### Test Procedure to calculate *α*, *C1* and *C2*

In order to verify the accuracy of the stress and strain distribution in the models, a MTS 810 machine in conjunction with a laser extensometer and an optical deformation measurement system, Aramis®, was used to conduct the tensile tests. Figure 3.3 illustrates the experimental setup and Figure 3.4 shows a tensile specimen that was painted with a random pattern. The Aramis® system uses this random pattern, applied to the surface of the target object, to create features that act as strain gages, which are then employed in calculating the strain distribution. The FE model of the tensile test was prepared for each material thickness using eight node solid elements. A mesh size study was performed and it was found that a model consisting of 12,500 elements with an aspect ratio of one, and three elements through the material thickness was sufficient to obtain a mesh-independent solution. With this mesh size, at the displacement range when necking started during experimentation, the model showed a reduction in the cross section, mimicking the onset of necking. The model was solved using LS-DYNA (V971 R6.1.2). Table 3.1 shows the mechanical properties for each material used in the FE model and Table 3.2 presents the Swift work hardening law constants. In the FE model, one end of the specimen was fixed and the displacement was applied to the opposite end to simulate an actual tensile test procedure performed under displacement control. The stress-strain behavior for post-necking was calculated for the two methods using Eq. 3.11 and Eq. 3.15. For each method, the predicted load vs displacement curve was extracted from the FE model and compared to the experimental data. The true stress-strain and the load-displacement data obtained from the data acquisition system of the MTS tensile testing system were used in the procedure presented in Figure 3.3.

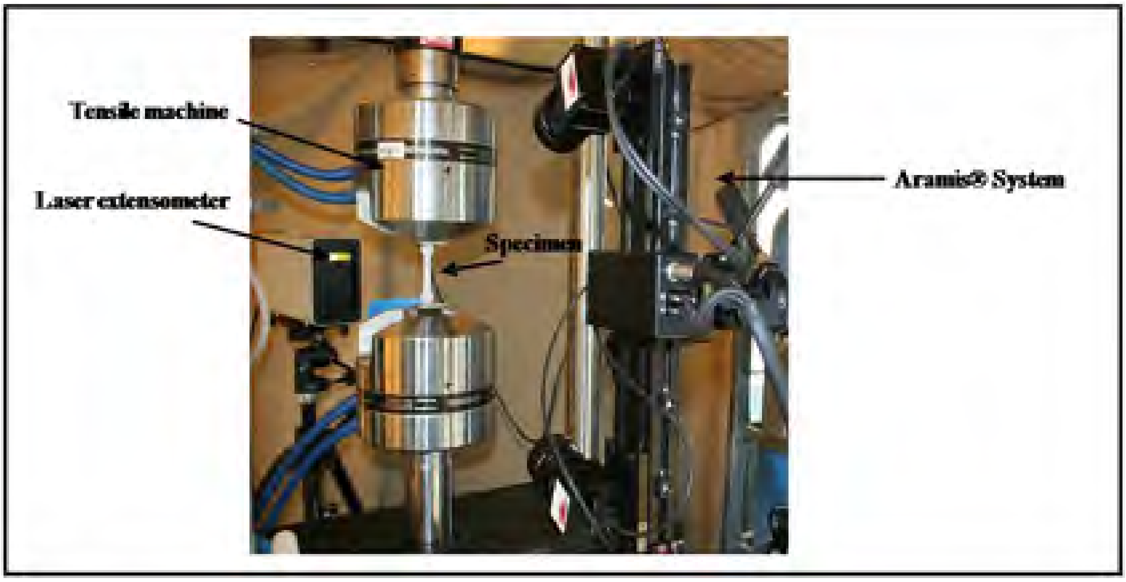

Figure 3.3: An experimental apparatus for free expansion tests.

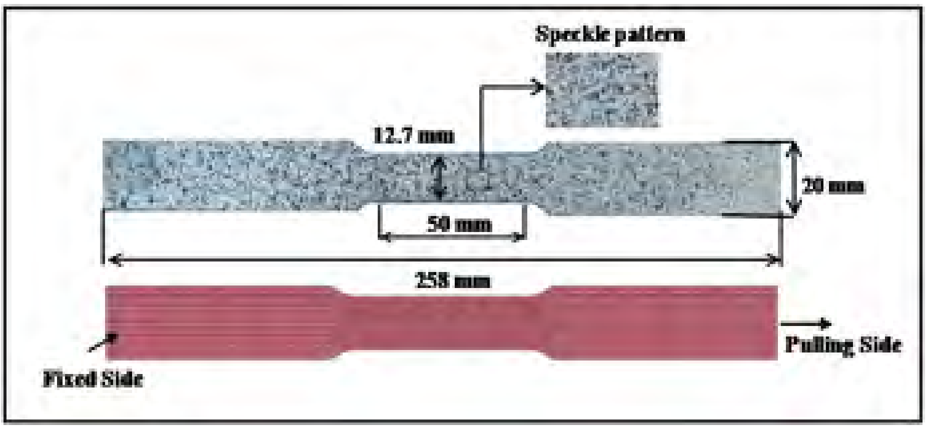

Figure 3.4: Specimen used for uniaxial tensile testing and the mesh used for FE modeling.

Table 3.1: Mechanical properties for annealed materials.

| **Material** | **Elastic Modulus (GPa)** | **Yield Strength (MPa)** |
|---|---|---|
| IN 718 | 204 | 440 |
| Ti6Al4V | 110 | 880 |
| SS 321 (0.9 mm thick) | 193 | 250 |
| SS 321 (1.2 mm thick) | 193 | 260 |

Table 3.2: Swift work hardening constants for IN 718, Ti6Al4V and SS 321.

| **Material** | $k$ | $n$ | $\varepsilon_0$ |
|---|---|---|---|
| IN 718 (0.9 mm thick) | 2053.4 | 0.62 | 0.071 |
| Ti6Al4V | 1598.3 | 0.47 | 0.02 |
| SS 321 (0.9 mm thick) | 1492.4 | 0.49 | 0.021 |
| SS 321 (1.2 mm thick) | 1461.5 | 0.62 | 0.048 |

## Results and discussions

### 3.1.2 Weighted-average and new hardening methods

The weighted average method and the new hardening function were used to estimate the true stress-true strain curves for the post-necking region of different aerospace materials. Figure 3.5 compares the extrapolated curves obtained from the two approaches presented in this study (Figure 3.2) along with the curves obtained from the Swift and Hollomon laws (the upper and lower bounds). As seen from this figure, the weighted average method and the new hardening function are very close to each other and in good agreement for the extrapolated region. Table 3.3 ssummarizes the $\alpha$, $C_1$ and $C_2$ values for all materials tested in this study. Figure 3.6 shows the experimental load-displacement data along with the predicted simulation results obtained from the α values presented in Table 3.3 for IN 718, Ti6Al4V and SS 321 materials. In addition, the predicted results based on the Swift and Hollomon curves are presented for the pre- and post-necking conditions. As seen in Figure 3.6, after necking, the predicted results using the Swift and the Hollomon laws deviate considerably from the experimental data.

Table 3.3: New extrapolation hardening constants for after necking for IN 718, Ti6Al4V and SS 321.

| **Material** | **Thickness(mm)** | $\alpha$ | $C_1$ | $C_2$ |
|---|---|---|---|---|
| IN 718 | 0.9 | 0.33 | 0.55 | 1.77 |
| Ti6Al4V | 2 | 0.26 | 0.68 | 1.83 |
| SS 321 | 0.9 | 0.6 | 0.46 | 1.91 |
| SS 321 | 1.2 | 0.66 | 0.73 | 1.3 |

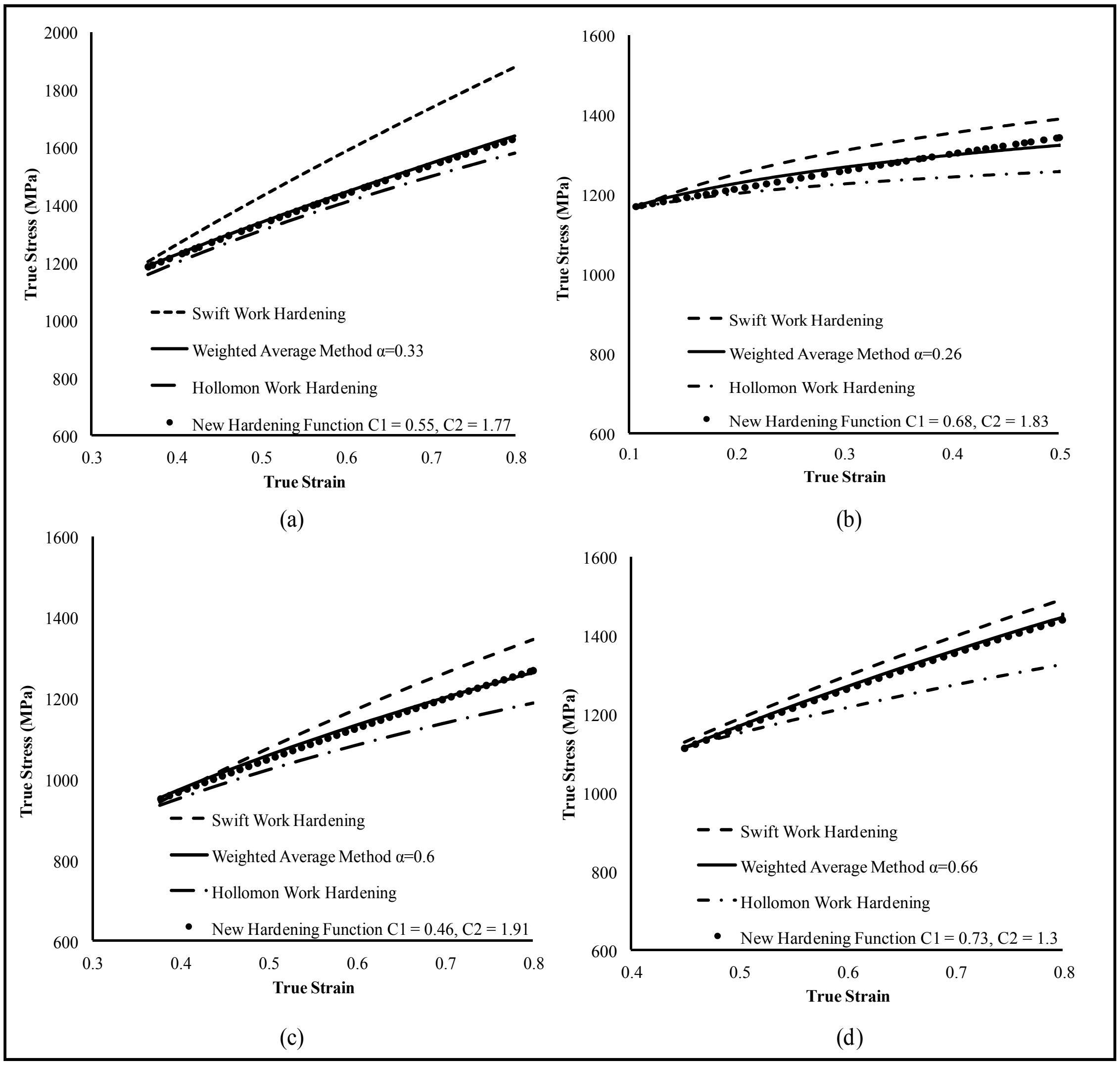

Figure 3.5: Comparison of true stress-true strain curves for post-necking phases (a) IN 718, (b) 2 mm Ti6Al4V, (c) 0.9 mm SS 321, (d) 1.2 mm SS 321.

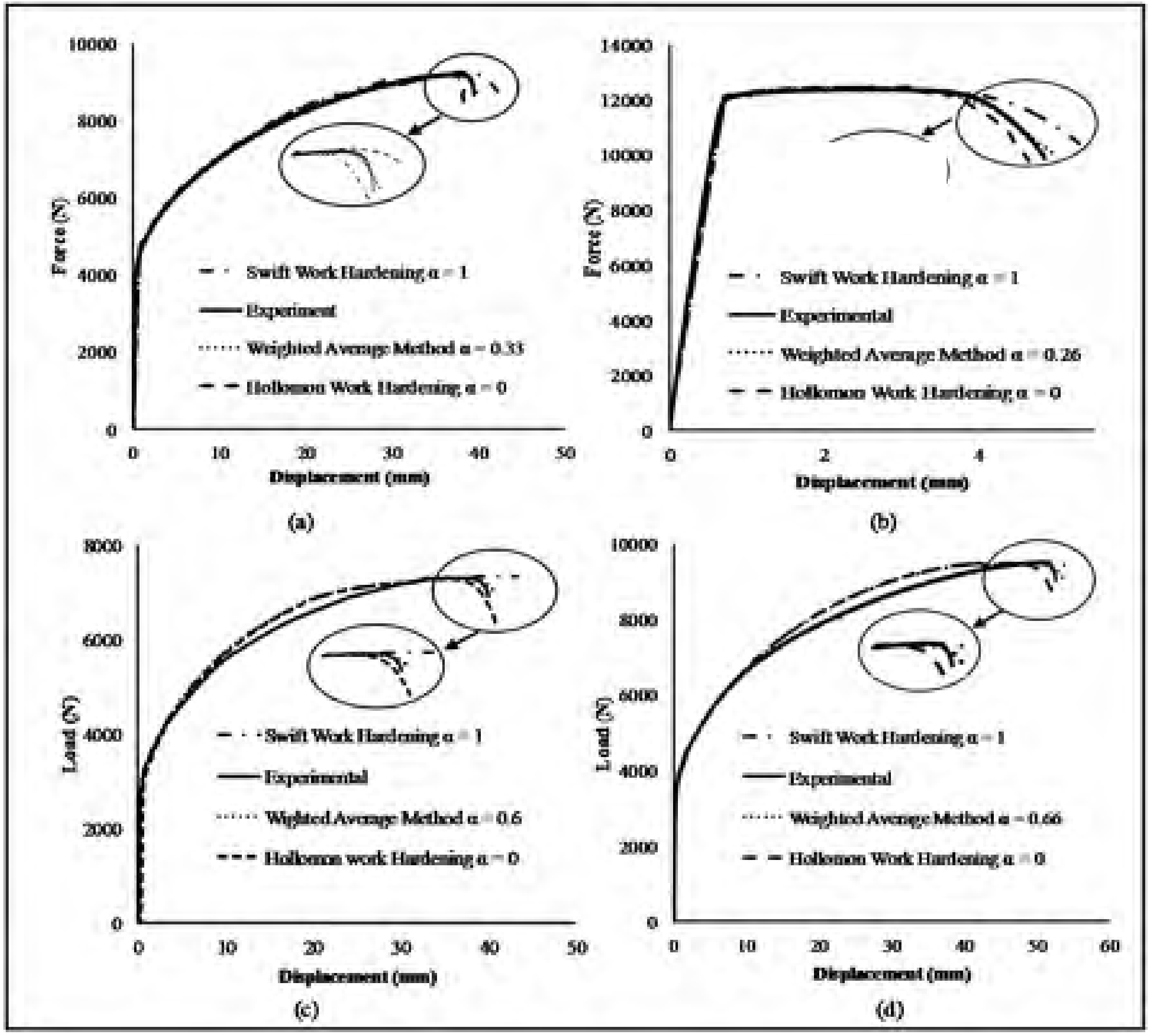

Figure 3.6: Comparison of load-displacement curves for: (a) IN 718, (b) Ti6Al4V, (c) 0.9 mm SS 321, (d) 1.2 mm SS 321.

Knowing of the α value in Eq. 3.11 or $C_1$ and $C_2$ constants in Eq. 3.15 allows the determination of the true stress-true strain after necking region. The results presented in Figure 3.6 show that the true stress-true strain curves obtained from the weighted average method and the new hardening function can predict the load-displacement with high accuracy.

It is noteworthy that it is difficult to obtain the local values of the strains and stresses at the neck region, especially for thin specimens. Therefore, without this approach, applying the conventional work hardening laws in the FE model is ineffective in capturing the descending trend in the experimental load-displacement curve after the neck. Also, unlike the proposed methods, a true stress-true strain relation, defined by conventional hardening laws, is neither suitable for damage modeling of metal forming processes nor modeling of the bi-axial forming conditions, such as bulge testing of tubes or sheets.

### 3.1.3 Validation of the new methodology

As mentioned before, the weighted average method and the new hardening function are in good agreement in the extrapolated region (Figure 3.5). For this reason, to validate the proposed methods, only the new hardening function was utilized. The material constants ($C_1$ and $C_2$), presented in Table 3.3, were implemented in the FE model to predict the punch-displacement of the 0.9 mm and 1.2 mm thick SS 321 and 0.9 mm thick Inconel 718 in a dome height testing process. The material was considered as isotropic elastic-plastic in the FE model Figure 3.7.a shows the FE model used to simulate the process, in which, due to symmetry conditions, only one quarter of the model was utilized. The simulation was performed in two steps. First the blank holder was moved in the z-direction to clamp the sheet metal between the blank holder and the die. Then, the hemi-spherical punch was displaced in the z-direction until a given displacement was reached. Meshing was performed in ANSYS 12 software and the model was solved using LS-DYNA (V971 R6.1.2). Figure 3.7.b shows the deformed sheets after experimentation. The sheets were flat and had different widths (12.7 mm, 50.8 mm, 76.2 mm, 127 mm and 177.8 mm) at the beginning of the process. In the model, a quadrilateral shell element with 5 integration points through the thickness was used for the sheet. The tooling (die, punch and the blank holder) were considered as a rigid body in the model. A mesh size study was performed and it was found that a model with 25,000 elements and an aspect ratio of one for the undeformed sheet was sufficient to obtain a mesh-independent solution. A fully integrated advanced Belytschko (Belytschko, Lin and Chen-Shyh, 1984) with the shell thickness change option activated was utilized as the shell element formulation. A surface-to-surface contact algorithm was applied to the contacting surface. Coulomb's friction was set to 0.15 in accordance with different reported values in literature for an unlubricated condition (Lou et al., 2012; Zhalehfar et al., 2013). After simulation, predicted punch-displacement results were extracted based on the Swift, Hollomon and the new hardening law and were compared with the experimental results. Table 3.4 summarizes all the results along with the error for each material model. Here, the simulations were stopped when the major strain in the simulation reached the strain value measured adjacent to the fracture location in the experiments. As demonstrated in Table 3.4, the Swift and Hollomon hardening laws respectively underestimate and overestimate the punch-displacements. In contrast, the new hardening function can predict the punch-displacement with higher accuracy, i.e. with less than 2.6% error, for all the specimens tested in this study.

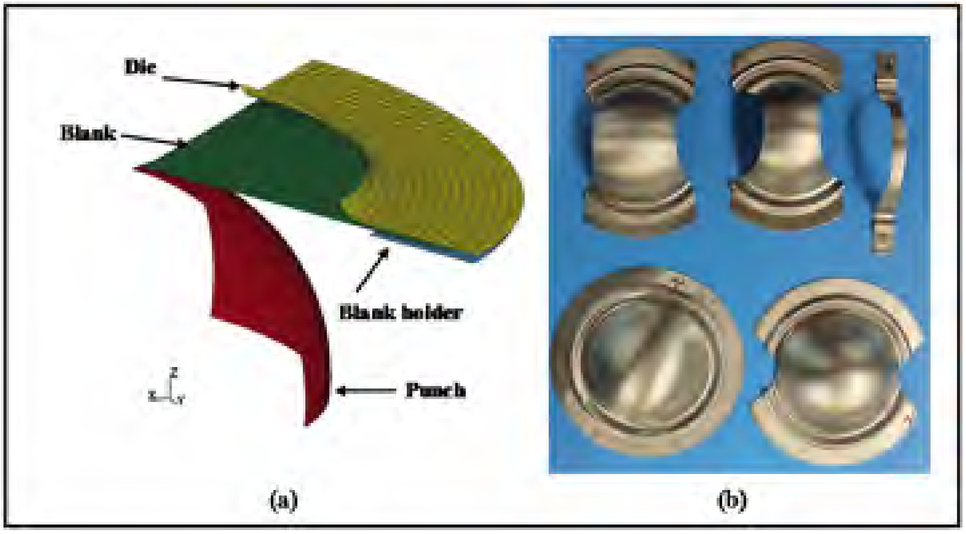

Figure 3.7: FE modeling of dome height test and deformed shapes of specimens of SS 321.

Table 3.4: Comparison of the punch-displacement for SS 321 and IN 718.

| **Material** | **Size (mm)** | **Swift (mm)** | **Hollomon (mm)** | **NHF (mm)** | **Experiment (mm)** | **Error (%) between prediction and experimental** | | |
|---|---|---|---|---|---|---|---|---|
| | | | | | | **Swift** | **Hollomon** | **NHF** |
| SS 321 (0.9 mm) | 12.7 | 24.3 | 28.9 | 27.0 | $27.3^{+0.4}_{-0.4}$ | -11.0 | 5.9 | -1.1 |
| | 50.8 | 46.5 | 55.8 | 51.7 | $52.2^{+0.2}_{-0.2}$ | -11.0 | 6.9 | -1.0 |
| | 76.2 | 46.0 | 53.0 | 50.0 | $49.6^{+0.1}_{-0.2}$ | -7.3 | 6.8 | -0.8 |
| | 127.0 | 38.1 | 46.4 | 43.4 | $43.0^{+0.4}_{-0.1}$ | -11.4 | 7.9 | 0.9 |
| | 177.8 | 51.5 | 58.5 | 55.3 | $55.0^{+1.1}_{-0.7}$ | -6.4 | 6.3 | 0.5 |
| SS 321 (1.2 mm) | 12.7 | 24.7 | 29.0 | 27.0 | $27.3^{+0.3}_{-0.4}$ | -9.5 | 6.2 | -1.1 |
| | 50.8 | 46.7 | 54.2 | 52.0 | $51.0^{+0.2}_{-0.3}$ | -8.4 | 6.3 | 1.9 |
| | 76.2 | 46.5 | 52.5 | 48.5 | $49.6^{+0.1}_{-0.2}$ | -6.3 | 5.8 | -2.2 |
| | 127.0 | 39.0 | 45.4 | 44.1 | $43.7^{+0.3}_{-0.1}$ | -10.7 | 3.9 | 0.9 |
| | 177.8 | 49.2 | 55.0 | 50.8 | $52.3^{+1}_{-0.7}$ | -5.9 | 5.2 | -2.6 |
| IN 718 (0.9 mm) | 12.7 | 23.8 | 29.0 | 27.0 | $27.3^{+0.15}_{-0.5}$ | -8.1 | 6.2 | -0.3 |
| | 50.8 | 38.7 | 44.1 | 42.3 | $42.9^{+1.1}_{-0.5}$ | -6.5 | 2.8 | -0.6 |
| | 76.2 | 40.2 | 44.6 | 42.0 | $42.2^{+1.7}_{-4.7}$ | -4.7 | 5.7 | -0.2 |
| | 127.0 | 34.1 | 38.5 | 35.7 | $36.5^{+0.3}_{-0.3}$ | -6.6 | 5.5 | -0.8 |
| | 177.8 | 41.7 | 49.2 | 43.0 | $44.0^{+1.5}_{-1.3}$ | -5.2 | 7.3 | -1.0 |

Note: NHF = new hardening function

## Conclusions

Based on the approach proposed in this work to determine the true stress-true strain curve of different aerospace materials using the weighted average method and a new hardening function, the following conclusions can be drawn:

- Compared to the conventional methods, the proposed procedures are simpler for finding the material behavior after necking.
- As investigated, the simulation results for the punch-displacement of the dome height test were within 2.6% of the experimental data, when using the extrapolated true stress-true strain curves from the new hardening function proposed in this section.
- The true stress-true strain curves in the post-necking region of several aerospace materials were determined using the proposed approaches (Figure 3.2) and the curves were validated through experimentation with dome height testing.
- The finite element models assumed isotropic behavior for each material and future work is required to include the effect of anisotropy.

# CHAPTER 4

## BURSTING FAILURE LIMIT PREDICTION OF TUBE HYDROFORMING BASED ON A NEW DUCTILE FRACTURE CRITERION FOR AEROSPACE ALLOY

* This section has been submitted to the Journal of Computational material science: M. Saboori, H. Champliaud, J. Gholipour, A. Gakwaya, J. Savoie, P. Wanjara, Extension of flow stress–strain curves of aerospace alloys after necking.

Tube hydroforming (THF) of aerospace components and materials without any defect, such as wrinkling, buckling and bursting encounter many difficulties. In contrast to wrinkling failure, bursting failure is irrecoverable. To achieve an accurate prediction of the bursting failure and forming limit diagram at fracture (FLDf) in THF of aerospace materials, a new ductile fracture initiation criterion is proposed through a new user material model in the 3D finite element software LS-DYNA. The new ductile fracture criterion is based on the effect of stress triaxiality, stress concentration factor and effective plastic strain on the nucleation, growth and coalescence of voids. To evaluate the accuracy of the new material model, some different ductile approaches were considered and compared with each other (Cockcroft, Oh, Brozzo, Oyane and Ko criteria) through a new user materials in LS-DYNA commercial software. Bursting points and the FLDf of different aerospace alloys, such as stainless steel 321 (SS 321) and inconel 718 (IN 718) were generated and compared with the experiments. The new fracture criterion was found to be successful to predict accurately the bursting points and FLDf of the tested materials.

### Introduction

The reliable numerical simulation of the THF process of aerospace materials depends on correct prediction of possible damage or failures in this process. Although the use of finite element analysis (FEA) for prediction the deformation behavior of THF before failure are increasingly available, reliable prediction of failure still remains an issue. To effectively design and manufacture a hydroformed aerospace part, it is critical to use a reliable failure criterion in this process. To evaluate the forming severity of the THF process, studies have been performed on two main important failures; (i) necking and (ii) ductile fracture. However, in practical cases, the necking criterion may not predict the forming limit for a wide range of hydroforming processes. Especially, in case of aluminum alloys (5000, 6000 and 7000 groups) the bursting failure is often observed without appearance of clear localized necking or thinning due to their low ductility (Lei, Kang and Kang, 2001). It means that in the case of aluminum alloys, the fracture occurs prior to the onset of localized necking which is influenced by the work-hardening characteristic and the normal anisotropy. Therefore, the analytical approaches based on the necking instability theories are not always applicable for tubes. Moreover, for some materials with strain hardening constant above 0.4 (e.g. austenitic stainless steel and high strength steel alloys), ductile fracture is commonly appeared than necking, since these alloys fail with negligible thickness reduction ((Bressan and Williams, 1983), (Korhonen and Manninen, 2008) and (Lou et al. 2012).

Korhonen and Manninen (Korhonen and Manninen, 2008) pointed out the effects of strain sign on the failure modes. It was shown that for austenitic steels, the ductile fracture is more common for the left hand side of the forming limit diagram. Moreover, onset of the necking takes place in tension while ductile fracture is observed not only in tension but also in shear and compression ((Lou et al., 2012) and (Lou and Huh, 2012)). The first concept of the forming limit diagram was presented in 1965 (Keeler, 1965), on the basis of diffused necking for the right side of the forming limit diagram. Goodwin (Goodwin, 1968a) completed the FLD by mapping up the left side. After the classic works of (Hill, 1952) and (Swift, 1952), numerous models based on the necking and thickness reduction (Stoughton and Zhu, 2004), (Yoshida and Suzuki, 2008) were developed to determine the forming limit diagrams. Nevertheless, most of these models are applicable only to highly ductile materials such as mild steel and some series of aluminum alloys. Since limited models are available for an accurate prediction of necking failure and forming limit of austenitic materials and tubular materials.

Various ductile fracture criteria (DFCs) have been studied to predict the onset of fracture (Lei, Kang and Kang, 2001) and (Lei, Kim and Kang, 2002). A DFC at various stress triaxialities was presented by (Michael et al., 2008) to study the effect of stress triaxiality on the onset of fracture and evolution of damage in ductile metals. The accuracy of DFC directly affects the precision of predicted results, thus the accurate determination of micro and/or macro parameters based on physical mechanism of ductile fracture, nucleation, growth, and coalescence of void is indispensable for any accurate damage model. Cockcroft and Latham (Cockcroft and Latham, 1968), Brozzo (Brozzo, Deluca and Rendina, 1972), Oh (Oh, Chen and Kobayashi, 1979b), Oyane (Oyane et al., 1980), and more recently Bao and Wierzbicki (Bai and Wierzbicki, 2010; Bao and Wierzbicki, 2004) , Ko (Ko et al., 2007), Lou (Lou et al., 2012), and Lou and Huh (Lou and Huh, 2012) developed different phenomenological damage models based on nucleation, growth and coalescence of microscopic voids.

Many researchers (Han and Kim, 2003), (Ozturk and Lee, 2004), (Liu et al., 2009), (Chen, Zhou and Chen, 2010), (Lou et al., 2012) and (Lou and Huh, 2013) verified the applicability of the phenomenological damage models to predict the formability of sheet metals. Although many studies of ductile fracture have already been undertaken, none of them are implemented to estimate bursting failure in THF. All attempts involved with bursting failure in hydroforming process are based on experiments and surprisingly only there are limited ductile damage models available in the literature (Lei, Kim and Kang, 2002), (Lei et al., 2003), (Kim et al., 2004b), (Song et al., 2005), (Saboori et al. 2011). The main concern of the present work is about the plastic behavior and possibility of precise prediction of burst pressure in aerospace austenitic steel alloys, SS 321 and IN 718 using a new ductile fracture criterion. The effect of the stress triaxiality, the stress concentration factor and the effective plastic strain on the nucleation, growth and coalescence of voids was considered. A numerical procedure for both plasticity and fracture was developed and implemented into 3D explicit commercial FE software (LS-DYNA) through a new user material subroutine. The comparison of bursting pressure and the FLDf results proved the accuracy and validity of the developed ductile model.

## Ductile Fracture Criteria

Accumulation of plastic deformation in THF process leads tube to deform from the uniform deformation to diffuse instability, localization instability and fracture at the end zone. Generally, in the beginning stages when the material is deformed, voids will be initiated at a certain equivalent strain, $\bar{\varepsilon}_i$, with further deformation causing the growth and coalescence of the voids, consequently the fracture will be observed at a certain equivalent strain, $\bar{\varepsilon}_f$. This behavior shows that the forming limit in THF depends greatly upon the deformation history. commonly, at least one of the following rules are considered as the hypothesis of all ductile fracture criteria: (i) the deformation path, since the current stress-strain state is not enough to characterize the damage state, (ii) the hydrostatic stress, $\sigma_m$, because ductility grows rapidly as $\sigma_m$ decreases, (iii) an adequate ratio of stresses, namely the triaxiality stress ratio, $\frac{\sigma_m}{\bar{\sigma}}$, in which $\bar{\sigma}$ is the equivalent stress, so that the general state of plasticity and fracture is better described. Therefore, a ductile fracture criterion could be expressed in a general form as:

$$\int_{\bar{\varepsilon}_i}^{\bar{\varepsilon}_j} f(\sigma, \bar{\sigma}, \sigma_m, \dots)\, d\bar{\varepsilon} = D \tag{4.1}$$

where $f$ is a function depending on the stress state $(\sigma, \bar{\sigma}, \sigma_m, \dots)$, $\bar{\varepsilon}$ is the equivalent strain, $\bar{\varepsilon}_i$ is the magnitude of equivalent strain when the damage starts to accumulate, $\bar{\varepsilon}_j$ is the current intensity of strain and $D$ is a physical property relevant to material properties and it is always taken as a constant and so-called “ damage indicator”. Osakada and Mori (Osakada and Mori, 1978) have reported that the strain at which voids is initiated depends on the pressure. However, it can be assumed that the value of $\bar{\varepsilon}_i$ is equal to zero (Oyane et al., 1980) since the void initiation is start after the elastic deformation. When the upper limit of the integral attains the critical fracture strain of the material, $\bar{\varepsilon}_j = \bar{\varepsilon}_f$ the damage indicator reaches a critical value $D = D_c$. Various ductile fracture criteria for metalworking processes were developed based on different hypotheses, empirically and theoretically.

Cockcroft and Latham (Cockcroft and Latham, 1968) assumed that the maximum principal stress is the most relevant factor in the initiation of fracture. This criterion is therefore defined in terms of plastic work associated to the principal stress along the path of the equivalent plastic strain as described below:

$$\frac{1}{C_1}\int_0^{\bar{\varepsilon}_f} \sigma^* \, d\bar{\varepsilon} = D_{c1} \tag{4.2}$$

where $\sigma^*$ is maximum principal stress, Oh (Oh, Chen and Kobayashi, 1979b) modified the Cockcroft and Latham criterion by introducing the effect of stress concentration factor, $\frac{\sigma^*}{\bar{\sigma}}$, into the ductile fracture criterion as follows:

$$\frac{1}{C_2}\int_0^{\bar{\varepsilon}_f} \frac{\sigma^*}{\bar{\sigma}} d\bar{\varepsilon} = D_{c2} \tag{4.3}$$

where $\bar{\sigma}$ is the effective stress, the Cockcroft and Latham criterion was modified by Brozzo (Brozzo, Deluca and Rendina, 1972) to introduce the effect of hydrostatic stress based on the evidence that ductility diminishes with the hydrostatic stress. Brozzo criterion states that the fracture in a ductile material occurs when:

$$\frac{1}{C_3}\int_0^{\bar{\varepsilon}_f} \frac{2\sigma^*}{3(\sigma^* - \sigma_m)} d\bar{\varepsilon} = D_{c3} \tag{4.4}$$

where $\sigma_m$ is the mean stress, Oyane (Oyane et al., 1980) proposed a ductile fracture criterion based on the plasticity theory for porous materials as below:

$$\frac{1}{C_4}\int_0^{\bar{\varepsilon}_f} (\frac{\sigma_m}{\bar{\sigma}} + C_5) d\bar{\varepsilon} = D_{c4} \tag{4.5}$$

More recently, Ko (Ko et al., 2007) proposed another modification of the Cockcroft-Latham criterion to consider the influence of the hydrostatic stress in order to correlate their experimental results:

$$\frac{1}{C_6}\int_0^{\bar{\varepsilon}_f}\frac{\sigma^*}{\bar{\sigma}}\left(3\frac{\sigma_m}{\bar{\sigma}}+1\right)d\bar{\varepsilon}=D_{c5} \qquad (x)=\begin{cases}-x, & x<0\\ x, & x\geq 0\end{cases} \quad (4.6)$$

in Eqs. 4.2-4.6, $C_1$ to $C_6$ are the material constants in ductile fracture criteria. In all these criteria, fracture initiates when the accumulated damage ($D_{c1}$ to $D_{c5}$) reaches to unity.

## Development of a new criterion for ductile fracture of THF process

In the microscopic viewpoint, ductile fracture surfaces appear rough and irregular. The surface consists of many microvoids and dimples. The main assumption behind most ductile fracture criteria developed recently is that equivalent strain to fracture is a function of stress triaxiality, $\frac{\sigma_m}{\bar{\sigma}}$. According to Figure 4.1, Luo and Wierzbicki (Luo and Wierzbicki, 2010) determined the influence of a wide range of the triaxiality on fracture equivalent strain with four distinct branches separated by five typical stress states (from uniaxial compression ($\frac{\sigma_m}{\bar{\sigma}}$ =*-1/3*) to the balanced biaxial tension ($\frac{\sigma_m}{\bar{\sigma}}$ =*2/3*). The branch for stress triaxialities larger than 1/3 ($\frac{\sigma_m}{\bar{\sigma}}$ =*1/3* means uniaxial tension) corresponds to fracture controlled by the mechanism of void nucleation, growth, and coalescence (branch I and II). Tensile testing on smooth and notch specimen or dome test are used for this branch. The fourth branch describes the so-called shear decohesion fracture under negative stress triaxiality (branch IV). Usually the compression tests on short cylinders are used for this branch. Finally, there is a third regime (branch III) in which fracture is a combination of the two simple modes describes above. Pure shearing and combined loading tests are usually used to determine fracture locus in this branch.

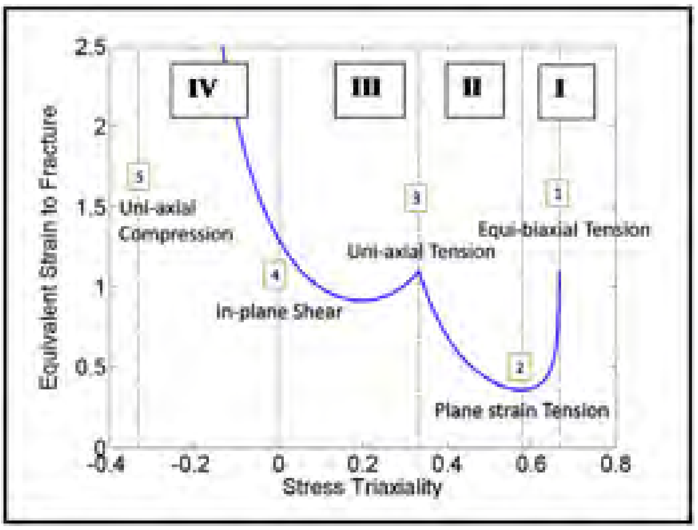

Figure 4.1: Comparison of the fracture locus in the plane of equivalent fracture strain and stress triaxiality, (Luo and Wierzbicki, 2010).

In the THF process of ductile materials the fracture locus are located in branch I and II ($\frac{\sigma_m}{\bar{\sigma}} \geq 1/3$). Therefore, the damage-fracture processes of THF for ductile materials can be described in terms of three stages, i.e. nucleation of voids or cavities, growth of cavities with continued deformation, and finally, coalescence of the voids including micro-cracks. These mechanisms were extensively investigated experimentally, theoretically and numerically (Gurson, 1975) and (Weck and Wilkinson, 2008). Moreover, many reported works on coupled and uncoupled ductile fracture criteria exists in the literature (Cockcroft and Latham, 1968), (Brozzo, Deluca and Rendina, 1972), (Oh, Chen and Kobayashi, 1979b), (Oyane et al., 1980), and more recently, various hypotheses into coupled and uncoupled ductile fracture were proposed (Ko et al., 2007), (Xue, 2007), (Xue, 2008), (Xue and Wierzbicki, 2008), and (Tvergaard and Nielsen, 2010).

According to review of literature, further investigation is still required to define the appropriate method to model and consider the aforementioned deformation characteristics of a material (e.g. nucleation, growth and coalescence of the voids), as well as application of them in the THF of aerospace materials through uncoupled damage model.

In the course of this study, the influence of these three stages will be analyzed separately, and then a proper damage model will be developed for THF in the following section.

### 4.1.1 Void nucleation model

Gurson (Gurson, 1975) and Fleck (Fleck, Hutchinson and Tvergaard, 1989) used plastic deformation theory to explain that void nucleation initiates by debonding or cracking the particles at a certain strain, then the overall stress-strain starts to display softening phenomenon, comparable to that observed in materials that their particles do not debond or crack.

Two models were developed for voids nucleation: (i) stress-controlled nucleation by Goods and Brown ((Goods and Brown, 1979) and Argon, Im and Safoglu (Argon, Im and Safoglu, 1975)) and (ii) strain-controlled nucleation by Gurson (Gurson, 1975) which indicates that the nucleation rate is proportional to the equivalent plastic strain rate. Bao and Wierzbicki (Bao and Wierzbicki 2004) and Li (Li et al., 2011) pointed out that the stress based criterion cannot be estimated in the processes where the hydrostatic stress is negative. Lou (Lou et al., 2012) explained that a strain-based nucleation model is more reasonable than stress-based nucleation ones for the macroscopic modeling of ductile fracture. Kõrgesaar (Kõrgesaar and Romanoff, 2013) and Lou (Lou et al., 2012) modeled the void nucleation as a proportional function to the equivalent plastic strain. A simple strain-controlled void nucleation rule was adapted for the new damage model as follows:

$$D_1 = D_1(\bar{\varepsilon}_p) \tag{4.7}$$

where $\boldsymbol{D_1}$ is damage accumulation caused by nucleation of the voids and $\bar{\boldsymbol{\varepsilon}}_{\boldsymbol{p}}$ is the equivalent plastic strain.

### 4.1.2 Void growth model

Studies of void growth reveal that stress triaxiality $\frac{\sigma_m}{\bar{\sigma}}$ (defined as $\frac{\sigma_m}{\bar{\sigma}}$ with mean stress $\sigma_m = \frac{\sigma_{kk}}{3}$ and effective stress $\bar{\sigma}$=$\sqrt{3S_{ij}S_{ij}/2}$ with Sij as the stress deviator) is a key ductility-controlling parameter to characterize important void growth. High mean stress accelerates void growth while negative stress triaxiality $\frac{\sigma_m}{\bar{\sigma}}$ suppress void growth (Li et al., 2011), (Lou et al., 2012), (Nahshon and Hutchinson, 2008), (Bao and Wierzbicki, 2005). As aforementioned, during the THF the stress triaxiality is always having a positive value (*1/3*≤$\frac{\sigma_m}{\bar{\sigma}}$ *≥2/3*). It is noteworthy that when the tube material is pushed towards the expansion zone the triaxiality moves to 1/3 ($\frac{\sigma_m}{\bar{\sigma}}$ *=1/3*), when the displacement at the ends is restricted the triaxiality moves to 1/sqrt ($\frac{\sigma_m}{\bar{\sigma}}$), and when the ends of the tube is pulled, the triaxiality moves to 2/3 ($\frac{\sigma_m}{\bar{\sigma}}$ *=2/3*). The weighting function of the voids growth was suggested by Brokken (Brokken, Brekelmans and Baaijens, 1998). In particular, Brokken's weight function prevents the accumulated damage from diminishing when the weighting value is negative. In this research, the weighting function suggested by Brokken is applied in a new ductile fracture criterion as shown below:

$$D_2 = D_2(\langle 1 + 3\frac{\sigma_m}{\bar{\sigma}} \rangle) \qquad \langle x \rangle = \begin{cases} x \;\; when & x \geq 0 \\ 0 \; when & x < 0 \end{cases} \tag{4.8}$$

where $D_2$ is damage accumulation caused by growth of the voids.

### 4.1.3 Void Coalescence model

The final stage of ductile fracture is void coalescence. After the onset of void coalescence the effective stress drops rapidly due to localization in the ligament. Pardoen and Hutchinson (Pardoen and Hutchinson, 2000) developed a micromechanically-based simple constitutive model for the void coalescence stage. The provided equation for the onset of coalescence is a function of the maximum principal stress and normalized by the effective stress as follow:

$$D_3 = D_3(\frac{\sigma_{max}}{\bar{\sigma}}) \tag{4.9}$$

where $D_3$ is damage accumulation caused by coalescence of the voids, $\sigma_{max}$ is the maximum principal stress, and $\bar{\sigma}$ is the effective stress.

### 4.1.4 New ductile fracture criterion

A new ductile fracture criterion was suggested as Eq. 4.10 in order to consider the fracture characteristics of a ductile material by the described mechanisms of nucleation, growth, and coalescence of voids as mentioned before. This equation consisted of terms to consider: (i) the deformation characteristics and as a function to consider the effect of stress triaxiality for voids growth, (ii) the effective strain was assumed proportional to the void nucleation, and (iii) void coalescence was considered as the ratio of the maximum principal stress to effective stress, when the loading path and plastic deformation were not proportional:

$$\frac{1}{C_7}\int_0^{\varepsilon_f}\left(\frac{\sigma_{max}}{\bar{\sigma}}\right)^{C_8}\left(\langle 1+3\frac{\sigma_m}{\bar{\sigma}}\rangle\right)^{C_9} d\varepsilon_f = D_{c6} \quad \left\{\langle x\rangle = \begin{cases} x \ \ when \quad x \geq 0 \\ 0 \ when \quad x < 0 \end{cases}\right. \tag{4.10}$$

Like in the aforementioned criteria, the fracture initiates when the accumulated damage ($D_{c6}$) reaches to unity. All suggested criteria Cockcroft, Oh, Brozzo, Oyane, Ko and the new fracture locus were implemented in LS-DYNA software through a new user material code combined with von Mises's plasticity to predict the bursting fracture in the free expansion process of the aerospace alloys (SS 321, IN 718) with end feeding and without end feeding. Each fracture criteria was calculated and checked in each incremental time steps.

## Material characterization and criteria calibration

To obtain an accurate stress-strain behavior of aerospace material, Saboori (Saboori et al. 2014) developed a new online procedure to characterize the mechanical response of the material for hydroforming applications based on the free expansion testing. As presented in (Saboori et al. 2014), the Swift hardening law could better predict the material behavior of SS 321 and IN 718.

It is well understood that in sheet and tube forming processes, the strain path changes after occurrence of localized necking. Once a localized neck forms, the deformation transits quickly into plane strain condition and continue until the fracture occurrence, which is considered as one of the difficulties to measure the stress and strain after this phenomenon (necking formation). As a result, predicted results of forming limit will be certainly affected. In this paper, to remedy this lack of accuracy, the material constants are determined with a FE-based inverse calibration procedure combined with the dome test and tensile test experiments that were employed to extract the critical damage values ($C_1$to $C_9$) ((Luo and Wierzbicki, 2010), (Liu et al., 2009)). This inverse method is believed to be valid in calibration of critical damage values ((Bonora et al., 2005) , (Bai and Wierzbicki, 2008), (Liu et al., 2009)). Figure 4.2 shows the tensile test (Bonora et al. 2005) and hourglass specimens with different widths (50.8 mm, 76.2 mm and 127 mm) that were adopted to obtain experimental fracture data to calibrate all damage models reviewed above and the new aforementioned damage criterion. These data contained fracture limits for 6 different deformation paths, which provided a more robust comparison of performances of different fracture models. Table 4.1 presents the calculated mean values of $C_i$ for all ductile fracture criteria.

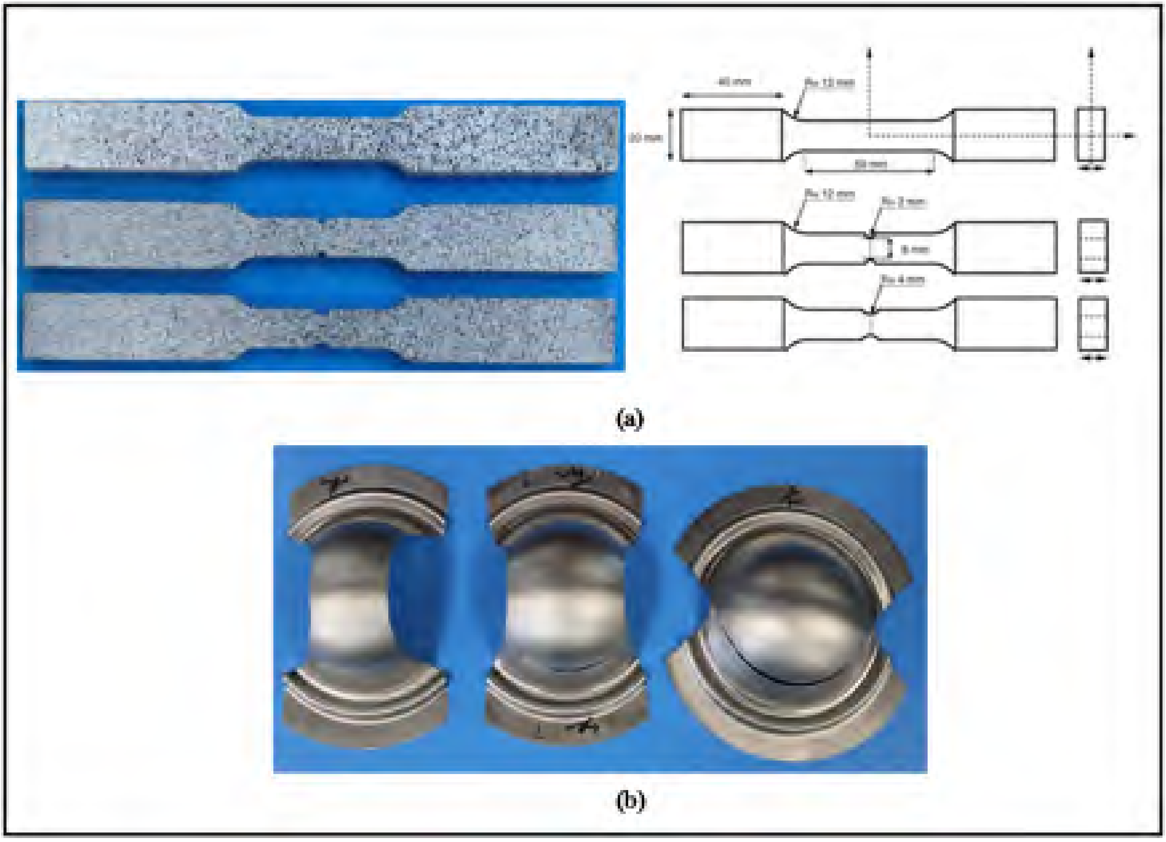

Figure 4.2: SS 321 samples for damage constants evaluation (a) tensile specimens with various geometries, (b) Hourglass shapes.

Table 4.1: Average material constants in ductile fracture criteria.

| **Material** | $C_1$ | $C_2$ | $C_3$ | $C_4$ | $C_5$ | $C_6$ | $C_7$ | $C_8$ | $C_9$ |
|---|---|---|---|---|---|---|---|---|---|
| SS 321 (0.9 mm) | 517.2 | 0.49 | 0.52 | 0.24 | 0.15 | 0.98 | 0.60 | 0.176 | 1.04 |
| SS 321 (1.2 mm) | 520.1 | 0.51 | 0.53 | 0.24 | 0.15 | 1.01 | 0.63 | 0.178 | 1.06 |
| IN 718 (0.9 mm) | 610.2 | 0.62 | 0.61 | 0.33 | 0.18 | 1.08 | 0.65 | 0.188 | 1.08 |

## Implementation for Fracture Prediction

In order to simulate bursting/or fracture initiation during free expansion process of the aerospace material, the cutting-plane algorithm as introduced by Simo and Ortiz ((Simo and Ortiz, 1985) and (Ortiz and Simo, 1986)), was implemented on elastic prediction and plastic correction technique into LS-DYNA. In this method, stresses at integration points are usually obtained by integrating nonlinear constitutive equations in an incremental form. This algorithm was proposed to bypass the need for computing the gradients of the yield function and the flow rule. The Newton-Raphson method is used to evaluate the gradients. The method is described as follows:

At the beginning of a load step, the values of stress and strain $\sigma_0$ and $\varepsilon_0$ are given, and the stress $\sigma$ can be calculated at the next step for a strain increment $\Delta\varepsilon$.

The total strain increment tensor is assumed to be the sum of the elastic strain increment tensor and the plastic strain increment tensor:

$$d\varepsilon_{ij} = d\varepsilon_{ij}{}^{e} + d\varepsilon_{ij}{}^{p} \tag{4.11}$$

The stress increment tensor corresponding to this increment in total strain tensor can be determined by a constitutive relation as follows:

$$\mathrm{d}\sigma_{\mathrm{ij}} = \mathrm{B}^{\mathrm{ep}}\mathrm{d}\varepsilon_{\mathrm{ij}} \tag{4.12}$$

where $B^{ep}$ is the elasto-plastic constitutive matrix. Assuming that the whole increment is purely elastic, then Hooke's law gives the relation between stresses and elastic strains as:

$$d\sigma_{ij} = \sigma_0 + Bd\varepsilon_{ij}{}^{e} = \sigma_0 + B\left(d\varepsilon_{ij} - d\varepsilon_{ij}{}^{p}\right) = \sigma_{ij}{}^{*} - Bd\varepsilon_{ij}{}^{p} \tag{4.13}$$

where $\sigma_{ij}{}^{*}$ is the trial stress tensor, the incremental stress tensor is expressed in terms of the volumetric and deviatoric strain in the following form as follows:

$$d\sigma_{ij} = 2Gd\varepsilon_{ij} + \lambda d\varepsilon_m \tag{4.14}$$

Where $G,\ \lambda$ and $d\varepsilon_m$ are introduced as plastic shear modulus, lamé modulus, and incremental hydrostatic strain, respectively. For the rate independent isotropic hardening material that obeys von Mises yield criterion the flow rule function is given as follow:

$$\phi\left(\sigma_{ij}, \bar{\varepsilon}^p\right) = \sqrt{\frac{3}{2} S_{ij} S_{ij}} - Y(\bar{\varepsilon}^p) \tag{4.15}$$

where the deviatoric stress tensor is computed by $S_{ij} = \sigma_{ij} - \left({}^{1}\!/_{3}\right)\sigma_{kk}\delta_{ij}$ and $Y(\bar{\varepsilon}^p)$ defines the true stress–true strain curve of the materials. $\delta_{ij}$ is named as the Kronecker delta and is given as below:

$$\delta_{ij} = \begin{cases} 0 & if\ \ i \neq j \\ 1 & if\ \ i = j \end{cases} \tag{4.16}$$

If the yield condition is satisfied by the elastic prediction, the constitutive integration is complete and Eq. 4.13 is shown as:

$$d\sigma_{ij} = {\sigma_{ij}}^* \tag{4.17}$$

Otherwise, the plastic strain increment tensor is determined from the yield function plastic correction and is implemented as follow:

$$d{\varepsilon_{ij}}^p = d\gamma \frac{\partial \phi}{\partial \sigma_{ij}} = \frac{3}{2} d\bar{\varepsilon}^p \frac{S_{ij}}{Y(\bar{\varepsilon}^p)} \tag{4.18}$$

In the above equations $\gamma$ represents the plastic multiplier and the flow stress curve is obtained as:

$$Y = K(\bar{\varepsilon}_0 + \bar{\varepsilon}^p) \tag{4.19}$$

where hardening law is as below:

$$dY = hd\bar{\varepsilon}^p \tag{4.20}$$

Thus, the stress increment is given by

$$d\sigma_{ij} = \sigma_{ij}{}^{*} - d\gamma B\frac{\partial \phi}{\partial \sigma_{ij}} \tag{4.21}$$

and the following relation must be satisfied before and after the plastic straining of $d\bar{\varepsilon}^p$:

$$\phi\left(\sigma_{ij} + d\sigma_{ij}, \bar{\varepsilon}^p + d\bar{\varepsilon}^p\right) = \phi\left(\sigma_{ij}, \bar{\varepsilon}^p\right) + \frac{\partial \emptyset}{\partial \sigma_{ij}} d\sigma_{ij} + \frac{\partial \emptyset}{\partial \bar{\varepsilon}^p} d\bar{\varepsilon}^p = 0 \tag{4.22}$$

The above relation reduces to a form of

$$\frac{\partial \emptyset}{\partial \sigma_{ij}} d\sigma_{ij} - \frac{dY}{d\bar{\varepsilon}^p} d\bar{\varepsilon}^p = 0 \tag{4.23}$$

Then the equivalent plastic strain increment is obtained as below:

$$d\bar{\varepsilon}^p = \frac{1}{H}\frac{\partial \emptyset}{\partial \sigma_{ij}} d\sigma_{ij} = \frac{1}{H}\frac{3}{2}\frac{S_{ij} d\sigma_{ij}}{Y(\bar{\varepsilon}^p)} \tag{4.24}$$

where $H = \frac{d\bar{\sigma}}{d\bar{\varepsilon}^p}$ is the effective plastic strain incremental $d\bar{\varepsilon}^p$ and is the only unknown that could be solved by Newton-Raphson iteration. Once $d\varepsilon^p$ is known, the solution can be obtain by:

$$\bar{\sigma}_{new} = \bar{\sigma}_{old} + Hd\bar{\varepsilon}^p \tag{4.25}$$

The deviatoric stress can also be solved by:

$$S_{ij}^{new} = S_{ij}^{old}\left(\frac{\bar{\sigma}_{new}}{\bar{\sigma}_{new} + 3Gd\bar{\varepsilon}^p}\right) \tag{4.26}$$

The stress components are calculated by:

$$\sigma_{ij}^{new} = S_{ij}^{new} + \sigma_m \tag{4.27}$$

Therefore, the value $D_{ij}$ for specific fracture criteria of element $j$ at deformation step $i$ is defined based on the obtained stress and strain components as follows:

$$\frac{1}{C_f}\sum f(\sigma,\bar{\sigma},\sigma_m \ldots)_{ij}\,\bar{\varepsilon}_{ij}^{p}\,d\bar{\varepsilon}_{ij} = D_{ij} \tag{4.28}$$

where $i$ and $j$ are the deformation step and the number of element, respectively. The occurrence of fracture is determined by comparing the value of the integral at a given material point to the critical value $C_f$ of corresponding fracture criterion. When $D_{ij}$ reaches unity, the corresponding element is assumed to fracture and is deleted in the simulation. Figure 4.3 illustrates a flow chart of the iterative finite element analysis procedure with the algorithm of the fracture criteria characterization that was implemented in LS-DYNA through the new user material subroutine (see ANNEX III).

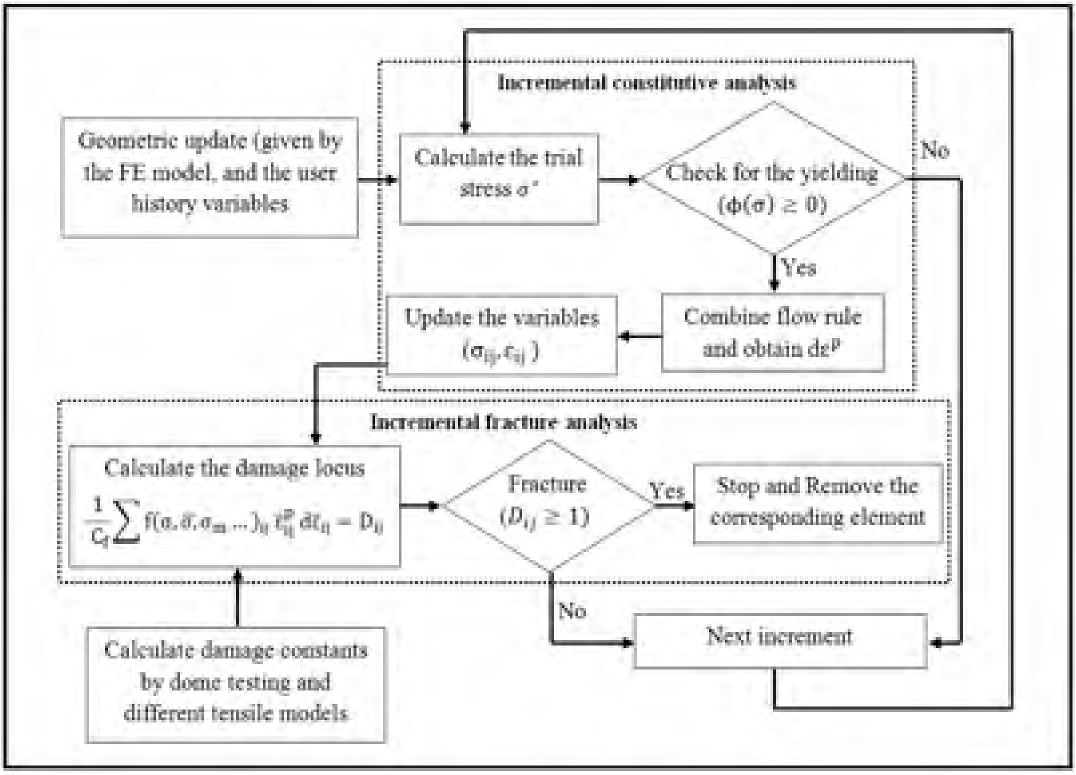

Figure 4.3: Flowchart for fracture prediction during free expansion process.

## Predicting of fracture forming limit curves in the THF process

### 4.1.5 Numerical approach using ductile fracture criterion

In this section the reviewed fracture locus and the new model were applied to commercial FE software, LS-DYNA 3D, to predict fracture forming limit curves during THF. The free expansion with and without end feeding of SS 321 with 0.9 and 1.2 mm thicknesses with 50.8 mm diameters was simulated. Figure 4.4 shows the mesh used for the die and a tube in the FE modeling. A quadrilateral shell element with 5 integration points through the thickness was used for the model. The fully integrated advanced Belytschko (Belytschko, Lin and Chen-Shyh, 1984) with the shell thickness change option activated was utilized as the shell element formulation. By varying the mesh size, it was found that 12,446 elements, with an aspect ratio of one were sufficient to obtain a nearly mesh-independent solution with accurate results. The die was modeled as a rigid body and the tube as a deformable material. In the model, a surface-to-surface contact algorithm was applied to the interface between the tube and the die with Coulomb’s friction set to 0.1 in accordance with different reported values in the literature for an non lubricated condition ((Vollertsen and Plancak, 2002) and (Abrantes, Szabo-Ponce and Batalha, 2005)). To mimic the experimental loading conditions in the FE model, the internal pressure was applied on each element of the meshed tube and increased linearly. It is noteworthy that in the present work, the effect of anisotropy on the mechanical response was not considered in the FE model of the free expansion process. To this end, as shown in Table 4.2, the effective true stress-true strain data employed in the FE model were based on the aforementioned study (Saboori et al. 2014).

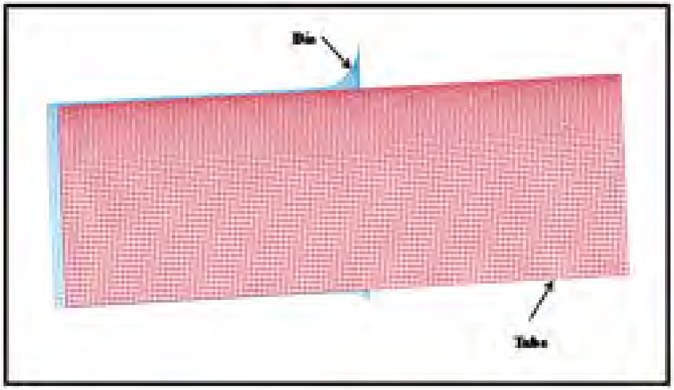

Figure 4.4: Mesh used in the FE model.

Table 4.2: True stress–strain relations (Saboori et al. 2014).

| Material | Thickness (mm) | Swift model $\bar{\sigma} = k_s(\varepsilon_0 + \bar{\varepsilon}_p)^{n_s}$ |
|---|---|---|
| SS 321 | 0.9 | $\bar{\sigma} = 1427.45(0.035 + \varepsilon_p)^{0.53}$ |
| SS 321 | 1.2 | $\bar{\sigma} = 1397.81(0.052 + \varepsilon_p)^{0.63}$ |
| IN 718 | 0.9 | $\bar{\sigma} = 1880.6(0.072 + \varepsilon_p)^{0.59}$ |

### 4.1.6 Experimental approach

In order to find the failure forming limit curve for SS 321 in the THF process, a series of free expansion tests were executed. Figure 4.5 illustrates the 3D CAD model of the die used for the free expansion tests and Table 4.3 shows the two setup experimental conditions (free expansion without and with end feeding). Figure 4.6 shows the setup used for THF trials, which involved the use of a 1000 ton hydroforming press capable of applying 400 MPa of internal pressure and equipped with the Aramis® system. The major strains and the minor strains at bursting were measured on the tube surface by using the Aramis® system. During the experiments without end feeding tests the ends of the tubes were maintained fixed in place and sealed using two end plungers, while for the tests with the end feeding the two plungers contribute to push the material inside the die cavity. The loading sequence of the free expansion tests is presented in Figure 4.7 for tubes with 0.9 mm and 1.2 mm thicknesses. Axial feed displacement with the same internal pressure level at each loading path means that different loading histories can be assigned for each free expansion test, as shown in Figure 4.7. As a result, the free expanded tubes after bursting for different loading paths are illustrated in Figure 4.8. To ensure the consistency of the data, each condition was repeated at least twice.

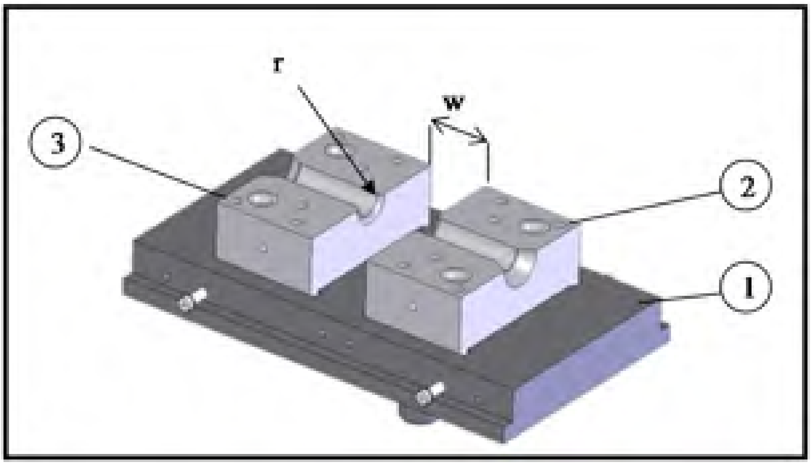

Figure 4.5: CAD of the die-set showing (1) the lower shoe, (2) the lower right cavity and (3) lower left cavity.

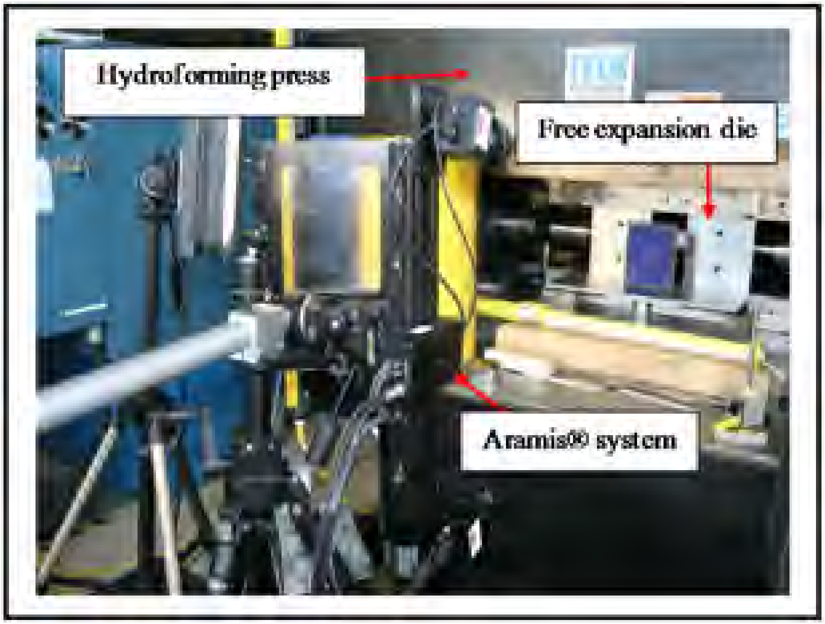

Figure 4.6: Experimental setup for the free expansion tests.

Table 4.3: Experimental conditions for the first and second set of the free expansion trials.

| Materials | $L_0$ (mm) | $D_0$ (mm) | w (mm) | r (mm) |
|---|---|---|---|---|
| SS 321 (0.9 mm and 1.2 mm thick) and IN 718 (0.9 mm thick) (without end feeding) | 381 | 50.8 | 101.8 | 7.5 |
| SS 321 (0.9 mm and 1.2 mm thick) and IN 718 (0.9 mm thick) (with end feeding) | 304 | 50.8 | 101.8 | 7.5 |

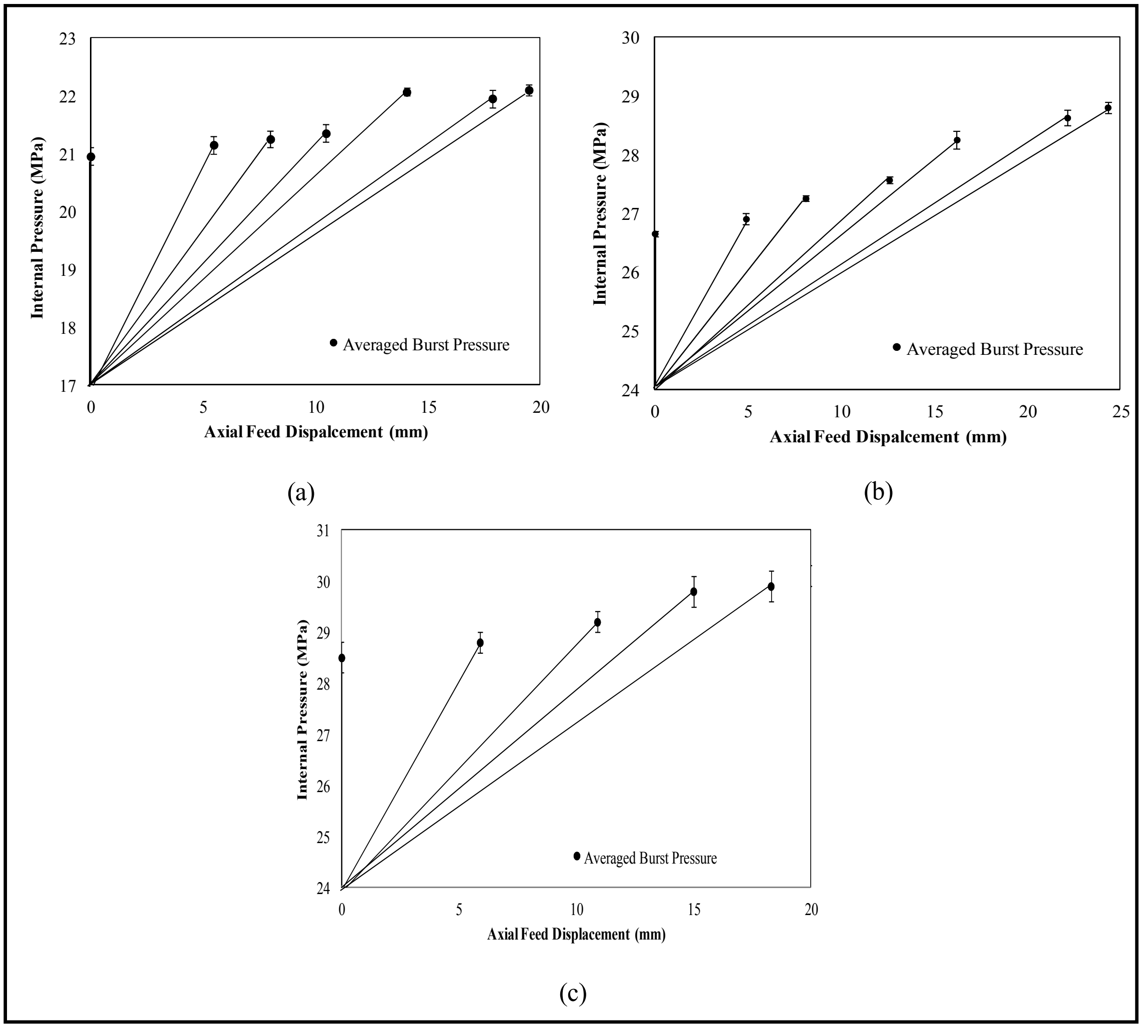

Figure 4.7: Different loading paths (a) 0.9 mm SS 321, (b) 1.2 mm SS 321 and (c) 0.9 mm IN 718.

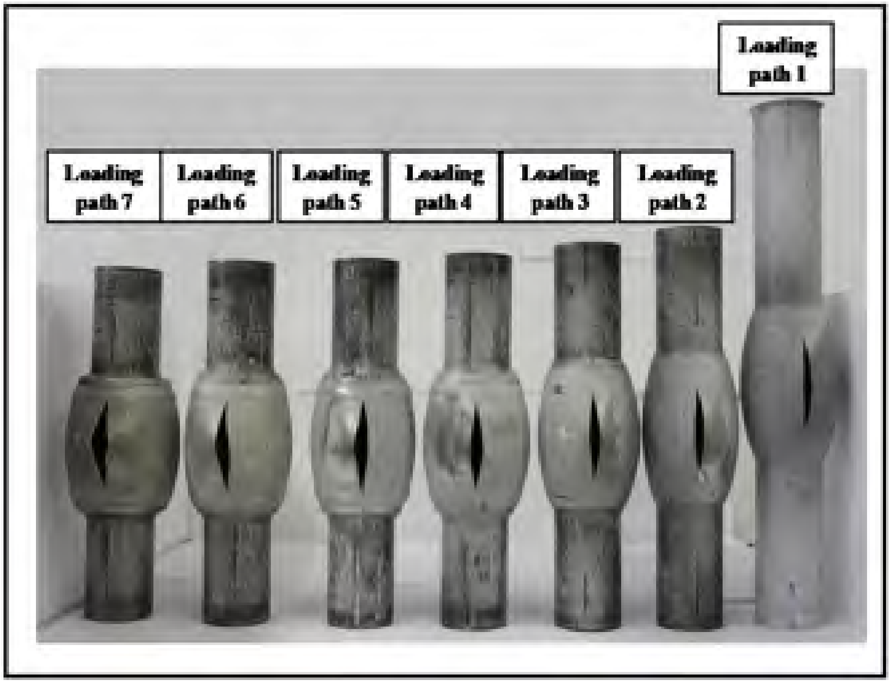

Figure 4.8: Free expansion test results with different loading paths for SS 321, 0.9 mm thickness.

### Results and discussion

As mentioned previously, the free expansion tests were performed with and without end feeding up to the rupture/burst of the tube for each thickness examined in this work (i.e. SS 321 with 0.9 mm, 1.2 mm and IN 718 with 0.9 mm thicknesses) in order to determine the forming limit curves of THF process under different loading conditions. Also the FE modeling of the free expansion with and without end feeding was carried out based on the new implemented user material for different aforementioned ductile fracture criteria and the new ductile fracture that was developed during this research.

The predicted burst pressure results for all fracture criteria were compared with the experimental results for plane strain condition (no end feeding) in Table 4.4. As summarized in this table, the ductile damages with one material constant overestimate the bursting pressure, while, the fracture with two underestimate the bursting pressure. In contrast, the new ductile fracture can predict the bursting pressure with higher accuracy with >1% for all tested specimens as demonstrated in Table 4.4.

Table 4.4: Comparison of the predicted burst pressures for without end feeding condition.

| **Material** | **SS 321 (0.9 mm) (MPa)** | **SS 321 (1.2 mm) (MPa)** | **IN 718 (0.9 mm) (MPa)** | **Error SS 321 (0.9 mm)** | **Error SS 321 (1.2 mm)** | **Error IN 718 (0.9 mm)** |
|---|---|---|---|---|---|---|
| Experiment | 21 | 26.7 | 28.5 | - | - | - |
| Cockcroft | 22.6 | 28.3 | 23.6 | 7.6 | 6 | 17.1 |
| Oh | 19.2 | 29 | 26 | 8.6 | 8.6 | 8.7 |
| Brozzo | 22.4 | 27.4 | 22.8 | 6.7 | 5.4 | 20.0 |
| Oyane | 21.6 | 28.1 | 30.3 | 2.3 | 2.6 | 6.3 |
| Ko | 23.8 | 29.4 | 30.6 | 13.3 | 10.1 | 7.3 |
| New criterion | 21.1 | 26.8 | 27.5 | 0.5 | .4 | 3.5 |

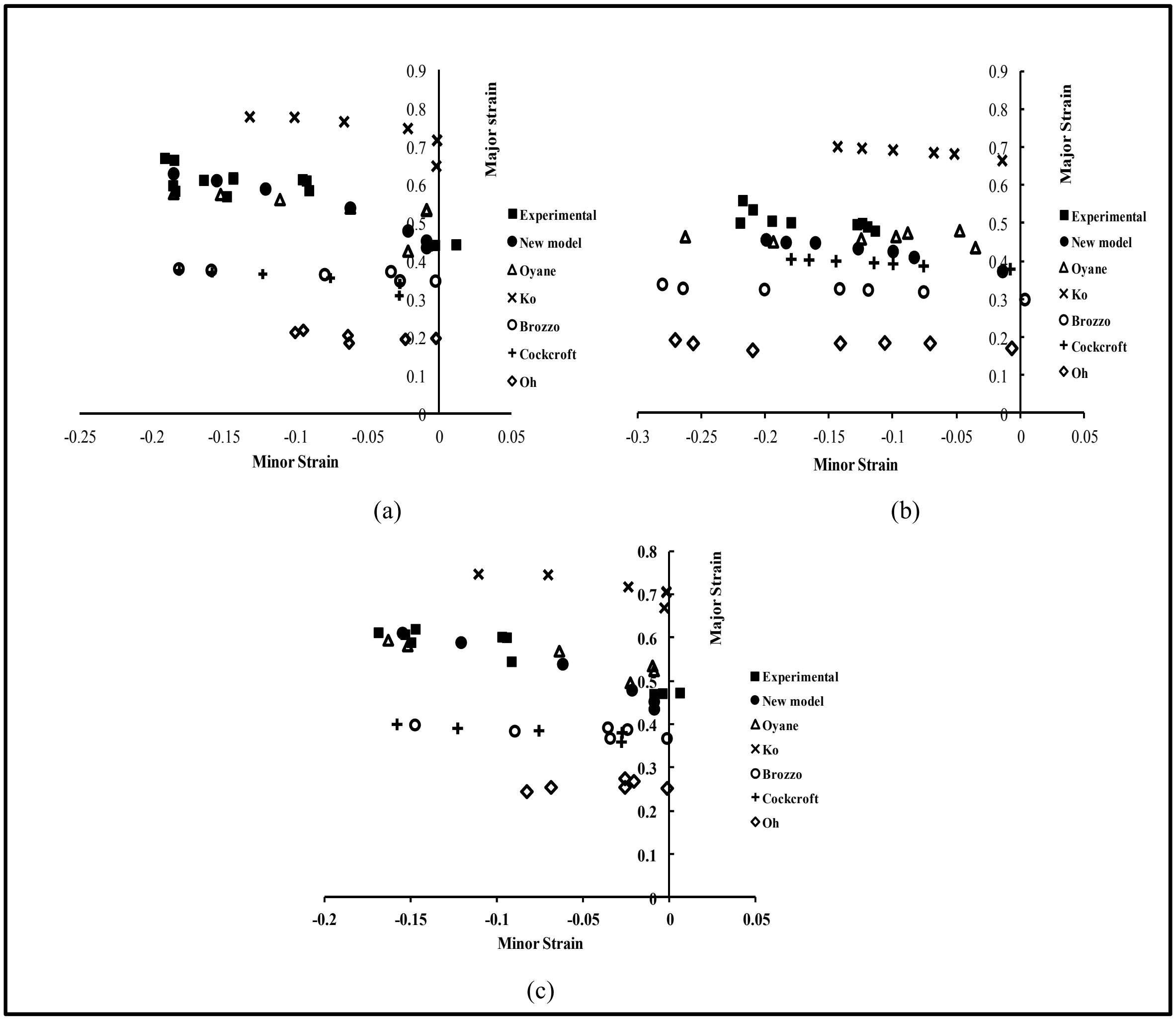

(a) (b)

(c)

Figure 4.9: Comparison between FLDf (a) 0.9 mm SS 321,
(b) 1.2 mm SS 321, (c) 0.9 mm IN 718.

As represented in Figure 4.9, the predicted fracture forming limit curves were compared with experimental results to evaluate the predictability of various ductile fracture criteria. Comparison demonstrated that the fracture forming limit curves of Ko and Oyane overestimated fracture strains while the Oh and Brozzo underestimated the fracture strains. Fracture curve predicted by the proposed ductile fracture criterion and Oyane fracture criterion were closer to the experimental results compare to other ductile fracture criteria. Oh, Brozzo, Ko and Cockcroft ductile fracture criteria made the most conservative prediction in the plane strain condition while other ductile fracture criteria (the new ductile fracture and

Oyane) made the least conservative prediction in the plain strain condition. Furthermore, similar inconsistency appeared with the experimental data for other loading paths for all fracture criteria except for the new and the Oyane fracture criterion. The above calculations showed that the prediction results based on a single material constant C were not accurate, but the results based on two (Oyane) and the proposed new damage model (three material constants) were much more accurate.

Furthermore, the value of material constant C had effect on the height but no effect on the curvature of the fracture forming limit curves; Brozo, Ko, Cockcroft and Oh cannot predict the fracture forming limit curves properly with a single material constant for the tested materials. Therefore the new criterion can handle the change of shape and height simultaneously.

## Conclusion

Based on the approach proposed in this work to determine the FLDf of SS 321 and IN 718 using the new ductile damage criterion and five conventional ductile fracture criteria for THF of aerospace material the following conclusions can be drawn:

- The experimental and the numerical FLDfs generated and the bursting pressure points were predicted for SS 321 with 0.9 mm, 1.2 mm and IN 718 with 0.9 mm thicknesses. The data set can help to design more accurately the THF process for aerospace applications.
- Compared to other ductile damage criteria, the new damage criterion based on three constants and considering the effect of void initiation, growth and coalescence predict the onset of failure more accurately. This maybe because the other ductile fracture criteria were developed for bulk metals rather than sheet or tube metals.
- The predicted bursting point were within 3% of the experimental data when using the Oyane criterion and less than 1% when using the new damage criterion

- Consequently, it is shown that the developed UMAT proposed in this study will provide a feasible method to satisfy the increasing demands for assessing the FLDf in THF of aerospace materials.

# CHAPTER 5

# CASE STUDY

As it was demonstrated in the Chapter 4, burst is a one of the major modes of failure of austenitic steel alloys tubes formed by THF. Clearly, an accurate prediction of this limit state (bursting) is essential for establishing a reliable working envelope for the process. The present chapter presents the application of the new damage model described in chapter 4 in two cases that are typically seen in some aero-engine components such as struts. As it will be shown later, only three different tensile specimen with different shapes (Bonora tensile models) were selected to calibrate the new damage model for multistep tube hydroforming processes (round to square and round to V shapes). The numerical bursting pressure results for SS 321 and IN 718 with 0.9 mm thickness for both materials and no end feeding condition were compared with the experiments for all tested materials. Results showed that acceptable agreements were observed.

## Case Studies

### 5.1.1 Round to square model (3D)

The simplest real multistep THF model application that can be used for the geometry at hand is a round to square shape. Exploiting the symmetries of the load and setup (see Figure 5.1), only one eighth of the tube and the die block were used for the FE model. Specifically, the tube length was sectioned midway longitudinally and a quarter section of the halved tube was simulated. The FEM for the round-to-square THF process was developed using ANSYS 14.5 software as the mesh generator and LS-DYNA as the FEM solver. The model consisted of two parts: (a) tube and (b) rigid die. A four node shell element was used for meshing the tube with Belytschko shell element formulation (Belytschko, Lin et al. 1984). Five integration points through the thickness were considered. In total, 17680 nodes and 17599 quadratic shell elements were used to generate the tube model. For the contact condition between the tube and the die, a surface to surface contact with a Coulomb friction value of 0.12 was used in the model (Vollertsen and Plancak, 2002).

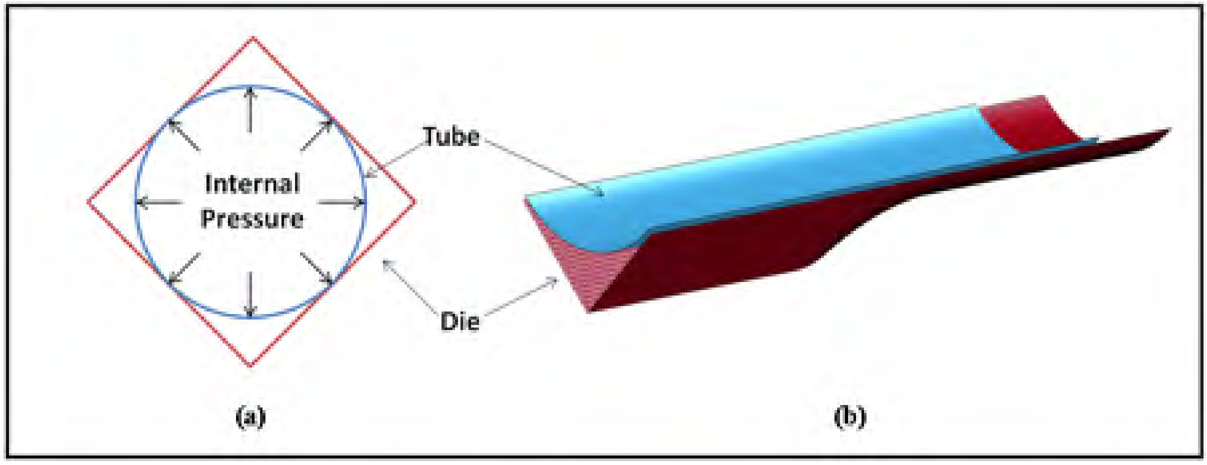

Figure 5.1: Round-to-square hydroforming process (a) schematic cross section, (b) tube and die in the FEM (Mojarad Farimani et al., 2013).

The material properties of the tubes were extracted from the methodology that was presented Saboori et al. (Saboori et al., 2014b) for SS 321 and In 718 with 0.9 mm thickness. The die was considered as rigid.

### 5.1.2 Round to V model (3D)

In another case study, a more complex shape (round to V shape) was simulated by the new damage model, Figure 5.2 shows the FE model of performing die and the hydroforming die was illustrated in Figure 5.3. Preforming of the tubes consisted of crushing the tube in a closed die. The FE model of the preforming and hydroforming processes included three parts: (i) the tube, (ii) the upper die and (iii) the lower die. ANSYS 14.5 was used as the mesh generator software and LS-DYNA as the FEM solver. Due to the symmetry condition in the tube length, the model was simplified; only half of the tube length was used in the simulations and the symmetry boundary conditions were applied to the boundary nodes along the symmetry plane. A total of 81012 four-node Belytschko-Tsay shell elements (Belytschko, Lin et al. 1984) with five integration points through the thickness and and with an aspect ratio of one were used to generate the tube model. For the contact condition between the tube and the die, a Coulomb friction law with the value of 0.05 was employed for crushing and for the hydroforming process the friction value was set to 0.12 (Mojarad Farimani et al., 2014).

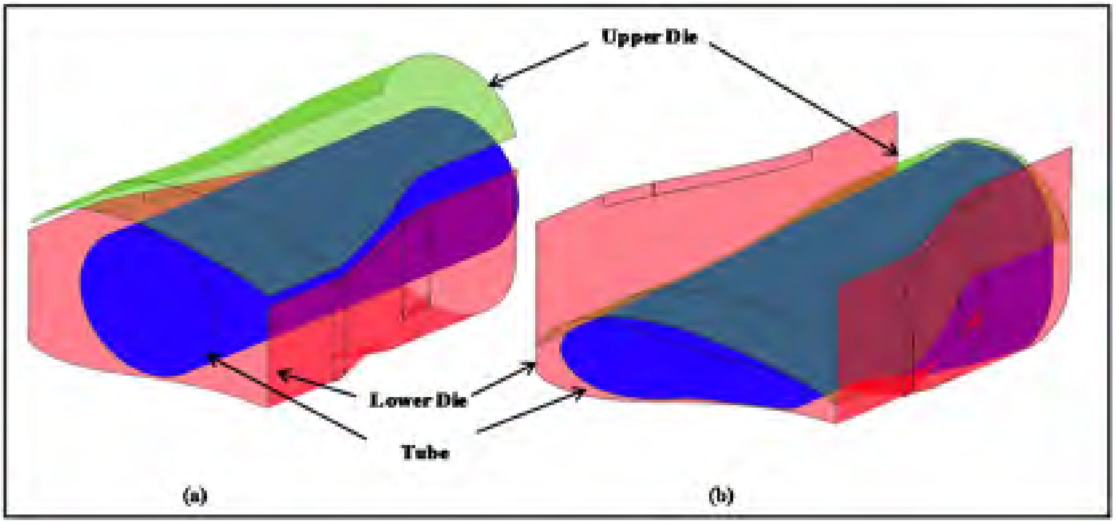

Figure 5.2: FE model of the preforming process (a) initial stage (b) final stage

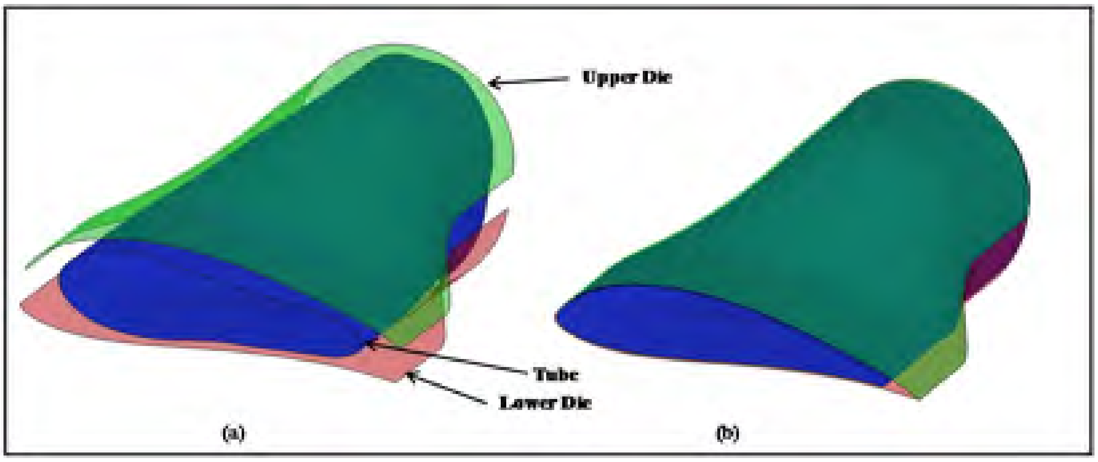

Figure 5.3: FE model of the hydroforming process (a) initial stage (b) final stage

### Damage constants calibration

As described in chapter 4, in order to calibrate the new damage model, tensile test (Bonora et al. 2005) and hourglass specimens were adopted to obtain experimental fracture data for the aforementioned new damage model (Eq. 4.10). Table 5.1 shows two different testing groups for damage calibration. As shown in this table both test groups give almost the same values, therefore, in this study only test results of the simplest specimens (Bonora) was selected to predict the bursting pressure.

Table 5.1: Material constants for the new ductile fracture criterion.

| **Material** | **Dome test specimens** | | | **Bonora test specimens** | | |
|---|---|---|---|---|---|---|
| | $C_7$ | $C_8$ | $C_9$ | $C_7$ | $C_8$ | $C_9$ |
| SS 321 (0.9 mm) | 0.59 | 0.18 | 1.03 | 0.61 | 0.17 | 1.05 |
| IN 718 (0.9 mm) | 0.64 | 0.19 | 1.06 | 0.65 | 0.19 | 1.09 |

## Results

Figure 5.4 shows the deformed configuration of tubes at the bursting points for round to square and round to V shapes. As shown in this figure the model predicts the bursting location at the expected locations. In the first case study (round to square shape), for SS 321 the burst was located at the top, while for IN 718 the burst was located at the side. The experimental and simulation burst pressure results are presented here to show the validity of this new damage model for real THF processes of aerospace materials.

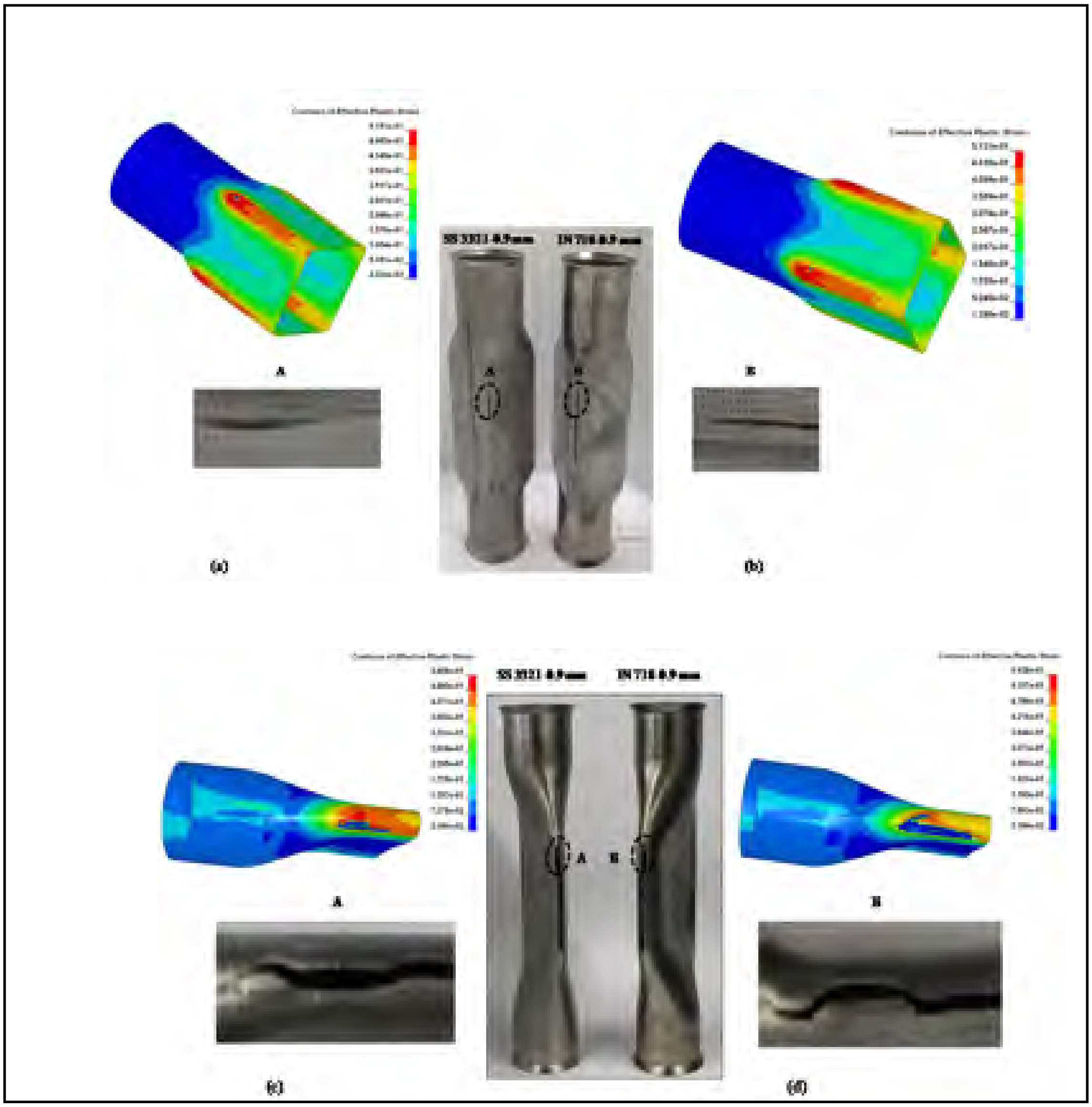

Figure 5.4: Results from numerical damage simulations of round to square experiments using the 3D model (a) round to square 0.9 mm SS 321, (b) round to square 0.9 mm IN 718 (c) round to V 0.9 mm SS 321 and (d) round to V 0.9 mm IN 718.

As shown in Table 5.2 the maximum error for SS 321 and IN 718 tubes with 0.9 mm is less than 6% for the round to square shape and the maximum error for the round to V shape with the same thickness is less than 7.5%. This shows that, the calibration method and the new damage model can be used in multistep THF processes correctly. It is noteworthy that for all case studies the model underestimate burst pressure which in on the safe side.

Table 5.2: Comparison of the predicted burst pressures for without end feeding condition.

| **Material** | **Round to square** | | | **Round to V** | | |
|---|---|---|---|---|---|---|
| | **Experiment (MPa)** | **Simulation (MPa)** | **Error (%)** | **Experiment (MPa)** | **Simulation (MPa)** | **Error (%)** |
| SS 321 (0.9 mm) | 136.0, 142.0, 144.0<br>Average (140.7) | 132.8 | -5.6 | 121.0, 128.0, 132.0<br>Average (127.0) | 118 | -7.0 |
| IN 718 (0.9 mm) | 165.0, 176.0, 174.0<br>Average (171.7) | 163.4 | -5.0 | 154.0, 156.0, 156.0<br>Average (155.3) | 144.0 | -7.3 |

## CONCLUSION

Numerical analyses were conducted to study the round to square THF process. The burst pressure points based on the new decoupled damage model were investigated. Then, the results from experimental and FEA were compared to verify the developed FE damage model.

The comparison between the FEM results and the experimental data showed that the new damage model is accurate enough for prediction of bursting point (less than 8% errors).

The Bonora tensile test group was accurate enough to determine the new damage model constants. As shown inTable 5.1, the difference between the constant values are small, then it would be more cost effective to select just Borora tensile test model to find the damage constants.

# CHAPTER 6

# THESIS SUMMARY

## Introduction

Failure during tube hydroforming is a common problem occuring in several tube hydroforming industrial sectors, such as aerospace, automobile, etc. It becomes an even more important issue when the part to be formed is made of super alloys, such as Inconel. Any solution to prevent or predict bursting or another failure during this process should start with a comprehensive study of the fundamentals of material behavior. Then, the failure prediction and prevention will require more accurate material models and close attention.

The experimental and numerical research work presented in this thesis consisted of three parts which put together are construct the main objective of this research work (Figure 6.1). The first parts of this study is devoted to a new combined analytical and experimental study to determine the material characterization for tube hydroforming by doing free expansion tests of SS 321, SS 304, In 718 and AA-0 6061. The second part focuses on determination of material behavior after the onset of instability, including predictive analytical-numerical weighted average method and a new work hardening function that is developed for ductile materials. The burst prediction and a new user material model for FE modeling of tube hydroforming process of ductile materials is the subject of the last part of this thesis. As described in the introduction, all these three aspects are related to others and were designed for prediction of material behavior and developing a new user material which is one of the main research objective(s) of this work (Figure 6.1).

This chapter presents a discussion of the obtained results in each part and aims to link them with the proposed research objectives in this work.

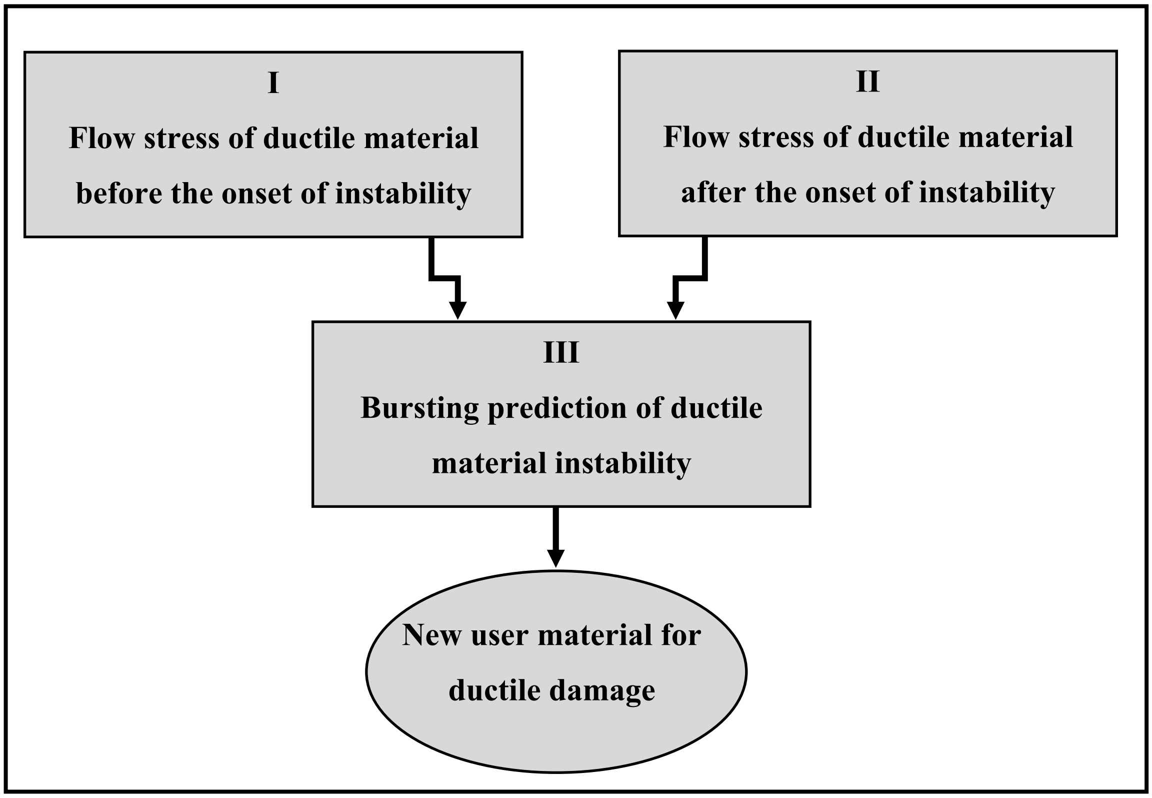

Figure 6.1: Main stages of the research objectives.

## Material characterization for tube hydroforming

In recent years, process simulations have been increasingly used to determine the feasibility of a hydroforming process or to optimize the THF process parameters. The material model used as an input for the FE simulations plays an important role in reliable prediction of the results. In general, the material parameters for FE modeling applications are determined by different methods such as tensile testing, free expansion/bulge testing and dome height testing. During tensile testing, the specimen is subjected to a uni-axial state of stress, which does not reflect the bi-axial state of deformation encountered during THF. Moreover, intermediate processes such as rolling, sizing and welding involved in the manufacturing of tubes from sheets affect the formability of the tubular material. Therefore, material data for THF would benefit in being extracted from tubular samples tested under a biaxial state of stress.

Several studies concerning the determination of properties for tubular materials have been reported in literature (Aue-U-Lan, Ngaile and Altan, 2004; Imaninejad, Subhash and Loukus, 2004; Vollertsen and Plancak, 2002). Specifically, Aue and Ngaile (Aue-U-Lan, Ngaile and Altan, 2004) optimized the THF process by validating their simulations using experiments. The effects of friction and material properties on formability of tubes were shown in their study. Imaninejad (Imaninejad, Subhash and Loukus, 2004) showed that strain hardening has the greatest influence on the formability of the tubes. Hwang (Hwang and Wang, 2009) determined the flow stress for zinc-copper and carbon steel alloys by using hydraulic bulge (free expansion) testing.

Flow stress during the bulge testing is strongly affected by the bulge profile, Koç (Koç, Aue-u-lan and Altan, 2001) proposed a combination of an online and offline measurement procedure to determine the necessary parameters (longitudinal and circumferential radius of curvature, as well as expansion and thickness at the maximum bulge height) to calculate the stress-strain curve. Hwang and Lin (Hwang and Lin, 2002) assumed that the profile of the bulged zone was elliptical. More recently, Hwang (Hwang, Lin and Altan, 2007) calculated the stress-strain curve from the experimental data using online measurement of the bulge height by assuming an elliptical bulge profile and measuring the thickness by cutting the tubes at different stages of the hydroforming process. Bortot (Bortot, Ceretti and Giardini, 2008) developed an offline analytical approach using a coordinate measuring machine (CMM) to measure the bulge profile and the tube thickness at different stages of the process.

Though research work on THF is well underway, up to now, most of these studies have focused on aluminum alloys and mild steels, mainly for automotive applications. Fundamental knowledge of the THF process is still very limited for most aerospace materials, such as nickel base superalloys and stainless steels. To advance the knowledge related to the THF for aerospace materials, tube bulge hydroforming in a free expansion die is a good method for studying the biaxial deformation of tubes. Therefore, it could be inferred that the tube profile and the accuracy of the calculated stress and strain strongly affects the flow stress curve before onset of instability. The presented outcomes were written as a journal article (see chapter 2) that was published in International Journal of Advanced Manufacturing and Technology in 2014.

### Work hardening laws

Work hardening model is one of the principal factors in FE modeling of THF process. Although most of the existing research works in literature aim to predict the material behavior before the onset of instability, it is in term of work hardening perspective that the formability of tubular nickel base superalloys and stainless steels were not evaluated. Therefore, further studies by means of modeling of material behavior during the THF process need to be carried out. Based on the previous studied that was done for nickel base superalloys and stainless steels the Swift hardening law was used in prediction of material behavior before necking. In chapter two more focus was paid to determine the Swift hardening law constant by using the bulge test.

A conference article on work hardening law was presented in the 16th ESAFORM Conference on Material Forming, which was held in Aveiro, Portugal, in April 2013 (see APPENDIX III).

### Study the material behavior after the onset of instability for ductile materials

Investigations on material behavior after onset of necking were conducted using some experimental, analytical and numerical methods such as FE simulations. It is noteworthy to mention that due to the complexity of material behavior after the onset of instability, most of the previous studies were based on round specimens (Bridgman, 1952; Mirone, 2004). One of the objectives of this thesis in chapter three is to address this issue by trying to understand how to accurately determine the mechanical properties of some aerospace alloys, such as IN 718, SS 321, Ti6Al4V after the onset of necking by developing a methodology based on uniaxial tensile testing. Another objective of this section of the thesis is to develop a procedure/method that can be applied to all type of uniaxial specimens (the flat or the round geometries). Two semi analytical methods, the weighted-average and the novel hardening approaches are proposed to determine the flow behavior after necking. As shown in the chapter three, the application of the weighted average method in FE modeling is simpler, but this method could not be used for an exponential hardening function due to complexity in the analytical derivation. Then FE modeling was used as a tool to obtain the predicted load displacement results of the two above methods, which were later compared with the experimental results.

The presented outcomes based on the new work hardening law and weighted average method were exposed in two conferences articles (see APPENDIX IV) and one journal article. The conference papers were presented in the 15th ESAFORM Conference on Material Forming, which was held in Erlangen, Germany, in March 2012 and in proceeding of Materials Science & Technology 2013, Montreal, Canada. The major contribution was submitted to Journal of Computational Materials Science (see chapter 3)

### Failure modeling of THF process for ductile materials

Knowing that the best setting levels of unknown material parameters to minimize each error are not similar for all metal forming processes, the question drawn is how to obtain the best setting levels of unknown material parameters to reach the accurate and optimum damage model prediction. This issue becomes more complex considering that for some metal forming process such as THF the forming process parameters such as end feeding and friction condition can precede or delay the onset of failure during the process. Therefore, in this study, as discussed in chapters two and three, the numbers of assumptions were reduced. The main concerns considered in this work are as follows:

(1) Determine the material behavior before onset of necking more accurately.
(2) Determine the material behavior after the onset of necking for sheet to find damage constants for THF process more accurately.
(3) Develop an elastic-plastic new user material model based on the influenced parameters for the THF process of aerospace materials.

Hence the importance of applying new modifications to the decoupled damage model is necessary. We conducted a study to develop an elastic-plastic damage model for simultaneously predict the onset of failure during the THF process and implement it to a commercial finite element software (LS-Dyna). This part of the work has led to a conference article that was presented in ESAFORM 2011 (APPENDIX I) and a journal article which was submitted to International Journal of Solids and Structures, 2014 (see chapter 4).

## Key contributions and outcomes of the thesis

The key contribution of this thesis can be summarized in the following main points:

1. The generated pool of data presented in this research work provides then a valuable data base for the alloys that were studied in this research. Specifically, to determine the stress-strain curve by the free expansion test, a novel online measurement approach was developed using a 3D automated deformation measurement system (Aramis®) to extract the coordinates of the bulge profile during the test. These coordinates were used to calculate the circumferential and longitudinal curvatures, which were then utilized to determine the effective stresses and effective strains at different stages of the THF process. It is noteworthy that with this approach all the data is generated through a single test in contrast to the conventional methods that use multiple tests to generate the same type of data. In addition, as the curvatures are calculated with the experimental coordinates, there is no assumption (circular, elliptical, etc.) associated to the shape of the section, thus resulting in more accurate analytical results with the methodology presented in this thesis. The flow stresses obtained from the free expansion tests were compared with those obtained from tensile testing of the specimens extracted from the tubes for the materials considered in this work, i.e. SS 304L, SS 321, IN 718 and AA 6061-0. The result showed that the new methodology was more accurate than tensile testing.

2. A tool was developed to determine the true stress-strain curve in post-necking regime for different aerospace alloys, such as Inconel 718 (IN 718), Stainless steel 321 (SS 321) and Titanium (Ti6Al4V). Uniaxial tensile tests based on ASME E8M-11standard were

performed to determine the true stress-strain before necking. Two different methods, a weighted-average method and a new hardening equation were utilized to extend the true stress-strain curve for post necking. These curves were used as the flow stress models to simulate dome test. The simulation results of the dome test were within 2.6 % of the experimental data when using the true stress-true strain curve generated based on the approach proposed in this work.

3. A new damage model based on stress triaxiality, the concentration factor and three constants was developed to determine the FLDf and the bursting point for SS 321. An inverse FE modeling of different tensile test shapes and hourglass specimens with different widths (12.7 mm, 50.8 mm, 76.2 mm, 127 mm and 177.8 mm) were adopted to obtain experimental fracture data to calibrate the critical damage values that was developed in this research. This new damage model was implemented in a 3D commercial FE software (LS-DYNA) through a new user material. The simulation results of bursting points were within 1% of the experimental data when using the new damage model. Also, the FLDf generated by the new user material was closer to the experimental data.

The new developed user material was used to predict the bursting point in some real THF process (round to square and round to V shapes). The simulation results of bursting points were within 6% of the experimental data for the round to square shape and within 7% for the round to V shape when using the new damage model.

# CONCLUSION

Recently, finite element analysis enabled the creation of better designs by identifying failure modes early on, reducing the cost of prototyping and helping to avoid warranty costs down the road especially in aerospace industries. The main purpose of using these numerical tools in the simulation of THF is to accurately model the material behavior and to predict the occurrence of failure in the aerospace alloys during its design and development phases. However, due to the high complexity, nonlinearity and interactivity of several phenomena involved in the THF process, the numerical results may not match well the experiments. Many efforts have been made to improve numerical tools in order to reproduce industrial applications in a reliable manner. The introduction of a new methodology to evaluate the flow stress, mechanical characterization and damage model for providing better predictability have been the subject of this thesis to meet the requirements of aerospace manufacturers such as Pratt & Whitney and Bell Helicopter.

One of the failures that can occur during a THF process is the bursting occurrence. Usually, this phenomenon is preceded by the occurrence of a plastic instability, a localized neck, which is taken as the criterion for the rejection of a part. Usually, the forming limit diagram at the onset of necking is used for finding the limit value for a metal forming process. However, the usage of high strength materials has brought new challenges during the formability study and to the numerical simulation of metal forming processes especially for a complex process such as the THF. These new materials are characterized by higher values of tensile strength but present lower ductility when compared to the traditional materials. This lower ductility makes these materials particularly inclined to fracture during processing, without any prior indication of necking occurrence. This unexpected fracture raises questions on the use of the conventional forming limit diagram concept based on the localized necking to evaluate the formability of these materials and has promoted the need for introducing new failure criteria to predict such a behavior. The trend of this research work was to improve the forming limit diagram concept by the use of theories that introduce ductile failure indicators based on the definition of an internal variable that represents the state and evolution of internal degradation of the mechanical properties of the material.

The work presented in this research work follows the trend and interest shown by industries on such theories, and aims to contribute to the improvement of numerical material models in predicting fracture in the tube hydroforming process by adopting ductile damage models, within the framework of decoupled damage theory. For this purpose, first, a new methodology was presented to predict the true stress-true strain before the onset of necking for the tube hydroforming process, which has the minimum number of assumptions to evaluate the flow stress accurately. Then a novel methodology was developed to generate the flow stress after the onset of the instability, namely the weighted average method and the new work hardening equation, in order to determine the damage constants for the new decoupled damage model based on the inverse method. A decoupled damage model behavior was formulated further by considering the effect of stress triaxiality and strain paths. Then for the implementation of the new damage model, a decoupled plasticity and damage algorithm was proposed. A comparison between experiments and numerical models has shown that the new decoupled algorithm can predict the failure point in tube hydroforming operations without a significant loss in the accuracy of the evolution of progressive plastic softening that is considered in a coupled plasticity and damage algorithm.

The proposed new user material model was applied to a nickel base superalloy (IN 718) and a stainless steel alloy (SS 321) to predict FLDfs and bursting points. One may conclude that the new damage model can provide satisfactory failure predictions in accordance with experimental results. Therefore, this new damage model introduces a lower complexity in the constitutive model and consequently, reduces computational time compared to the coupled damage model with plastic softening algorithm.

By using the proposed methodology for considering the effective stress triaxiality state in the damage model and correction of work hardening results have shown that the selected procedure can improve fracture predictions. Likewise, this new methodology based on all aforementioned steps (chapter 2 to 4) is a powerful tool for aerospace industries in the feasibility study and development stages of new products.

# FUTURE WORKS

Some perspectives concerning the continuity of the present work and potential topics for future research are listed below:

- Extensive experimental program for damage models validation. An effort should be devoted in the development of a methodology for identification of damage constants to be used in such models.
- Develop inverse techniques and minimization procedures to fully characterize the developed models and determine failure forming limit diagram behavior for different materials.
- Enhancement of decoupled and coupled damage models by adopting the effect of friction and end feeding during the THF process. However, the effect of strain paths was considered in the developed damage model.
- Development and application of more advanced experimental setup, to capture the flow stress behavior of tube after the onset of necking up to onset of bursting to improve material behavior modelling.
- Extension of the constitutive models by using more advanced plasticity models and including strain rate sensitivity and anisotropic dependency parameters towards the increase of accuracy in failure predictions.
- Expanding experimental and simulation works using an optimization algorithms based on the new damage model to produce a part by the THF process without any failure.

# APPENDIX I

## PREDICTION OF BURST PRESSURE USING DECOUPLED DUCTILE FRACTURE CRITERIA FOR TUBE HYDROFORMING OF AEROSPACE ALLOYS

14th International Conference on Metal Forming-ESAFORM 2011
April 27-29, 2011, Belfast, Northern Ireland
AIP Conference Proceedings , p. 301-306. Melville, NY, USA : American Institute of Physics.

M. Saboori[ab], J. Gholipour[b], H. Champliaud[a], A. Gakwaya[c] J. Savoie[d] and P. Wanjara[b]

[a]École de technologie supérieure, Montreal, Canada,
[b]Institute for Aerospace Research of NRC, Aerospace Manufacturing Technology Centre, Montreal, Canada
[c]Laval University, Quebec city, Canada
[d]Pratt & Whitney Canada, Special Process Development Group, Longueuil, Canada

**Abstract** One of the failure modes in tube hydroforming (THF) is bursting. To predict the burst pressure in the THF process, Brozzo's decoupled ductile fracture criterion was used in conjunction with a dynamic nonlinear commercial finite element software, Ls-Dyna, and the criterion was evaluated using the data obtained from the free expansion (tube bulging) tests performed on 0.9 mm and 1.2 mm thick stainless steel (SS) 321 tubes. The predicted burst pressures were compared with the experimental results for both thicknesses. The predicted burst failure of the tube bulging, based on the Brozzo's criterion, demonstrated a good agreement with the experimental data, indicating that the present approach for predicting the burst failure for the tube bulging can be extended to predict formability limits in THF applications.

**Keywords** Decoupled ductile fracture criterion, Tube bulging, Free expansion, Tube hydroforming

# APPENDIX II

## STUDY OF TRUE STRESS-STRAIN CURVE AFTER NECKING FOR APPLICATION IN DUCTILE FRACTURE CRITERIA IN TUBE HYDROFORMING OF AEROSPACE MATERIAL

15th International Conference on Metal Forming-ESAFORM 2012
March 14-16, 2012, Erlangen, Germany
Key Engineering Materials, 504-506. , p. 95-100. Trans Tech Publications Ltd.

M. Saboori[ab], H. Champliaud[a], J. Gholipour[b], A. Gakwaya[c], J. Savoie[d] and P. Wanjara[b]

[a]École de technologie supérieure, Montreal, Canada,
[b]NRC Aerospace, Aerospace Manufacturing Technology Centre, Montreal, Canada
[c]Laval University, Quebec city, Canada
[d]Pratt & Whitney Canada, Longueuil, Canada

**Abstract.** The increased demand for weight reduction and manufacture of complex shapes with tube hydroforming (THF) requires more accurate material models to achieve highly reliable results from simulations. Conventional flow behaviours of materials implemented in commercial finite element (FE) software are not capable of describing accurately the material behaviour after localization. Utilization of the stress-strain data after necking can improve the quality of the FE analysis by employing realistic data for extrapolating the stress-strain curve. In this paper, the objective was to develop a simple tool that can determine the true stress-strain curve after necking in order to predict the material behaviour of aerospace alloys such as stainless steel 321 (SS321). Standard uniaxial tensile tests (ASME E8M-04) were performed to determine the true stress-strain before necking. A weighted-average method and a new hardening equation were proposed to extend the curve after necking.

**Keywords:** Work hardening law, Material behaviour, Weighted average method, Diffuse necking

# APPENDIX III

## EFFECT OF MATERIAL MODEL ON FINITE ELEMENT MODELING OF AEROSPACE ALLOYS

16th International Conference on Metal Forming-ESAFORM 2013
April 22-24, 2013 Aveiro, Portugal
Key Engineering Materials, 554-557. , p. 151-156. Zurich-Durnten, Switzerland : Trans Tech Publications Ltd.

M. Saboori[ab], J. Gholipour[b] ,H. Champliaud[a], A. Gakwaya[c], J. Savoie[d] and P. Wanjara[b]

[a]École de technologie supérieure, Montreal, Canada,
[b]NRC Aerospace, Aerospace Manufacturing Technology Centre, Montreal, Canada
[c]Laval University, Quebec city, Canada
[d]Pratt & Whitney Canada, Longueuil, Canada

**Abstract** Increasing acceptance and use of hydroforming technology within the aerospace industry requires a comprehensive understanding of critical issues such as the material characteristics, friction condition and hydroformability of the material. Moreover, the cost of experiments can be reduced by accurate finite element modeling (FEM) entails the application of adapted constitutive laws for reproducing with confidence the material behavior. In this paper, the effect of different constitutive laws on FEM of tubular shapes is presented. The free expansion process was considered for developing the FEM. Bulge height, thickness reduction and strains were determined at the maximum bulge height using different constitutive models, including Hollomon, Ludwik, Swift, Voce and Ludwigson. In order to minimize the effect of friction, the free expansion experiments were performed with no end feeding. The simulation results were compared with theexperimental data to find the appropriate constitutive law for the free expansion process.

**Keywords:** Free expansion test, Tube bulge test, Constitutive law, Hydroforming

# APPENDIX IV

# DEVELOPMENT OF AN INVERSE METHOD FOR MATERIAL CHARACTERIZATION

Materials Science and Technology Conference and Exhibition 2013, MS and T 2013 (Montreal, QC, Canada, Oct. 27-31, 2013), p. 694-701. Warrendale, PA, USA : Association for Iron and Steel Technology.

M. Saboori[ab], J. Gholipour[b] ,H. Champliaud[a], A. Gakwaya[c], J. Savoie[d] and P. Wanjara[b]

[a]École de technologie supérieure, Montreal, Canada,
[b]NRC Aerospace, Aerospace Manufacturing Technology Centre, Montreal, Canada
[c]Laval University, Quebec city, Canada
[d]Pratt & Whitney Canada, Longueuil, Canada

**Abstract** Conventional engineering analysis involves the determination of material properties under uniaxial loading conditions. The true stress-true strain curves generated through this way have been used in finite element modeling (FEM) of various forming processes. However, this method is only valid up to the onset of necking; after this point the stress state is not uniaxial and the discrepancies between FEM results and experimental data are significant. In this paper a new work hardening equation for predicting material behavior after the instability was used for stainless steel 321 (SS 321) and Inconel 718 (IN 718). A finite element model based on an inverse method was devised with the aim of determining the properties of isotropic materials after instability. To facilitate the process of material characterization, an algorithm was developed using LS-DYNA and Matlab software. Verification of this methodology was carried out by comparing the experimental load-displacement data (obtained by tensile testing) with the simulation results.

**Keywords:** Inverse Method, Finite-element simulation, Material properties

# LIST OF REFERENCES

Abrantes, JP, A Szabo-Ponce and GF Batalha. 2005. « Experimental and numerical simulation of tube hydroforming (THF) ». *Journal of materials processing technology,* vol. 164, p. 1140-1147.

Aguir, Hamdi, Hédi BelHadjSalah and Ridha Hambli. 2011. « Parameter identification of an elasto-plastic behaviour using artificial neural networks–genetic algorithm method ». *Materials & Design,* vol. 32, n$^{o}$ 1, p. 48-53.

Ahmadi, S, AR Eivani and A Akbarzadeh. 2009. « An experimental and theoretical study on the prediction of forming limit diagrams using new BBC yield criteria and M–K analysis ». *Computational Materials Science,* vol. 44, n$^{o}$ 4, p. 1272-1280.

Ahmed, M, and MSJ Hashmi. 1997. « Estimation of machine parameters for hydraulic bulge forming of tubular components ». *Journal of materials processing technology,* vol. 64, n$^{o}$ 1, p. 9-23.

Ahmetoglu, Mustafa, and Taylan Altan. 2000. « Tube hydroforming: state-of-the-art and future trends ». *Journal of Materials Processing Technology,* vol. 98, n$^{o}$ 1, p. 25-33.

Ahmetoglu, Mustafa, Kevin Sutter, XJ Li and T Altan. 2000. « Tube hydroforming: current research, applications and need for training ». *Journal of Materials Processing Technology,* vol. 98, n$^{o}$ 2, p. 224-231.

Anderson, Mélissa. 2010. « Tube hydroforming of aerospace alloys: material characterization methods ». École de technologie supérieure.

Anderson, Ted L. 2005. *Fracture mechanics: fundamentals and applications*. CRC press.

Argon, AS, J Im and R Safoglu. 1975. « Cavity formation from inclusions in ductile fracture ». *Metallurgical Transactions A,* vol. 6, n$^{o}$ 4, p. 825-837.

Asnafi, Nader. 1999. « Analytical modelling of tube hydroforming ». *Thin-Walled Structures,* vol. 34, n$^{o}$ 4, p. 295-330.

Assempour, Ahmad, Hamid Khakpour Nejadkhaki and Ramin Hashemi. 2010. « Forming limit diagrams with the existence of through-thickness normal stress ». *Computational Materials Science,* vol. 48, n$^{o}$ 3, p. 504-508.

Aue-U-Lan, Yingyot, Gracious Ngaile and Taylan Altan. 2004. « Optimizing tube hydroforming using process simulation and experimental verification ». *Journal of Materials Processing Technology,* vol. 146, n$^{o}$ 1, p. 137-143.

Ávila, Antonio F, and Evanio LS Vieira. 2003. « Proposing a better forming limit diagram prediction: a comparative study ». *Journal of materials processing technology,* vol. 141, n° 1, p. 101-108.

Bai, Yuanli, and Tomasz Wierzbicki. 2008. « A new model of metal plasticity and fracture with pressure and Lode dependence ». *International Journal of Plasticity,* vol. 24, n° 6, p. 1071-1096.

Bai, Yuanli, and Tomasz Wierzbicki. 2010. « Application of extended Mohr–Coulomb criterion to ductile fracture ». *International Journal of Fracture,* vol. 161, n° 1, p. 1-20.

Banabic, Dorel, Frédéric Barlat, Oana Cazacu and Toshihiko Kuwabara. 2010. « Advances in anisotropy and formability ». *International journal of material forming,* vol. 3, n° 3, p. 165-189.

Bao, Yingbin, and Tomasz Wierzbicki. 2004. « On fracture locus in the equivalent strain and stress triaxiality space ». *International Journal of Mechanical Sciences,* vol. 46, n° 1, p. 81-98.

Bao, Yingbin, and Tomasz Wierzbicki. 2005. « On the cut-off value of negative triaxiality for fracture ». *Engineering fracture mechanics,* vol. 72, n° 7, p. 1049-1069.

BARATA DA ROCHA, Augusto. 1985. « Mise en forme des tôles minces: instabilité plastique, anisotropie et endommagement ».

Belytschko, Ted, Jerry I Lin and Tsay Chen-Shyh. 1984. « Explicit algorithms for the nonlinear dynamics of shells ». *Computer methods in applied mechanics and engineering,* vol. 42, n° 2, p. 225-251.

Bohme, W, D-Z Sun, W Schmitt and A Honing. 1992. « Application of micromechanical material models to the evaluation of Charpy tests ». *Advances in local fracture/damage models for the analysis of engineering problems*, p. 203-216.

Bonora, Nicola, Domenico Gentile, A Pirondi and Golam Newaz. 2005. « Ductile damage evolution under triaxial state of stress: theory and experiments ». *International Journal of Plasticity,* vol. 21, n° 5, p. 981-1007.

Bortot, P, E Ceretti and C Giardini. 2008. « The determination of flow stress of tubular material for hydroforming applications ». *Journal of Materials Processing Technology,* vol. 203, n° 1, p. 381-388.

Bressan, JD, and JA Williams. 1983. « The use of a shear instability criterion to predict local necking in sheet metal deformation ». *International Journal of Mechanical Sciences,* vol. 25, n° 3, p. 155-168.

Bridgman, Percy Williams. 1952. *Studies in large plastic flow and fracture with special emphasis on the effects of hydrostatic pressure*. McGraw-Hill.

Brokken, Dirk, WAM Brekelmans and FPT Baaijens. 1998. « Numerical modelling of the metal blanking process ». *Journal of Materials Processing Technology,* vol. 83, n° 1, p. 192-199.

Brozzo, P, B Deluca and R Rendina. 1972. « A new method for the prediction of formability limits in metal sheets ». In *Proc. 7th biennal Conf. IDDR*.

Veuillez sélectionner un type de document autre que « Generic » afin de faire afficher la référence bibliographique.

Butuc, MC, D Banabic, A Barata da Rocha, JJ Gracio, J Ferreira Duarte, P Jurco and DS Comsa. 2002. « The performance of Yld96 and BBC2000 yield functions in forming limit prediction ». *Journal of materials processing technology,* vol. 125, p. 281-286.

Butuc, MC, JJ Gracio and A Barata da Rocha. 2003. « A theoretical study on forming limit diagrams prediction ». *Journal of Materials Processing Technology,* vol. 142, n° 3, p. 714-724.

Butuc, MC, JJ Gracio and A Barata da Rocha. 2006. « An experimental and theoretical analysis on the application of stress-based forming limit criterion ». *International Journal of Mechanical Sciences,* vol. 48, n° 4, p. 414-429.

Carleer, B, G Van Der Kevie, L De Winter and B Van Veldhuizen. 2000. « Analysis of the effect of material properties on the hydroforming process of tubes ». *Journal of Materials Processing Technology,* vol. 104, n° 1, p. 158-166.

Chen, Jieshi, Xianbin Zhou and Jun Chen. 2010. « Sheet metal forming limit prediction based on plastic deformation energy ». *Journal of Materials Processing Technology,* vol. 210, n° 2, p. 315-322.

Chen, K. 2002. « A bursting failure criterion for tube hydroforming ». *Metal Forming,* vol. 2014, p. 11-05.

Chen, Kuo-Kuang. 2001. « The bulge of tubes and a failure criterion for tube hydroforming ». *Fuel,* vol. 1, p. 1126.

Chen, Kuo-Kuang, Ronald J Soldaat and Robert M Moses. 2004. « Free expansion bulge testing of tubes for automotive hydroform applications ». *SAE transactions,* vol. 113, n° 5, p. 391-399.

Chow, CL, SJ Hu and M Jie. 2003. « Forming limit analysis of sheet metals based on a generalized deformation theory ». *Journal of engineering materials and technology,* vol. 125, n° 3, p. 260-265.

Chow, CL, and XJ Yang. 2002. « Bursting for fixed tubular and restrained hydroforming ». *Journal of materials processing technology,* vol. 130, p. 107-114.

Chu, E, and Yu Xu. 2004. « Hydroforming of aluminum extrusion tubes for automotive applications. Part I: buckling, wrinkling and bursting analyses of aluminum tubes ». *International Journal of Mechanical Sciences,* vol. 46, n° 2, p. 263-283.

Chu, E, and Yu Xu. 2008. « Influences of generalized loading parameters on FLD predictions for aluminum tube hydroforming ». *Journal of materials processing technology,* vol. 196, n° 1, p. 1-9.

Chu, E, Yu Xu, RW Daxies and GJ Grant. 2006. « Failure predictions for aluminum tube hydroforming processes ». *Proceedings of SAE2006, SAE Paper*, n° 2006-01, p. 0543.

Cockcroft, MG, and DJ Latham. 1968. « Ductility and the workability of metals ». *J Inst Metals,* vol. 96, n° 1, p. 33-39.

Considère, A. 1870. « Poussée des terres ». In *Annales des Ponts et Chaussées.* Vol. 19, p. 547.

Cooreman, S, D Lecompte, H Sol, J Vantomme and Dimitri Debruyne. 2007. « Elasto-plastic material parameter identification by inverse methods: Calculation of the sensitivity matrix ». *International journal of solids and structures,* vol. 44, n° 13, p. 4329-4341.

Doege, E, and K Dröder. 1997. « Processing of magnesium sheet metals by deep drawing and stretch forming ». *Matériaux et techniques,* vol. 85, n° 7-8, p. 19-23.

Dohmann, F, and Ch Hartl. 1997. « Tube hydroforming—research and practical application ». *Journal of Materials Processing Technology,* vol. 71, n° 1, p. 174-186.

E8, Astm. 2011. « Standard test methods for tensile testing of metallic materials ». *Annual book of ASTM standards,* vol. 3.

Farzin, M, HR Javani, M Mashayekhi and R Hambli. 2006. « Analysis of blanking process using various damage criteria ». *Journal of materials processing technology,* vol. 177, n° 1, p. 287-290.

Fleck, NA, JW Hutchinson and V Tvergaard. 1989. « Softening by void nucleation and growth in tension and shear ». *Journal of the Mechanics and Physics of Solids,* vol. 37, n° 4, p. 515-540.

Fuchizawa, S, and M Narazaki. 1993. « Bulge test for determining stress-strain characteristics of thin tubes ». *Advanced technology of plasticity,* vol. 1, p. 488-493.

FUCHS, FJJR. 1966. « Hydrostatic pressure--its role in metal forming ». *Mech Eng,* vol. 88, n$^o$ 4, p. 34-40.

Gänser, H-P, EA Werner and FD Fischer. 1998. « Plasticity and ductile fracture of IF steels: experiments and micromechanical modeling ». *International Journal of Plasticity,* vol. 14, n$^o$ 8, p. 789-803.

Garrison Jr, WM, and NR Moody. 1987. « Ductile fracture ». *Journal of Physics and Chemistry of Solids,* vol. 48, n$^o$ 11, p. 1035-1074.

Ghosh, Amit K, and Joseph V Laukonis. 1977. « Influence of Strain-Path Changes on the Formability of Sheet Steel ». *Sheet Metal Forming and Energy Conversion. ASM, Metals Park, Ohio. 1977, 167-178.*

Goods, SH, and LM Brown. 1979. « Overview No. 1: The nucleation of cavities by plastic deformation ». *Acta Metallurgica,* vol. 27, n$^o$ 1, p. 1-15.

Goodwin, Gorton M. 1968a. « Application of strain analysis to sheet-metal- forming problems in the press shop ». *MET ITAL,* vol. 60, n$^o$ 8, p. 767-774.

Goodwin, Gorton M. 1968b. Application of strain analysis to sheet metal forming problems in the press shop. SAE Technical Paper.

Graf, Alejandro, and William Hosford. 1993. « Effect of changing strain paths on ». *Metallurgical transactions A,* vol. 24, n$^o$ 11, p. 2503-2512.

Graf, Alejandro, and William Hosford. 1994. « The influence of strain-path changes on forming limit diagrams of A1 6111 T4 ». *International Journal of Mechanical Sciences,* vol. 36, n$^o$ 10, p. 897-910.

Graf, Alejandro, and William F Hosford. 1990. « Calculations of forming limit diagrams ». *Metallurgical Transactions A,* vol. 21, n$^o$ 1, p. 87-94.

US Patent 2,203,868. 1940. *Apparatus for making wrought metal T's.*

Green, DE, and TB Stoughton. 2004. « Evaluating hydroforming severity using stress-based forming limits ». *In Second Annual Hydroforming Conference.*

Groche, P. 2004. « v. Breitenbach G., Tubular semi-finished product characterisation and optimisation for tube hydroforming ». In *Proceedings of international conference on innovations in metal forming*. p. 23-24.

Groche, P, G v Breitenbach and R Steinheimer. 2003. « Investigation of the influence of the pre-hydroforming processes and development of characterization methods for the testing of steel semi-products for hydroforming ». *Proceeding of Tube Veracruz, Veracruz, Mexico*.

Groche, Peter, and Gerrit v Breitenbach. « Tubular semi-finished product characterisation and optimisation for tube hydroforming ».

Guan, Yabo, Farhang Pourboghrat and Woong-Ryeol Yu. 2006. « Fourier series based finite element analysis of tube hydroforming: An axisymmetric model ». *Engineering computations,* vol. 23, n° 7, p. 697-728.

Gurson, Arthur L. 1975. *Continuum theory of ductile rupture by void nucleation and growth. Part I. Yield criteria and flow rules for porous ductile media*. Brown Univ., Providence, RI (USA). Div. of Engineering.

Gutierrez, MA, V Picozzi, J Ripodas, L Gunnarsson, G Breitenbach, M Schneider, W Urech and I Pascual. 2007. « Investigation of the influence of the pre hydroforming processes and development of characterization methods for the testing of steel semi-products for hydroforming-HYDROTEST ». *EUR*, n° 22447, p. 1-248.

Han, Heung Nam, and Keun-Hwan Kim. 2003. « A ductile fracture criterion in sheet metal forming process ». *Journal of Materials Processing Technology,* vol. 142, n° 1, p. 231-238.

Hartl, Ch. 2005. « Research and advances in fundamentals and industrial applications of hydroforming ». *Journal of Materials Processing Technology,* vol. 167, n° 2, p. 383-392.

Hashmi, MSJ, and R Crampton. 1985. « Hydraulic bulge forming of axisymmetric and asymmetric components: comparison of experimental results and theoretical predictions ». In *Twenty-Fifth International Machine Tool Design and Research Conference*. p. 541-549.

Hill, R. 1979. « Theoretical plasticity of textured aggregates ». *Math. Proc. Cambridge Philos. Soc.,* vol. 85, n° 1, p. 179-191.

Hill, R t. 1952. « On discontinuous plastic states, with special reference to localized necking in thin sheets ». *Journal of the Mechanics and Physics of Solids,* vol. 1, n° 1, p. 19-30.

Hockett, JE, and OD Sherby. 1975. « Large strain deformation of polycrystalline metals at low homologous temperatures ». *Journal of the Mechanics and Physics of Solids,* vol. 23, n° 2, p. 87-98.

Holmberg, Stefan, Bertil Enquist and Per Thilderkvist. 2004. « Evaluation of sheet metal formability by tensile tests ». *Journal of materials processing technology,* vol. 145, n° 1, p. 72-83.

Horstemeyer, MF, S Ramaswamy and M Negrete. 2003. « Using a micromechanical finite element parametric study to motivate a phenomenological macroscale model for void/crack nucleation in aluminum with a hard second phase ». *Mechanics of Materials,* vol. 35, n° 7, p. 675-687.

Hu, Jack, Zdzislaw Marciniak and John Duncan. 2002. *Mechanics of sheet metal forming*. Butterworth-Heinemann.

Hwang, Yeong-Maw, and Yi-Kai Lin. 2002. « Analysis and finite element simulation of the tube bulge hydroforming process ». *Journal of materials processing technology,* vol. 125, p. 821-825.

Hwang, Yeong-Maw, Yi-Kai Lin and Taylan Altan. 2007. « Evaluation of tubular materials by a hydraulic bulge test ». *International Journal of Machine Tools and Manufacture,* vol. 47, n° 2, p. 343-351.

Hwang, Yeong-Maw, Yi-Kai Lin and Han-Chieh Chuang. 2009. « Forming limit diagrams of tubular materials by bulge tests ». *Journal of Materials Processing Technology,* vol. 209, n° 11, p. 5024-5034.

Hwang, YM, and CW Wang. 2009. « Flow stress evaluation of zinc copper and carbon steel tubes by hydraulic bulge tests considering their anisotropy ». *Journal of Materials Processing Technology,* vol. 209, n° 9, p. 4423-4428.

Imaninejad, M, G Subhash and A Loukus. 2004. « Experimental and numerical investigation of free-bulge formation during hydroforming of aluminum extrusions ». *Journal of materials processing technology,* vol. 147, n° 2, p. 247-254.

Jansson, Mikael, Larsgunnar Nilsson and Kjell Simonsson. 2008. « Tube hydroforming of aluminium extrusions using a conical die and extensive feeding ». *Journal of Materials Processing Technology,* vol. 198, n° 1, p. 14-21.

Jie, M, CH Cheng, LC Chan and CL Chow. 2009. « Forming limit diagrams of strain-rate-dependent sheet metals ». *International Journal of Mechanical Sciences,* vol. 51, n° 4, p. 269-275.

Jirathearanat, Suwat, Christoph Hartl and Taylan Altan. 2004. « Hydroforming of Y-shapes—product and process design using FEA simulation and experiments ». *Journal of Materials Processing Technology,* vol. 146, n° 1, p. 124-129.

Kachanov, L. 1986. *Introduction to continuum damage mechanics*, 10. Springer.

Kang, Sung-Jong, Hyoung-Kwang Kim and Beom-Soo Kang. 2005. « Tube size effect on hydroforming formability ». *Journal of materials processing technology,* vol. 160, n° 1, p. 24-33.

Keeler, Stuart P. 1965. « Determination of forming limits in automotive stampings ». *451221 SHEET METAL IND,* vol. 42, n° 461, p. 683-691.

Keeler, Stuart P, and Walter A Backofen. 1963. « Plastic instability and fracture in sheets stretched over rigid punches ». *ASM TRANS Q,* vol. 56, n° 1, p. 25-48.

Kilfoil, Leo Joseph. 2007. « In-plane plane strain testing to evaluate formability of sheet steels used in tubular products ».

Kim, Jeong, Sang-Woo Kim, Woo-Jin Song and Beom-Soo Kang. 2004a. « Analytical approach to bursting in tube hydroforming using diffuse plastic instability ». *International journal of mechanical sciences,* vol. 46, n° 10, p. 1535-1547.

Kim, Jeong, Sang-Woo Kim, Woo-Jin Song and Beom-Soo Kang. 2005. « Analytical and numerical approach to prediction of forming limit in tube hydroforming ». *International journal of mechanical sciences,* vol. 47, n° 7, p. 1023-1037.

Kim, Jeong, Yong-Wook Kim, Beom-Soo Kang and Sang-Moon Hwang. 2004b. « Finite element analysis for bursting failure prediction in bulge forming of a seamed tube ». *Finite elements in Analysis and Design,* vol. 40, n° 9, p. 953-966.

Kim, Sungtae, and Youngsuk Kim. 2002. « Analytical study for tube hydroforming ». *Journal of materials processing technology,* vol. 128, n° 1, p. 232-239.

Ko, Youn Ki, Jong Sub Lee, H Huh, HK Kim and SH Park. 2007. « Prediction of fracture in hub-hole expanding process using a new ductile fracture criterion ». *Journal of materials processing technology,* vol. 187, p. 358-362.

Koc, M, and T Altan. 1998. *Development of guidelines for part, process, and tooling design in the tube hydroforming (THF) process: Classification of the parts and analytical models for prediction of process parameters*. Report No. THF/ERC/NSM-98-R-34, The Ohio State University.

Koç, Muammer. 2003. « Tribological issues in the tube hydroforming process—selection of a lubricant for robust process conditions for an automotive structural frame part ». *Journal of manufacturing science and engineering,* vol. 125, n° 3, p. 484-492.

Koc, Muammer, and Taylan Altan. 2002. « Prediction of forming limits and parameters in the tube hydroforming process ». *International Journal of Machine Tools and Manufacture,* vol. 42, n° 1, p. 123-138.

Koç, Muammer, Yingyot Aue-u-lan and Taylan Altan. 2001. « On the characteristics of tubular materials for hydroforming—experimentation and analysis ». *International Journal of Machine Tools and Manufacture,* vol. 41, n° 5, p. 761-772.

Koc, Pino, and Boris Štok. 2004. « Computer-aided identification of the yield curve of a sheet metal after onset of necking ». *Computational Materials Science,* vol. 31, n° 1, p. 155-168.

Kõrgesaar, M, and J Romanoff. 2013. « Influence of softening on fracture propagation in large-scale shell structures ». *International Journal of Solids and Structures,* vol. 50, n° 24, p. 3911-3921.

Korhonen, AS, and T Manninen. 2008. « Forming and fracture limits of austenitic stainless steel sheets ». *Materials Science and Engineering: A,* vol. 488, n° 1, p. 157-166.

Kridli, GT, L Bao, PK Mallick and Y Tian. 2003. « Investigation of thickness variation and corner filling in tube hydroforming ». *Journal of Materials Processing Technology,* vol. 133, n° 3, p. 287-296.

Kuwabara, Toshihiko. 2007. « Advances in experiments on metal sheets and tubes in support of constitutive modeling and forming simulations ». *International Journal of Plasticity,* vol. 23, n° 3, p. 385-419.

Lang, LH, ZR Wang, DC Kang, SJ Yuan, Shi-Hong Zhang, Joachim Danckert and Karl Brian Nielsen. 2004. « Hydroforming highlights: sheet hydroforming and tube hydroforming ». *Journal of Materials Processing Technology,* vol. 151, n° 1, p. 165-177.

Lei, Li-Ping, Jeong Kim and Beom-Soo Kang. 2002. « Bursting failure prediction in tube hydroforming processes by using rigid–plastic FEM combined with ductile fracture criterion ». *International journal of mechanical sciences,* vol. 44, n° 7, p. 1411-1428.

Lei, Li-Ping, Jeong Kim, Sung-Jong Kang and Beom-Soo Kang. 2003. « Rigid–plastic finite element analysis of hydroforming process and its applications ». *Journal of Materials processing technology,* vol. 139, n° 1, p. 187-194.

Lei, LP, BS Kang and SJ Kang. 2001. « Prediction of the forming limit in hydroforming processes using the finite element method and a ductile fracture criterion ». *Journal of Materials Processing Technology,* vol. 113, n° 1, p. 673-679.

Lemaitre, Jean, and Horst Lippmann. 1996. *A course on damage mechanics*, 2. Springer Berlin.

Li, H, MW Fu, J Lu and H Yang. 2011. « Ductile fracture: experiments and computations ». *International Journal of Plasticity,* vol. 27, n° 2, p. 147-180.

Ling, Yun. 1996. « Uniaxial true stress-strain after necking ». *AMP Journal of Technology,* vol. 5, p. 37-48.

Liu, Gang, Shijian Yuan and Bugang Teng. 2006. « Analysis of thinning at the transition corner in tube hydroforming ». *Journal of materials processing technology,* vol. 177, n$^o$ 1, p. 688-691.

Liu, Hongsheng, Yuying Yang, Zhongqi Yu, Zhenzhong Sun and Yongzhi Wang. 2009. « The application of a ductile fracture criterion to the prediction of the forming limit of sheet metals ». *Journal of materials processing technology,* vol. 209, n$^o$ 14, p. 5443-5447.

Lou, Yanshan, and Hoon Huh. 2012. « Extension of a shear-controlled ductile fracture model considering the stress triaxiality and the Lode parameter ». *International Journal of Solids and Structures*.

Lou, Yanshan, and Hoon Huh. 2013. « Prediction of ductile fracture for advanced high strength steel with a new criterion: Experiments and simulation ». *Journal of Materials Processing Technology*.

Lou, Yanshan, Hoon Huh, Sungjun Lim and Keunhwan Pack. 2012. « New ductile fracture criterion for prediction of fracture forming limit diagrams of sheet metals ». *International Journal of Solids and Structures,* vol. 49, n$^o$ 25, p. 3605-3615.

Luo, Meng, and Tomasz Wierzbicki. 2010. « Numerical failure analysis of a stretch-bending test on dual-phase steel sheets using a phenomenological fracture model ». *International Journal of Solids and Structures,* vol. 47, n$^o$ 22, p. 3084-3102.

Manabe, Ken-ichi, and Masaaki Amino. 2002. « Effects of process parameters and material properties on deformation process in tube hydroforming ». *Journal of materials processing technology,* vol. 123, n$^o$ 2, p. 285-291.

Marciniak, Zdzislaw, and Kazimierz Kuczyński. 1967. « Limit strains in the processes of stretch-forming sheet metal ». *International Journal of Mechanical Sciences,* vol. 9, n$^o$ 9, p. 609-620.

Mariage, Jean-François. 2003. « Simulation numérique de l'endommagement ductile en formage de pièces massives ». Université de Technologie de Troyes.

McClintock, Frank A. 1963. « On the plasticity of the growth of fatigue cracks ». *Fracture of solids,* vol. 20, p. 65-102.

McClintock, Frank A. 1968. « A criterion for ductile fracture by the growth of holes ». *Journal of Applied Mechanics,* vol. 35, n$^o$ 2, p. 363-371.

Michael, B, C Oliver, A Daniel, D Larissa and A MARCÍLIO. 2008. « A ductile damage criterion at various stress triaxialities [J] ». *International Journal of Plasticity,* vol. 24, n° 10, p. 1731-1755.

Mirone, Giuseppe. 2004. « A new model for the elastoplastic characterization and the stress–strain determination on the necking section of a tensile specimen ». *International Journal of Solids and Structures,* vol. 41, n° 13, p. 3545-3564.

Mojarad Farimani, Saeed. 2013. « Experimental process development and aerospace alloy formability studies for hydroforming ». École de technologie supérieure.

Mojarad Farimani, Saeed, Henri Champliaud, Javad Gholipour Baradari, Jean Savoie and Priti Wanjara. 2013. « Numerical and Experimental Study of Tube Hydroforming for Aerospace Applications ». *Key Engineering Materials,* vol. 554, p. 1779-1786.

Mojarad Farimani, Saeed, Javad Gholipour Baradari, Henri Champliaud, Jean Savoie and Priti Wanjara. 2014. « Numerical and Experimental Study of Preforming Stage in Tube Hydroforming ». In *Key Engineering Materials*. Vol. 611, p. 1132-1138. Trans Tech Publ.

Nahshon, K, and JW Hutchinson. 2008. « Modification of the Gurson model for shear failure ». *European Journal of Mechanics-A/Solids,* vol. 27, n° 1, p. 1-17.

Narasimhan, K, and RH Wagoner. 1991. « Finite element modeling simulation of in-plane forming limit diagrams of sheets containing finite defects ». *Metallurgical Transactions A,* vol. 22, n° 11, p. 2655-2665.

Needleman, A. 1987. « A continuum model for void nucleation by inclusion debonding ». *Journal of applied mechanics,* vol. 54, n° 3, p. 525-531.

Nefussi, Germaine, and Alain Combescure. 2002. « Coupled buckling and plastic instability for tube hydroforming ». *International Journal of Mechanical Sciences,* vol. 44, n° 5, p. 899-914.

Ngaile, Gracious, Stefan Jaeger and Taylan Altan. 2004. « Lubrication in tube hydroforming (THF): Part II. Performance evaluation of lubricants using LDH test and pear-shaped tube expansion test ». *Journal of materials processing technology,* vol. 146, n° 1, p. 116-123.

Ngaile, Gracious, Bryan Pax, Taylan Altan, Nitin Jain, Brent Harman, Greg Homan and Xiaoxiang Shi. 2006. « Progressive die sequence design for deep drawing round cups using finite element analysis ». *Journal of manufacturing science and engineering,* vol. 128, n° 1, p. 366-369.

Ogura, Takashi. 1970. « Liquid bulge forming ».

Oh, SI, CC Chen and S Kobayashi. 1979a. « Ductile fracture in axisymmetric extrusion and drawing—part 2: workability in extrusion and drawing ». *Journal of Engineering for Industry,* vol. 101, n° 1, p. 36-44.

Oh, SI, CC Chen and S Kobayashi. 1979b. « Ductile Fracture in Axisymmetric Extrusion and Drawing—Part 2: Workability in Extrusion and Drawing ». *Journal of Engineering for Industry,* vol. 101, p. 36.

Orban, Hatem, and S Jack Hu. 2007. « Analytical modeling of wall thinning during corner filling in structural tube hydroforming ». *Journal of Materials Processing Technology,* vol. 194, n° 1, p. 7-14.

Ortiz, M, and JC Simo. 1986. « An analysis of a new class of integration algorithms for elastoplastic constitutive relations ». *International Journal for Numerical Methods in Engineering,* vol. 23, n° 3, p. 353-366.

Osakada, K, and K Mori. 1978. « Prediction of ductile fracture in cold forging ». *Ann. CIRP,* vol. 27, n° 1, p. 135-139.

Oyane, Moriya, Teisuke Sato, Kunio Okimoto and Susumu Shima. 1980. « Criteria for ductile fracture and their applications ». *Journal of Mechanical Working Technology,* vol. 4, n° 1, p. 65-81.

Ozturk, Fahrettin, and Daeyong Lee. 2004. « Analysis of forming limits using ductile fracture criteria ». *Journal of materials processing technology,* vol. 147, n° 3, p. 397-404.

Ozturk, Fahrettin, and Daeyong Lee. 2007. « A new methodology for ductile fracture criteria to predict the forming limits ». *Journal of Materials Engineering and Performance,* vol. 16, n° 2, p. 224-228.

Pardoen, T, and JW Hutchinson. 2000. « An extended model for void growth and coalescence ». *Journal of the Mechanics and Physics of Solids,* vol. 48, n° 12, p. 2467-2512.

Perra, Mark, and Iain Finnie. 2013. « Void growth and localization of shear in plane strain tension ». In *ICF4, Waterloo (Canada) 1977.*

Plancak, M, F Vollertsen and J Woitschig. 2005. « Analysis, finite element simulation and experimental investigation of friction in tube hydroforming ». *Journal of materials processing technology,* vol. 170, n° 1, p. 220-228.

Rice, J R_, and Dennis Michael Tracey. 1969. « On the ductile enlargement of voids in triaxial stress fields∗ ». *Journal of the Mechanics and Physics of Solids,* vol. 17, n° 3, p. 201-217.

Saboori, M, H Champliaud, J Gholipour, A Gakwaya, J Savoie and P Wanjara. 2014a. « Evaluating the flow stress of aerospace alloys for tube hydroforming process by free expansion testing ». *The International Journal of Advanced Manufacturing Technology*, p. 1-12.

Saboori, M, H Champliaud, J Gholipour, A Gakwaya, J Savoie and P Wanjara. 2014b. « Evaluating the flow stress of aerospace alloys for tube hydroforming process by free expansion testing ». *The International Journal of Advanced Manufacturing Technology,* vol. 72, n° 9-12, p. 1275-1286.

Veuillez sélectionner un type de document autre que « Generic » afin de faire afficher la référence bibliographique.

Saboori, Mehdi, Henri Champliaud, Javad Ghoulipor, Augustin Gakwaya, Jean Savoie and Priti Wanjara. 2012b. « Study of True Stress-Strain Curve after Necking for Application in Ductile Fracture Criteria in Tube Hydroforming of Aerospace Material ». *Key Engineering Materials,* vol. 504, p. 95-100.

Saboori, Mehdi, Javad Gholipour, Henri Champliaud, Augustin Gakwaya, Jean Savoie and Priti Wanjara. 2013a. « Development of an Inverse Method for Material Characterization ». In *Materials Science & Technology 2013*. (Montréal, 2013).

Saboori, Mehdi, Javad Gholipour, Henri Champliaud, Augustin Gakwaya, Jean Savoie and Priti Wanjara. 2013b. « Effect of Material Model on Finite Element Modeling of Aerospace Alloys ». *Key Engineering Materials,* vol. 554, p. 151-156.

Shabrov, MN, CL Briant, A Needleman, S Kim, E Sylven, DH Sherman and L Chuzhoy. 2004. « Void nucleation by inclusion cracking ». *Metallurgical and Materials Transactions A,* vol. 35, n° 6, p. 1745-1755.

Simha, C, Rassin Grantab and Michael J Worswick. 2007. « Computational analysis of stress-based forming limit curves ». *International Journal of Solids and Structures,* vol. 44, n° 25, p. 8663-8684.

Simha, C Hari Manoj, J Gholipour, A Bardelcik and MJ Worswick. 2005. « Application of an extended stress-based flow limit curve to predict necking in tubular hydroforming ». In *AIP Conference Proceedings*. Vol. 778, p. 511. IOP INSTITUTE OF PHYSICS PUBLISHING LTD.

Simha, C Hari Manoj, Javad Gholipour, Alexander Bardelcik and Michael J Worswick. 2007. « Prediction of necking in tubular hydroforming using an extended stress-based forming limit curve ». *Journal of Engineering Materials and Technology,* vol. 129, n° 1, p. 36-47.

Simo, JC, and Miguel Ortiz. 1985. « A unified approach to finite deformation elastoplastic analysis based on the use of hyperelastic constitutive equations ». *Computer methods in applied mechanics and engineering,* vol. 49, n° 2, p. 221-245.

Sokolowski, T, K Gerke, M Ahmetoglu and T Altan. 2000. « Evaluation of tube formability and material characteristics: hydraulic bulge testing of tubes ». *Journal of Materials Processing Technology,* vol. 98, n° 1, p. 34-40.

Song, WJ, J Kim and BS Kang. 2007. « Experimental and analytical evaluation on flow stress of tubular material for tube hydroforming simulation ». *Journal of materials processing technology,* vol. 191, n° 1, p. 368-371.

Song, Woo-Jin, Seong-Chan Heo, Tae-Wan Ku, Jeong Kim and Beom-Soo Kang. 2010. « Evaluation of effect of flow stress characteristics of tubular material on forming limit in tube hydroforming process ». *International Journal of Machine Tools and Manufacture,* vol. 50, n° 9, p. 753-764.

Song, Woo-Jin, Sang-Woo Kim, Jeong Kim and Beom-Soo Kang. 2005. « Analytical and numerical analysis of bursting failure prediction in tube hydroforming ». *Journal of materials processing technology,* vol. 164, p. 1618-1623.

Stören, S, and JR Rice. 1975. « Localized necking in thin sheets ». *Journal of the Mechanics and Physics of Solids,* vol. 23, n° 6, p. 421-441.

Stoughton, Thomas B. 2000. « A general forming limit criterion for sheet metal forming ». *International Journal of Mechanical Sciences,* vol. 42, n° 1, p. 1-27.

Stoughton, Thomas B, and Xinhai Zhu. 2004. « Review of theoretical models of the strain-based FLD and their relevance to the stress-based FLD ». *International Journal of Plasticity,* vol. 20, n° 8, p. 1463-1486.

Strano, Matteo, Suwat Jirathearanat, Shiuan-Guang Shr and Taylan Altan. 2004. « Virtual process development in tube hydroforming ». *Journal of materials processing technology,* vol. 146, n° 1, p. 130-136.

Swift, H_W. 1952. « Plastic instability under plane stress ». *Journal of the Mechanics and Physics of Solids,* vol. 1, n° 1, p. 1-18.

Tvergaard, Viggo, and Kim Lau Nielsen. 2010. « Relations between a micro-mechanical model and a damage model for ductile failure in shear ». *Journal of the Mechanics and Physics of Solids,* vol. 58, n° 9, p. 1243-1252.

Vollertsen, F, and M Plancak. 2002. « On possibilities for the determination of the coefficient of friction in hydroforming of tubes ». *Journal of materials processing technology,* vol. 125, p. 412-420.

Wagoner, Robert H, and Jean-Loup Chenot. 1997. *Fundamentals of metal forming*. Wiley New York.

Weck, Arnaud, and DS Wilkinson. 2008. « Experimental investigation of void coalescence in metallic sheets containing laser drilled holes ». *Acta Materialia,* vol. 56, n° 8, p. 1774-1784.

Weck, Arnaud, DS Wilkinson, Eric Maire and H Toda. 2008. « Visualization by X-ray tomography of void growth and coalescence leading to fracture in model materials ». *Acta Materialia,* vol. 56, n° 12, p. 2919-2928.

Xia, ZC. 2001. « Failure analysis of tubular hydroforming ». *Journal of engineering materials and technology,* vol. 123, n° 4, p. 423-429.

Xu, Yanwu. 2006. *Modern formability: measurement, analysis and applications*. Hanser Gardner Publications Cincinnati, OH.

Xue, Liang. 2007. « Damage accumulation and fracture initiation in uncracked ductile solids subject to triaxial loading ». *International Journal of Solids and Structures,* vol. 44, n° 16, p. 5163-5181.

Xue, Liang. 2008. « Constitutive modeling of void shearing effect in ductile fracture of porous materials ». *Engineering Fracture Mechanics,* vol. 75, n° 11, p. 3343-3366.

Xue, Liang, and Tomasz Wierzbicki. 2008. « Ductile fracture initiation and propagation modeling using damage plasticity theory ». *Engineering Fracture Mechanics,* vol. 75, n° 11, p. 3276-3293.

Yadav, Ajay D. 2008. « Process analysis and design in stamping and sheet hydroforming ». The Ohio State University.

Yang, B, WG Zhang and SH Li. 2006. « Analysis and finite element simulation of the tube bulge hydroforming process ». *The International Journal of Advanced Manufacturing Technology,* vol. 29, n° 5-6, p. 453-458.

Yao, Hong, and Jian Cao. 2002. « Prediction of forming limit curves using an anisotropic yield function with prestrain induced backstress ». *International journal of plasticity,* vol. 18, n° 8, p. 1013-1038.

Yoshida, Kengo, and Toshihiko Kuwabara. 2007. « Effect of strain hardening behavior on forming limit stresses of steel tube subjected to nonproportional loading paths ». *International journal of plasticity,* vol. 23, n° 7, p. 1260-1284.

Yoshida, Kengo, Toshihiko Kuwabara and Mitsutoshi Kuroda. 2007. « Path-dependence of the forming limit stresses in a sheet metal ». *International journal of plasticity,* vol. 23, n$^o$ 3, p. 361-384.

Yoshida, Kengo, and Noriyuki Suzuki. 2008. « Forming limit stresses predicted by phenomenological plasticity theories with anisotropic work-hardening behavior ». *International Journal of Plasticity,* vol. 24, n$^o$ 1, p. 118-139.

Yu, Song, Xiaolong Xie, Jie Zhang and Zhen Zhao. 2007. « Ductile fracture modeling of initiation and propagation in sheet-metal blanking processes ». *Journal of materials processing technology,* vol. 187, p. 169-172.

Yuan, Shijian, Xiaosong Wang, Gang Liu and ZR Wang. 2007. « Control and use of wrinkles in tube hydroforming ». *Journal of Materials Processing Technology,* vol. 182, n$^o$ 1, p. 6-11.

Zhalehfar, F, SJ Hosseinipour, S Nourouzi and AH Gorji. 2013. « A different approach for considering the effect of non-proportional loading path on the forming limit diagram of AA5083 ». *Materials & Design,* vol. 50, p. 165-173.

Zhang, ZL, M Hauge, J Ødegård and C Thaulow. 1999. « Determining material true stress–strain curve from tensile specimens with rectangular cross-section ». *International Journal of Solids and Structures,* vol. 36, n$^o$ 23, p. 3497-3516.

Zhano, KS, and ZH Li. 1994. « Numerical analysis of the stress-strain curve and fracture initiation for ductile material ». *Engineering fracture mechanics,* vol. 49, n$^o$ 2, p. 235-241.

Zribi, Temim, Ali Khalfallah and Hedi BelHadjSalah. 2013. « Experimental characterization and inverse constitutive parameters identification of tubular materials for tube hydroforming process ». *Materials & Design,* vol. 49, p. 866-877.